Oceanic Latent Heat Flux from Satellite data

by

Bart A. Brashers

A dissertation submitted in partial fulfillment
of the requirements for the degree of

Doctor of Philosophy

University of Washington

1998

Approved by _____
Chairperson of Supervisory Committee

Program Authorized
to Offer Degree _____

Date _____

Doctoral Dissertation

In presenting this dissertation in partial fulfillment of the requirements for the Doctoral degree at the University of Washington, I agree that the Library shall make its copies freely available for inspection. I further agree that extensive copying of this dissertation is allowable only for scholarly purposes, consistent with “fair use” as prescribed in the U.S. Copyright Law. Requests for copying or reproduction of this dissertation may be referred to University Microfilms, 1490 Eisenhower Place, P.P. Box 975, Ann Arbor, MI 48106, to whom the author has granted “the right to reproduce and sell (a) copies of the manuscript in microform and/or (b) printed copies of the manuscript made from microform.”

Signature _____

Date _____

University of Washington

Abstract

Oceanic Latent Heat Flux from SSM/I Data
by Bart A. Brashers

Chairperson of the Supervisory Committee: Professor Robert A. Brown
Department of Atmospheric Sciences

This thesis presents a new method of estimating ocean latent heat flux (LHF) using satellite data. The surface layer equations derived from Monin-Obukhov similarity theory are closed with empirical parameterizations, and patched to a mixed layer model yielding a two-layer PBL model. This is the first proof that such a model can be applied in non-strongly convective situations. Two new retrievals of moisture parameters are derived, one for the surface to 500 meter integrated water vapor (W_B) and one for the mixed-layer humidity (q_m). Inputs include total integrated water vapor retrieved from the Special Sensor Microwave Imager (SSM/I), sea surface temperature optimally interpolated from retrievals from the Advanced Very High Resolution Radiometer and buoy/ship measurements (OI SST), and ECMWF analyzed air-sea temperature difference (T - SST). An analytic relationship between W_B and near-surface humidity is presented as a replacement for the statistical relationship of Schulz et al. (1993). LHF is then calculated using the new SSM/I-based retrieval of ML-humidity, SSM/I retrieval of wind speed, OI SST, and ECMWF T - SST. Model errors are assessed, and the q_m method derived in this thesis is found to perform the best. Systematic errors are small, and random errors are 26 W/m^2. Monthly averages of LHF have been calculated using all available SSM/I data on a 1° by 1° grid for 1992-1997. Differences with other published climatologies, both those derived from SSM/I data and from traditional data, have been discussed. Differences between the current work and previous SSM/I methods are evenly split between model parameterization differences and the new moisture retrieval. Errors due to averaging the input variables and due to errors in merchant ship measurements dominate the differences between the current work and traditional climatologies. This analysis establishes the limiting factors in LHF calculation and produces the most accurate LHF climatology to date. It is the first full SSM/I climatology which will be made available to the general scientific community.

Table of Contents

List of Figures

List of Tables

Acknowledgments

I would like to take this opportunity to thank my advisor Dr. Bob Brown for his support and guidance through the years leading to this thesis. He helped me keep an eye on the “big picture” when I needed it, and forced me to pay attention to the smallest details when I needed it. I’d also like to thank Dr. Conway Leovy for the many many fruitful discussions and for reading this thesis, Dr. Lynn McMurdie for helping me organize my thoughts in writing and reading this work, and Dr. Chris Bretherton for many helpful discussions and cheerfully answering even my dumb questions. Thanks go as well to Dr. Ralph Foster, for many insightful discussions through the years.

I would also like to thank Dr. König-Langlo of the Alfred Wegener Institute for Polar and Marine Research in Bremerhaven, Germany for data from the R/V Polarstern; Dr. Sandra Yuter of the Mesoscale Group, Department of Atmospheric Science here at UW for data from TEPPS; Dr. Chris Fairall of NOAA/ERL for turbulence data from ASTEX and TOGA-COARE; Dr. Jim Johnson of NOAA/PMEL for data from ACE-1 and RITS93, Mr. Frank Wentz of Remote Sensing Systems Inc. for SSM/I data, and Dr. Shu-Hsien Chou for sharing the data files from her 1997 paper with me. Without their help and cooperation this work would not have been possible.

Thanks are also due to Marc Michelsen for his help with computer problems, programming tips, data storage help, and generally keeping the highest standard of computer facilities available throughout my tenure here at UW; and to Shirley Joaquin for managerial support.

Finally, thanks go to my family and particularly my fiance Margaret, for their continued support and for making this all worth while.

This work was performed under an Earth Observing System grant, NASA grant NAGW-2633, “Climate Processes over the Oceans”.

Chapter 1

Introduction

1.1) Introduction

The heat balance at the sea surface is of primary interest to climate modelers, since the models are sensitive to small imbalances integrated over long time. A small change in heat flux can drive changes in the sea surface temperature and cause the models to deviate from the observed climate. The two leading loss terms in the heat budget at the sea surface are latent heat flux due to evaporation and longwave radiation. Both depend strongly on the water vapor content of the lowest layer of air above the surface. A dry layer will both promote evaporation and transmit more upwelling longwave radiation. Randall et. al. (1992) showed that the parameterization of latent heat flux was the term with the most inter-model variability among 19 of the most advanced global climate models. Good-quality global measurements of evaporation are needed to establish a climatology to validate model assumptions and calibrate climate parameters, as well as to understand the basic physics of air-sea interaction. There exists a good possibility to obtain these data from existing satellite data.

Routine measurements are far too sparse globally to produce acceptable climatologies of latent heat flux, even when volunteer ship reports of temperature and relative humidity (which are of questionable quality) are included. Satellites provide good coverage, typically covering all points on the earth every few days, but don't measure evaporation directly. The Special Sensor Microwave Imager (SSM/I) a passive microwave radiometer, has been flown since 1987 and is likely to be flown for several years to come. In 1999 and 2000, the Advanced Microwave Scanning Radiometer (AMSR), the "next generation" radiometer with the characteristics of both the SSM/I and the Advanced Very High Resolution Radiometer (AVHRR), will be launched aboard a Japanese and an American satellite. We now have 10 years of SSM/I data, and will have at least several years of AMSR data, long enough to provide a reasonable climatology. Several retrievals of geophysical parameters from the SSM/I radiation measurements have been presented and are widely used, most noteably U (wind speed), W (total integrated water vapor), L (total integrated liquid water), W_B (bottom-layer integrated water vapor), ice detection, and some land-use parameters.

One might then seek a relationship between a parameter retrieved by the SSM/I and a parameter that can be used to calculate latent heat flux. Liu (1986), Miller and Katsaros (1992), Schulz et. al.

(1993), Schlüssel et al. (1995), Clayson and Curry (1996) and Chou et al. (1995, 1997) have all presented statistical relationships toward that end.

Statistics are a valuable tool to research scientists, and are frequently used when no physically-based relationships can be found. However, statistically-based relationships may not be valid in changing climate situations, and are often not portable from one geographic region to another even without climate change. Using a statistically-derived relation also ignores variation around a mean, or some tendency that may be due to resolvable physics. Many successful studies have been completed using these statistically-based methods, and some ~1 year climatologies have been produced. However, all the methods suffer from either bias or significant scatter, or both.

Liu's method was derived for use with monthly averages, but several studies have applied it to instantaneous data. However, it has serious regional biases in the range of -5 to 29 W/m^2, with r.m.s. scatter about each mean of more than 30 W/m^2. Schulz' method produces reasonable biases except south of 40˚ S where it is biased by up to 41 W/m^2, and r.m.s. scatter of about 30 W/m^2 as well. Schlüssel's method produces reasonable biases north of 60˚ S, but still has scatter of about 30 W/m^2. Chou's method gives negligible biases but is still plagued by r.m.s. scatter of about 30 W/m^2. If the distribution of samples from the SSM/I were gaussian, the r.m.s. error would cancel when taking a monthly mean, leaving only the biases. However, due to the nature of the satellite swath sampling patterns a gaussian distribution is not expected, and the r.m.s. errors of individual retrievals can contribute to the bias of the monthly-mean field. Thus it is important to develop a method that minimizes the scatter as well as the bias.

The goal of this thesis is to develop a physically-based relationship between satellite-retrievable parameters and sea surface latent heat flux (LHF) to be used over the world's oceans. Input parameters will be restricted to satellite data, rather than global circulation model output or analyses, whenever possible.

First, I will summarize the data used in this work, then I will present a bulk surface layer model, and explain how it relates to the bulk aerodynamic parameterization. I will then add a few components to the LKB model and choose the necessary empirical constants, and compare its output with direct measurements to show that it adequately estimates the latent heat flux. Then I will create a simple model of the lowest part of the planetary boundary layer by patching the augmented LKB model to a model of a well-mixed layer, such that the LKB model is driven with mixed-layer (ML) averages. I will show that using ML-values gives similar results compared with the more traditional 10 m values.

I will then review some of the more popular SSM/I retrievals, and show how some have been used to calculate LHF. Two new retrievals will be developed, using a multi-sensor approach that uses parameters retrieved by the SSM/I and by AVHRR. The errors of these retrievals will be evaluated.

A collection of atmospheric soundings launched from a variety of research vessels, along with their associated ship-board sensor logs, will be used to simulate SSM/I retrievals of *W* to validate the model and compare it to the statistically-based relationships. Then real SSM/I data will be used to assess the overall performance of the model, and partition the error into retrieval-based error and model-based error. Finally, a climatology will be calculated using all the available SSM/I data. This will be compared to climatologies from the UW boundary layer model PBL-LIB model as well as other published sources.

1.2) Introduction to the marine boundary layer

Almost everywhere over the world's oceans, the air is a degree or so colder than the sea surface temperature, and has a relative humidity near 75%. This makes both the sensible heat flux and the latent heat flux positive into the atmosphere. Turbulence near the surface, either shear-driven or buoyancy-driven, transports air from the molecular sub-layer where molecular diffusion dominates and establishes the surface layer where the profiles are logarithmic. The shear maintains the logarithmic form, keeping the layer from becoming well mixed, as it is always "renewed" with warmer moister air from below.

The buoyancy flux drives convection that mixes the layer above the surface layer, reaching to ~500 m in height. This "mixed layer" (ML) is very common over most of the worlds oceans. Samples are shown in Figure 2.3, page 29.

Two regimes can be identified by categorizing the marine boundary layer in terms of the wind direction compared to the sea surface temperature gradient. Cold advection, where the wind blows from cooler SSTs to warmer, promotes the buoyancy flux described above that tends to mix the ML. Warm advection tends to decrease the buoyancy flux, but is not often successful at shutting it completely off. The advection of high-humidity air tends to happen together with warm advection, but since the humidity part of the buoyancy flux is larger than the sensible part, the globally averaged buoyancy flux is still positive into the atmosphere. Additionally, removal of sensible heat from the ML by longwave radiational exchange with the upper atmosphere, and removal of water vapor by convective transport helps to establish this global non-zero average. Another factor adding to the prevalence of positive buoyancy flux is the fact that the Western boundary currents in the ocean (moving warm water away from the equator) are stronger then the Eastern boundary currents (moving cold water toward the equator). Since

the general circulation of the air around the sub-tropical high is in the same direction as the oceanic boundary currents, the stronger Western boundary current offsets much of the warm advection with its own oceanic warm advection.

The structure of the marine boundary layer can be diagnosed well from the types and frequency of clouds that co-exists with it. In the equator-ward branch of the circulation, the boundary layer is shallow, often topped with a single layer of stratus or stratocumulus. As the air is advected to higher and higher sea surface temperatures, the boundary layer grows and the cloud thickens until drizzle or radiative processes establish a region of negative buoyancy flux somewhere below cloud base. The upper layer (often call the cloud layer) decouples from the mixed layer and the depth of the PBL continues to grow. Only intermittently can air from the lower layer, originating in the surface layer, penetrate the region of negative buoyancy flux and bring high-humidity air to the upper layer. This structure is associated with cumulus under stratocumulus, with the cumulus being the intermittent events. Without the moisture they bring from the surface layer, the stratocumulus would evaporate due to entrainment of dry air from above the inversion as the layer grows. Eventually, as the air column nears the ITCZ, this happens and the cumulus-under-stratocumulus gives way to deeper and deeper cumulus. The surface layer and mixed layer are still there, but feel the effects of the deep convection through downdrafts of low equivalent potential temperature air (dry air cooled by evaporation that sinks all the way to the surface). These intermittent bursts of cool, dry air result in bursts of sensible and latent heat fluxes into the air.

As the circulation brings the air column out of the region of deep convection, toward cooler SSTs, the deep convection is suppressed by cutting off the surface buoyancy flux. We shift from cold to warm advection. The boundary layer depth falls, and clouds tend to be either fog or non-existent, depending on whether the advection of temperature is stronger than the advection of water vapor. That is, as heat leaves the ML (mostly through radiative losses but also some sensible heat loss to the ocean) it may cool fast enough cause the water vapor to condense to fog. The stable stratification tends to suppress the shear-driven turbulence in the surface layer, leading to reduced fluxes (regardless of their direction). The ML may still persist as a remnant, since little else is going on to destroy it.

As the circulation brings our hypothetical air column farther from the equator, the air may feel the effects of mid-latitude storms. Shear-driven turbulence overwhelms buoyancy-driven turbulence, and the surface fluxes are once again strong, leading to a well-mixed layer being established above the surface layer. The prevalence of stratus is once again indicative of a single well-mixed layer. Deeper convection forced by synoptic- to meso-scale convergence may affect the ML, especially through downdrafts of cold dry air that may not penetrate all the way to the surface. As the column swings equa-

torward again near the Easter boundary of the ocean, it leaves the storm track and we return to the starting point of the circulation.

1.3) The SSM/I Sensor

The Special Sensor Microwave Imager (SSM/I) is a passive microwave radiometer. It has been flown on United States Defense Meteorological Satellite Program (DMSP) satellites since 1987, on the F8, F10, F11, F13 and F14 satellites. They use sun-synchronous, near-polar (98.8° inclination) orbits with a mean altitude of 860 km and a period of 102 minutes. The orbits cross the equator on an ascending swath at approximately 06:00 Local Standard Time (LST), and on a descending swath at approximately 19:00 LST. The F11 has a slightly different orbit than the other DMSP satellites.

The radiometer measures both horizontal and vertical polarizations of radiation at 19.35, 22.23 (vertical polarization only), 37.0 and 85.5 GHz (Figure 1.1). It has a swath width of 1394 km, and an excellent continuous on-line calibration method. The radiation measurements are converted to equivalent brightness temperatures and archived by Remote Sensing Systems, Inc. (Wentz 1989, 1995) in 56 pixels (19, 22 and 37 GHz) and 93 pixels (85 GHz) across each swath, with a nominal footprint size of 25 x 25 km (19, 22 and 37 GHz) and 15 x 15 km (85 GHz).

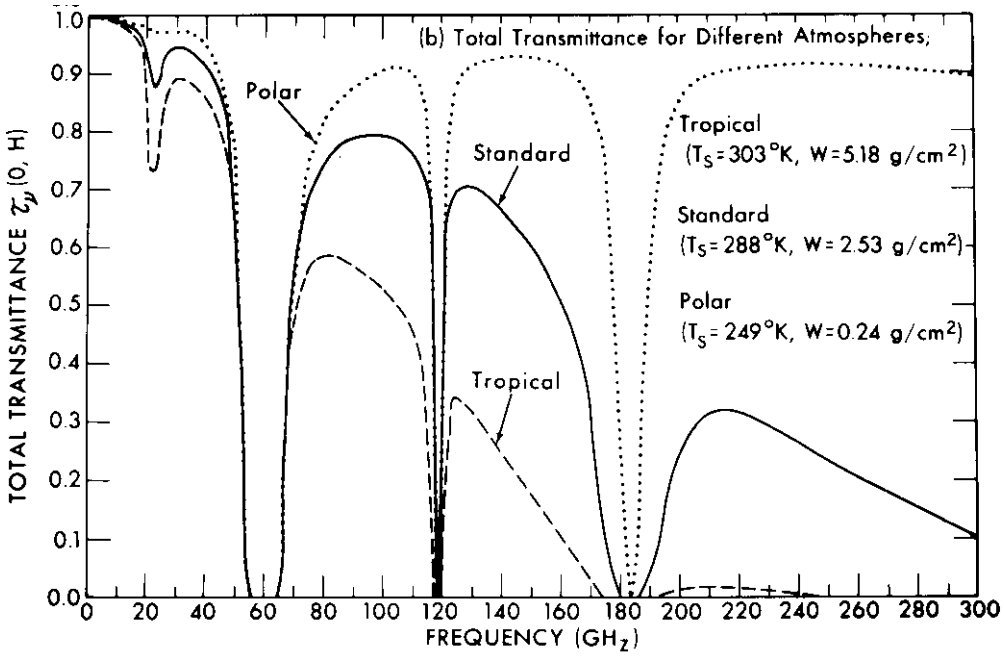

Figure 1.1 Vertical atmospheric transmittance vs. frequency for different atmospheric conditions (from Grody, 1976)

The longer wavelengths (19 and 22 GHz) channels are not very sensitive to cloud liquid water, but are suitable for measuring surface roughness and atmospheric water vapor. The 22 GHz channel is at the center of a weak water vapor resonance line at 22.235 GHz; the 19 GHz channel is in the 'wings' of this line, allowing a differential absorption technique to be used. There is a strong oxygen absorption band between 50 and 70 GHz, and non-resonant 'continuum absorption' from both dry air and water vapor increasing monotonically with increasing frequency. Thus the 37 and 85 GHz channel are located in spectral windows, but have different 'continuum absorption' rates. At the SSM/I frequencies, there is no appreciable scattering of microwave energy by cloud droplets, but the absorption coefficient for liquid water is much higher than for water vapor or oxygen. Due to the placement of the channels away from strong absorption lines, the radiation observed by the antenna is a mixture of radiation emitted by clouds, water vapor in the air, and the sea surface; and radiation emitted in the atmosphere and reflected by the sea surface.

Several geophysical parameters are retrieved from the observed brightness temperatures, most notably: W, the total integrated water vapor; L, the total integrated liquid water; U_{10}, the wind speed at 10 m (Wentz 1989, 1995); and W_B, the bottom layer integrated water vapor (Schulz et al. 1993). These retrievals are valid only under certain conditions. The area on the earth sampled by the instrument must be free from both land and sea ice, since both of these surfaces radiate much more brightly in the microwave than does the sea surface. Furthermore, clouds with sufficiently high liquid water content absorb and scatter the radiation, rendering the retrievals invalid. Thus these retrievals are valid only in the open ocean when there are only thin clouds. See Hollinger et. al. (1987) for more details on the SSM/I.

1.4) Methods for estimating LHF

There are four main ways to estimate the latent heat flux due to evaporation. The *eddy correlation* technique requires a time series of high-frequency measurements of vertical wind speed (W) and specific humidity (Q). The time series is sub-divided into periods where it looks reasonably stationary, between 20 and 60 minutes each. The total time series is partitioned into an average over that time period and a deviation from the average, $W = \overline{w} + w'$ and $Q = \overline{q} + q'$. The covariance between W and Q is then $\overline{w'q'}$, since the cross terms vanish in the averaging. This is the only direct measure of the water vapor flux. Multiplying by the air density (ρ) and the latent heat of vaporization for water (L_v) converts the water vapor flux to units of watts per square meter. Biases in the measurements of W and Q are not passed on to $\overline{w'q'}$, since it is only the fluctuations about a local mean that are used. However, errors due to interactions between the flow and the measurement instrument and supporting structure can be substantial (Högström 1988).

The *inertial dissipation* method also requires time series of high frequency measurements (commonly referred to as “turbulence data”). The dissipation of turbulent kinetic energy is estimated from the spectra of *W* and *Q* in the inertial subrange. This is then related via the budget equations to the flux of water vapor. Errors are similar to errors in the eddy correlation measurements, except that low-frequency contamination of the data (e.g. the rolling of a ship or buoy) does not affect the data in the inertial subrange very drastically.

The *profile method* requires time-averaged (bulk) measurements of horizontal wind speed, temperature and humidity at several heights in the atmospheric surface layer. The profiles expected from Monin-Obukhov similarity theory (e.g. Brown 1991) are fit to the measurements. The equations are then solved for the Obukhov length and roughness lengths, allowing one to calculate the latent heat flux. This technique was widely used in the early days of micrometeorology, but has fallen in disfavor in modern times. Error can be very large, especially if flow distortions are different at the different heights. Additionally, different averaging times are required to achieve stable statistics at different heights.

The *bulk method* is by far the most widely used today, since high-frequency (turbulence) data is rather expensive and difficult to take compared with hourly-averaged (bulk) data. The bulk aerodynamic equation is the result of classic similarity theory:

$$E = \rho L_v C_E U_{10}(q_0 - q_{10}) \tag{1.1}$$

where ρ is again the density of the air and L_v the latent heat of vaporization, U_{10} is the wind speed (in this case, at 10 m), q_0 is the specific humidity at the interface (surface), q_{10} is the specific humidity of the air (again at 10 m), and C_E is the transfer coefficient (a non-dimensional factor that must be determined from measurements). C_E can be derived for different heights other than 10 m, if desired.

1.4.1) Bulk method error analysis

The value of L_v as a function of temperature is known to high accuracy (Bolton 1980). Using the ideal gas law $\rho = P/R_d T_v$, where P is pressure, R_d is the gas constant for dry air and $T_v = T(1 + 0.61q)$ is the virtual temperature, we find that a 10 mb error in P or a 3 K error in T gives only a 1% error in ρ. C_E suffers from much larger errors. Table 1.1 lists experimentally determined values of C_E, along with the uncertainty when available, and the corresponding percent scatter (uncertainty ÷ value). The last row

summarizes the table (neglecting the highest and lowest values) by listing the mean and standard deviation of the values. We haven't been able to determine the value of C_E to within 10%.

Table 1.1 Values of C_E from experiments

Source	$10^3\, C_E$	% Scatter
Pond et al. (1971)	1.2 ± 0.2	17%
Friehe and Schmitt (1976)	1.32	
Kruspe (1977)	1.36 ± 0.25	18%
Garratt and Hyson (1975)	1.6 ± 0.3	19%
Francey and Garratt (1978)	1.5	
Fujitani (1981)	1.05	
Antonia et al (1978)	0.82 ± 0.15	18%
Smith (1974)	1.2	
Anderson and Smith (1981)	1.27 ± 0.26	20%
Smith and Anderson (1988)	1.2	
DeCosmo et al. (1996)	1.2 ± 0.24	20%
"Trimmed" overall	**1.25 ± 0.13 (10%)**	**18.6% ± 1.14%**

Figure 1.2 shows the error due to a changes in the input variables to the bulk aerodynamic LHF equation for a range of SSTs and wind speeds. T_{10} was taken to be SST - 1.25 K, and q_{10} was taken as 75% of the saturation at the SST. Except for (D), the ordinate shows the error in LHF for a unit error in the input variable, a derivative of sorts. We might set as goal for this equation to predict the LHF with 10 W/m^2. For typical midlatitude conditions (SST = 10° C, U_{10} = 10 m/s) the sensitivity to U_{10} is about 7 W/m^2 per m/s, indicating we need know the wind speed only within 1.4 m/s. The sensitivity to error in q_{10} is rather large: we need know it within 0.27 g/kg to have an acceptable (10 W/m^2) error in LHF. The sensitivity to SST is also very large: a maximum error of about 0.5 K can be tolerated. For tropical conditions (high SST but lower U_{10}) the error increases dramatically, reaching about 50 W/m^2 for a unit error in SST and about half that for U_{10}, while the sensitivity to q_{10} decreases since the typical wind speeds decrease. Also shown is the error due to a 10% error in C_E.

Given high enough quality measurement, the goal of 10 W/m^2 LHF error could be reached, were it not for the more fundamental uncertainty that stems from our lack of knowledge of the value of C_E. For

typical midlatitude conditions, the bulk aerodynamic formula can't predict the fluxes better than about 8 W/m^2. For the tropics, this number rises to near 12 W/m^2.

1.5) A brief history of SSM/I LHF methods

Several studies have attempted to find a relationship between SSM/I retrieved products and LHF, each aiming to find the specific humidity at 10 m (q_{10}) for use in the bulk aerodynamic formula (equation (4.1), page 59). The main idea is that integrated water vapor is measurable from space by the SSM/I

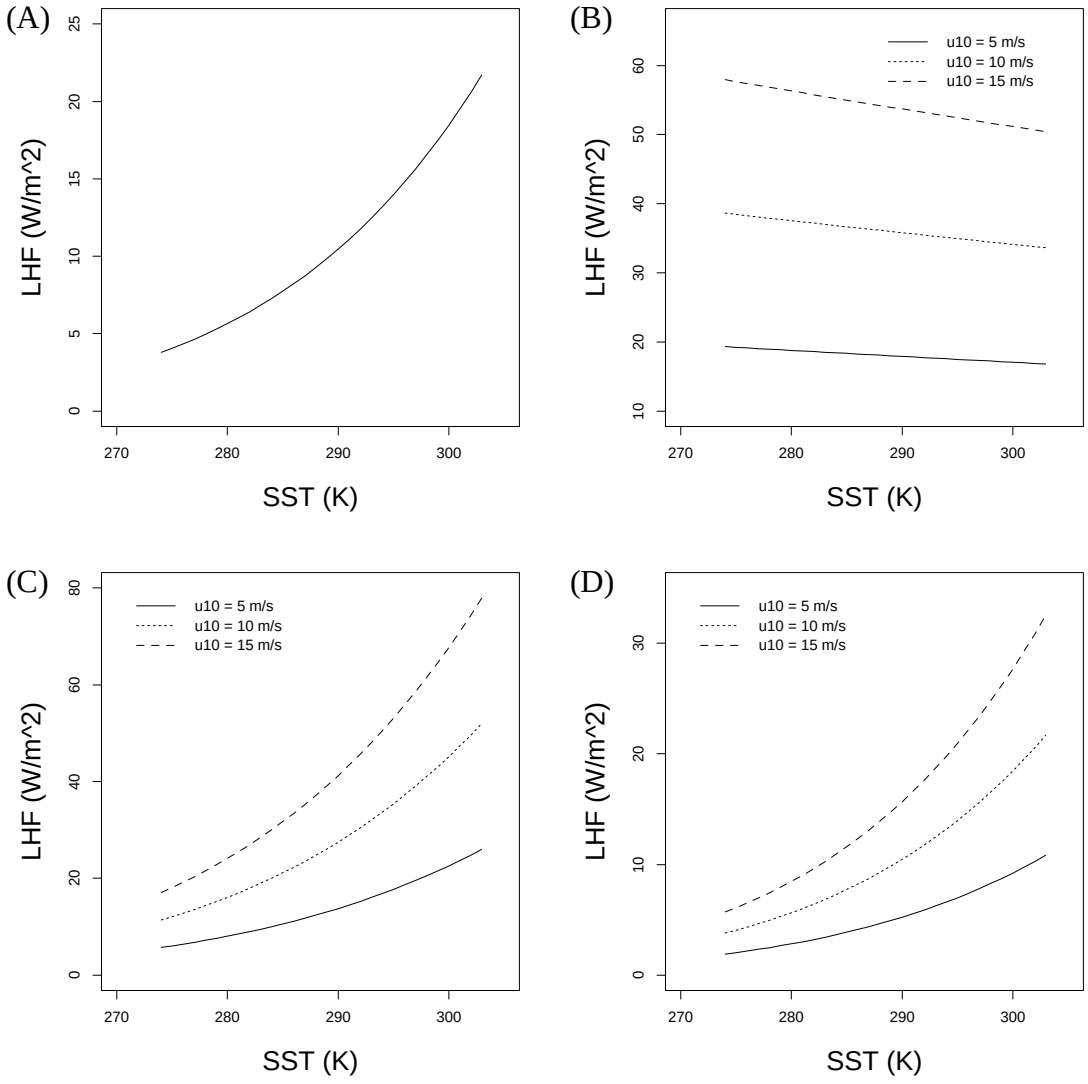

Figure 1.2 Error in LHF from the bulk aerodynamic formula, as a function of SST and wind speed, for unit errors in (A) wind speed (m/s), (B) specific humidity (g/kg), (C) sea surface temperature (K), and (D) a 10% error in the transfer coefficient. Sign of errors taken so LHF error is positive.

instrument, and a relationship between q_{10} and an SSM/I retrieval could be used to calculate the latent heat flux using the bulk aerodynamic formula and SSM/I data.

The integrated water vapor (a.k.a. precipitable water) is defined as

$$W \equiv \int_0^\infty q(z)\rho(z)dz \tag{1.2}$$

Liu and Niiler (1984) used the soundings from a 1-year period from 11 ocean weather ships and island stations to derive a 5th-order polynomial relation between monthly-mean *W* and the monthly-mean specific humidity at the lowest reported level in the sounding (*Q*). Note that although *Q* was not necessarily at 10 meters, it was designed to be used in place of q_{10} in equation (4.1). Liu (1986) was a much larger yet similar study, using 17 years of soundings from 46 mid-ocean small island or ship stations with the same goal and method. It further showed that on time scales of more than a few weeks, *W* was well correlated with *Q*, with a theoretical r.m.s. scatter of 0.4 g/kg, which corresponds to an error in the latent heat flux of 10 W/m^2 under typical conditions. However, they did not use any satellite data in their study. They only developed the *W:Q* relation, shown in Figure 1.3 along with a scatter plot of q_{10}

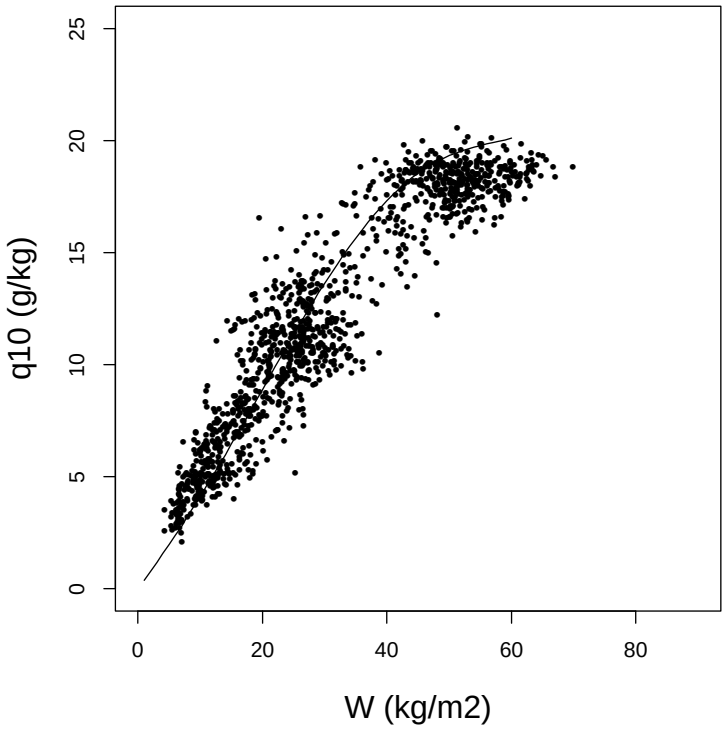

Figure 1.3 q_{10} vs. *W*, the source for the Liu (1986) retrieval, using the data described in Chapter 2.

vs. *W*. Liu and Niiler (1984) and Liu (1986) are very similar papers, the main difference being in scope. Henceforth, I shall refer to these collectively as “Liu’s method”.

Hsu and Blanchard (1989) applied the Liu (1986) relation to individual soundings, and found the error in the inferred *Q* to be about 1 g/kg. However, they averaged the error in each of their 13 experiments first, and then averaged the average errors by summing them and dividing by 13. The proper way to calculate the error would have been to sum the error from *all* the soundings, regardless of which experiment they were from, and then divide by the total number of soundings, or to weight each experiment’s error by the number of soundings in that experiment.

Esbensen et al. (1993) used 1 year of actual SSM/I data and took a critical look at the errors involved in each of the steps necessary to calculate latent heat flux using the Liu (1986) method. They found that the largest error is not from the satellite retrieval, but from applying the *W:Q* relation. Systematic discrepancies of over 2 g/kg were found in the tropics, as well as in the middle and high latitudes. The spatial pattern of the *W:Q* relation discrepancies could be readily interpreted in terms of dynamical and physical processes that maintain the vertical profile of water vapor in the atmosphere as a whole. In regions of persistent strong subsidence, most of the water vapor is trapped near the surface and the Liu (1986) method works reasonably well. But in regions of active convection, significant amounts of water vapor can exist aloft where it is acted upon by processes that are uncorrelated with the surface fluxes. The Liu (1986) method works less well in the tropics and in the storm tracks.

Miller and Katsaros (1992) and Clayson and Curry (1996) both derived regressions of the air-sea humidity difference against a quadratic function of *W* and SST (and U_{10} for the latter). The motivation was to reduce the excessive (> 2 g/kg) error found in applying Liu’s method to individual values instead of monthly mean values. However, both of these studies used only a limited geographic region to derive their retrievals (the Northwest Atlantic and the Equatorial Western Pacific, respectively) and are not globally applicable.

Schulz et al (1993) introduced two new variations on the now-familiar themes: (1) a new SSM/I retrieval for the bottom-layer integrated water vapor (W_B, defined below) and (2) a linear W_B:*Q* relation. Like Liu (1986), the general idea of Schulz et al. (1993) was to use a historical record of radiosonde reports to derive a statistical relationship between the specific humidity at the lowest sounding level and some measure of the integrated water vapor. Liu (1986) used *W*, while Schulz et al. (1993) used W_B, with the definition

$$W_B \equiv \int_0^{500m} q(z)\rho(z)dz \tag{1.3}$$

Schulz et al. (1993) used 542 globally distributed soundings, and took care to use only soundings from Meteorological field experiments rather than a mix of island stations and weather ships. The majority of his soundings, 345, came from the R/V Polarstern, a source I also use.

Using an advanced radiative transfer scheme, Schulz et al. (1993) found that the SSM/I measurements are sufficiently sensitive to W_B in the 19v, 22v, 37v and 19h channels (v - vertical polarization, h - horizontal polarization) to allow a retrieval with an accuracy of 0.6 kg/m^2. Since typical values of W_B range from 1-10 kg/m^2, this represents an error of about 10%, nearly the same as the error in the retrieval of *W*. The 19h channel is not used in Wentz's (1989) retrieval of *W*.

The arbitrary upper limit of the integration (500 m) was motivated in part by observational evidence that there often exists a well-mixed layer extending to about 500 m over the ocean surface. It's a compromise between a layer thin enough such that the water vapor content will be closely tied to the surface fluxes, yet thick enough to contain enough radiating matter for the SSM/I sensor to "see" it.

Schulz et al. (1993) then derived a linear W_B:Q relation from the same set of soundings. Figure 1.4 is a scatter plot of the two parameters (data described in Chapter 2) along with their W_B:Q linear relation. Q was again defined as the lowest sounding level, not necessarily 10 m. In fact, the R/V Polarstern's soundings report the independent sensor on the mast of the ship at 27 m for the lowest sounding level, which introduces some systematic bias. I've calculated this bias to be about 5%. Despite the good correlation shown in Figure 1.4, the overall r.m.s. error using this method exceeds 30 W/m^2, and the method is prone to biases.

Schlüssel et al. (1995) used a larger collection of soundings than Schulz et al. (1993) (Schlüssel was a co-author of Schulz et al. (1993)) and collapsed the two statistical steps in Schulz et al. (1993), the satellite retrieval and the W_B:Q relation, into one step. He derived a direct statistical retrieval of Q from the SSM/I brightness temperatures (T_b) using the 19v, 22v, 37v, 19h and 37h channels (note that Schulz et al. (1993) did not use 37h). Still, the overall error was comparable to Schulz et al. (1993).

Chou et al. (1995) developed an empirical orthogonal function (EOF) method that used both *W* and W_B to retrieve *Q*, derived from a collection of 23,117 FGGE IIb soundings. It uses 6 categories of EOF's, based on the value of *W*, in the hopes that the result will be more geographically portable than the more common regionally-based EOF methods. It also uses a full surface-layer model to calculate

LHF, rather than the more approximate bulk aerodynamic formula. Chou et al. (1997) fixed a few of the problems of Chou et al. (1995), but despite the advanced statistical EOF method the overall r.m.s. errors are nearly the same as Schulz et al. (1993).

The development of SSM/I-based methods for the retrieval of LHF, from Liu's monthly-mean method to Chou's EOF statistical method, represents great advances in satellite retrievals of latent heat flux. But even the best method (Chou et al. (1995, 1997), with its advanced statistical method and full surface-layer model) still has r.m.s. errors of about 30 W/m^2, 3 times larger than the target limit set forth by the COARE working group. There is room for improvement, that this thesis attempts to provide.

1.6) PBL-LIB

PBL-LIB is a collection of 18 FORTRAN programs in support of the main program, an implementation of R. A. Brown's large-scale marine planetary boundary layer model (Brown and Liu, 1982). The model is a two-layer similarity model that combines an "outer" Ekman solution and an "inner" log-layer solution of the primitive equations, and includes a parameterization for Organized Large Eddies (OLE). The "inner" solution is essentially the "LKB" model (Liu et al. 1979) described in section 4.3, page 59.

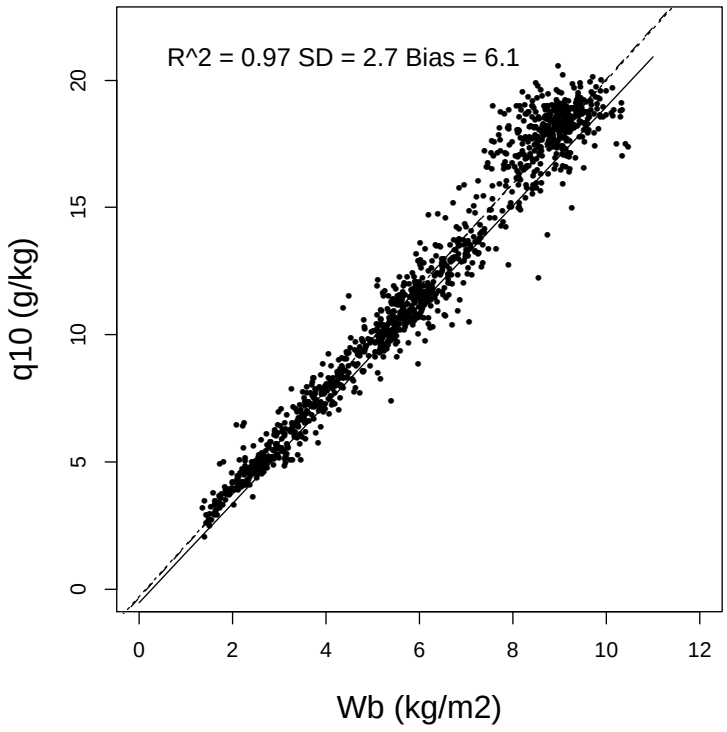

Figure 1.4 q_{10} vs. W_B, the source for the Schulz et al. (1993) correlation, using the data described in Chapter 2.

Brown (1970) solved a 6th-order reduced set of perturbation equations for the boundary layer and found solutions corresponding to the classic Ekman spiral (Ekman, 1905) plus a superimposed secondary flow in the form of counter-rotating helical roll vortices. The secondary flow is believed to be due to the “inflection point instability” (Brown, 1972). The effect of the secondary flow on the Ekman solution was then parameterized in terms of a stratification parameter. By choosing the appropriate length scales for the “outer” and “inner” solutions, and requiring that the solutions asymptote to the same solution at an intermediate patch height, a similarity model with a single similarity parameter was derived (Brown, 1981, 1982a). This similarity parameter is the ratio of the patch height (the depth of the surface layer) to the Ekman depth, and was found to be nearly constant with a value near 0.15. Variations by 20% about this value produced only small differences in the model behavior (Brown, 1982a). The classic similarity functions *A* and *B* can be predicted using this model, as can the values of the transfer coefficients in the bulk aerodynamic flux equations.

Operationally, the OLE parameterization affects the model output through the parameterization of the drag law. This model is essentially a function relating the geostrophic wind at the surface to u_*, the friction velocity. The function includes the effects of the OLE, near-surface stratification, thermal wind in the boundary layer, and variable surface roughness due to variations in wind speed. Inputs include fields of gridded sea level pressure (to find the geostrophic wind), sea surface temperature and near-surface air temperature and humidity (to find the stratification and the thermal wind). The thermal wind across the PBL can also be calculated by the model from the thickness of the surface-to-850 mb or surface-to-925 mb layer. Outputs include the near-surface wind including turning angle, the fluxes of momentum and sensible and latent heats, the geostrophic and thermal winds, and the divergence and vorticity of the surface wind.

This model has been inverted and applied to retrieving sea level pressure gradients from scatterometer data (Brown and Levy, 1986; Brown and Zeng 1998) and applied to southern hemisphere storm analysis (Levy and Brown, 1986, Brown and Zeng, 1998). Foster and Brown (1994, 1994a) have studied the differences between the model’s parameterization of the surface layer and that of the Goddard Labs global circulation model. Dickinson and Brown (1996) used this model along with scatterometer and SSM/I retrievals to study marine cyclones. Flamant et. al (1998) have applied this model to cold air outbreaks over the Mediterranean and found a contribution from the shear in the “mixed layer” to the entrainment process.

Figure 1.5 shows the near-surface wind speed and the surface sensible heat flux predicted by the model as a function of air-sea temperature difference at various geostrophic wind speeds. Figure 1.6

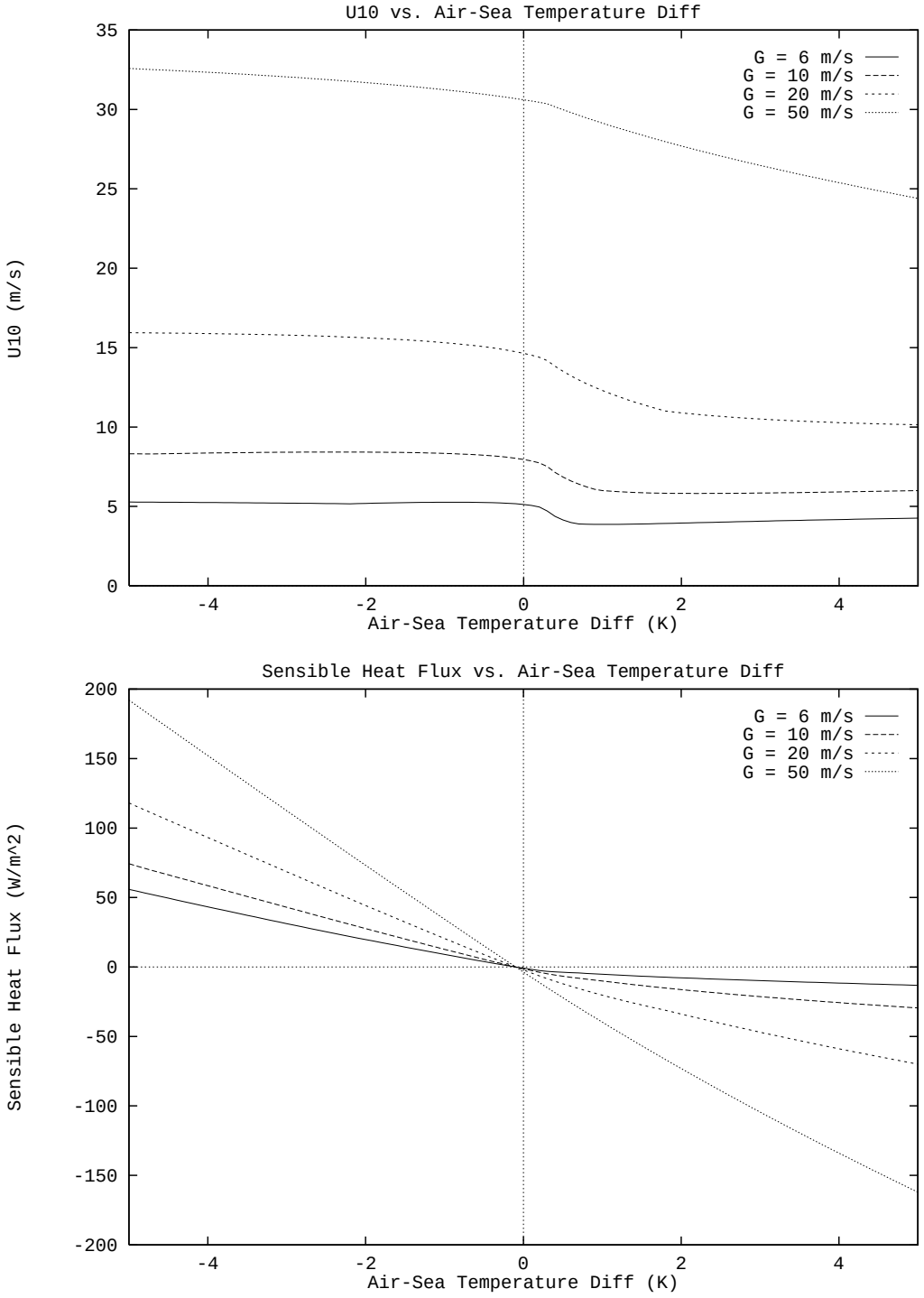

Figure 1.5 The (A) wind speed at 10m, and (B) sensible heat flux predicted by PBL-LIB as a function of the air-sea temperature difference, at various geostrophic wind speeds.

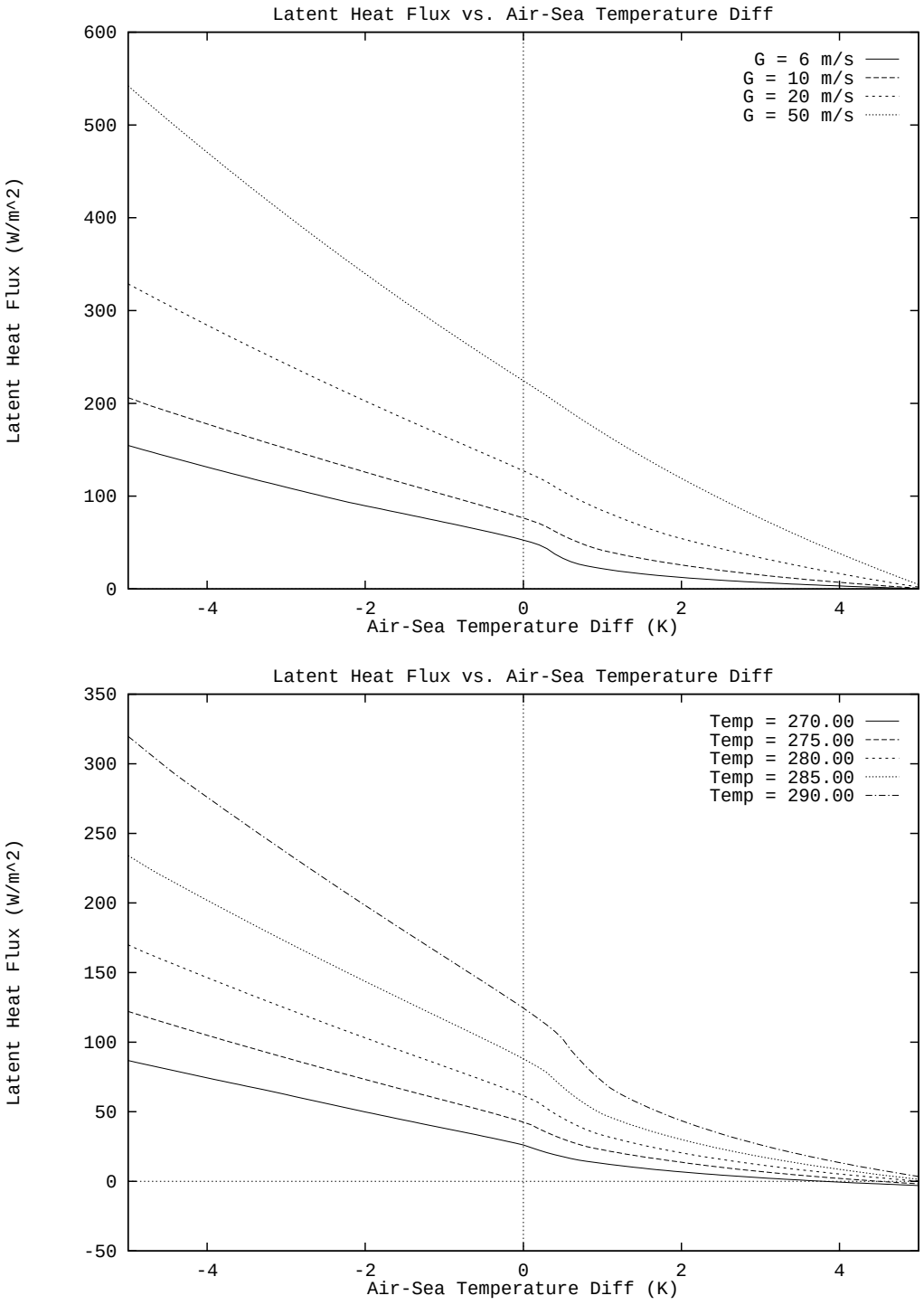

Figure 1.6 Latent heat flux predicted by PBL-LIB as a function of air-sea temperature difference and (A) geostrophic wind speed, and (B) near-surface air temperature.

shows PBL-LIB's calculation of latent heat flux, as a function of air-sea temperature difference, and at various geostrophic wind speeds and near-surface air temperatures.

As discussed in section 4.3, page 59, there are several empirical constants that must be experimentally determined, most notably the constants in the diabatic corrections to the log layer profiles (the Ψ's). Högström (1988) has attempted to retroactively correct the original constants of several researchers for flow distortions around their various sensor instruments by carefully measuring the distortions in a wind tunnel and developing correction factors. Figure 1.7 shows the effect of choosing the constants following Businger et al. (1971), Dyer (1974), Kondo (1975) and Dyer and Bradley (1982), along with the corresponding corrected constants from Högström (1988).

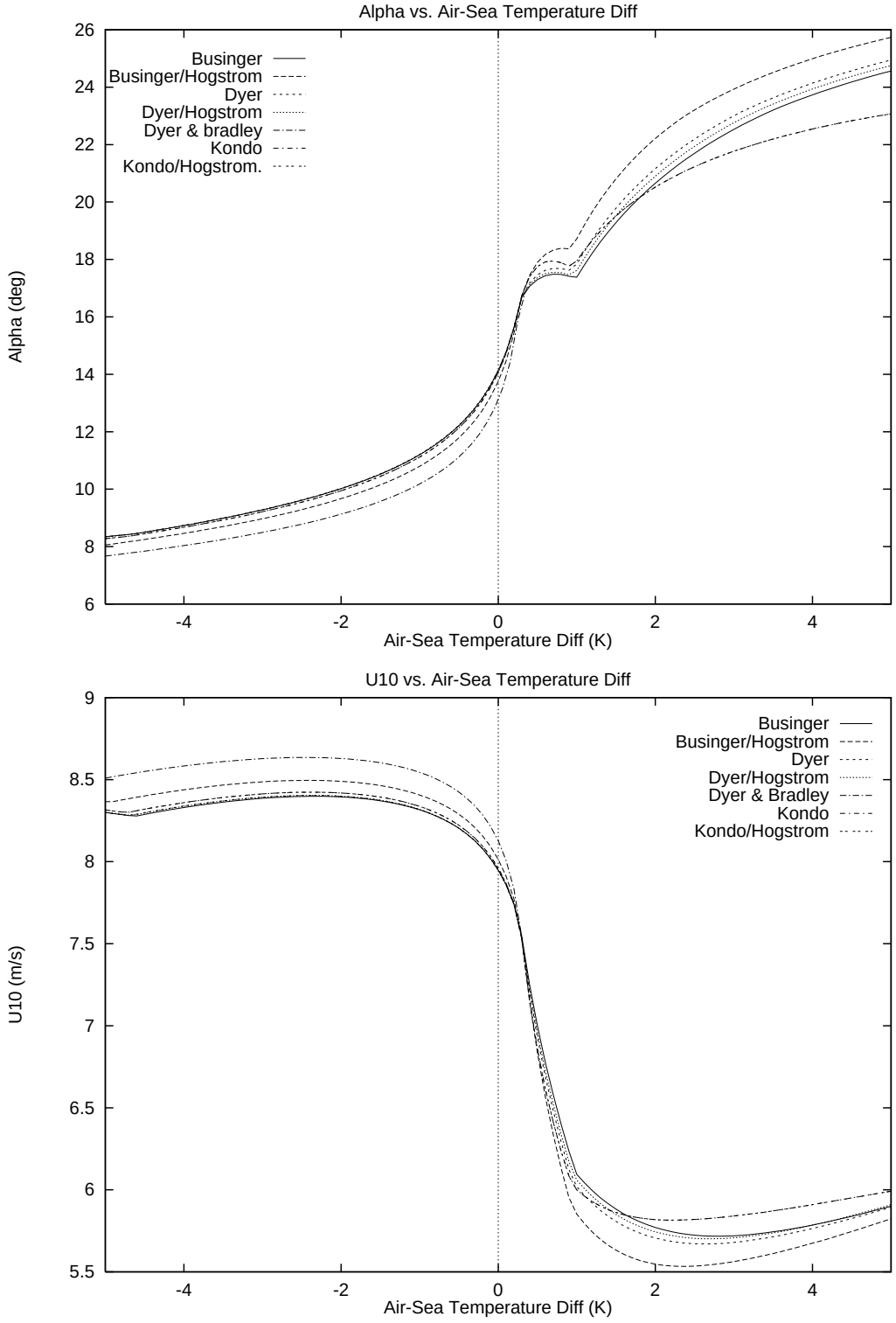

Figure 1.7 The effect of different choices of the constants in the parameterization of Ψ, on (A) turning angle and (B) wind speed at 10 m.

Chapter 2

The Data

The work to be presented in this thesis requires data from a variety of sources:

1. ECMWF analyses and Reynolds Optimum Interpolation (OI) sea surface temperature product.
2. SSM/I retrievals of the total integrated water vapor and wind speed.
3. A collection of high-resolution soundings launched from ships.
4. Each ship's sensor logs of wind speed; air temperature and humidity; and sea surface temperature.

2.1) ECMWF data and Reynolds Optimally Interpolated SST data

Our group regularly uses analyses from the European Centre for Medium-Range Weather Forecasting (ECMWF). This data is available from UCAR (ds111.1, "ECMWF TOGA Global Sfc Anals"). I will be using the data from 1992-1997 to calculate latent heat flux from PBL-LIB. No special pre-processing of the data was necessary.

Reynolds and Smith (1994) presented an optimum interpolation (OI) method to produce a global 1° by 1° gridded weekly sea surface temperature product. Their method ingests retrievals of SST from the advanced very high resolution radiometer (AVHRR) along with buoy and ship reports, and averages/interpolates to fill in missing data on the output grid. This data is produced operationally, and the products are freely distributed to the scientific community. I have downloaded the weekly OI SST data for 1992-1997 from UCAR (ds277.0, "Reynolds' CAC Global Sea Sfc Temp Anals") and applied a 1/4-1/2-1/4 binomial filter in time (following the authors' strong suggestion) to remove noise.

Figure 2.1(A) shows the OI SST vs. the ship-sensor SST, each interpolated to the launch times of the soundings. There is generally good agreement, but there are some outliers. Further investigation shows that most of these are from the Polarstern, when its SST record was changing by several degrees over a few hour's time, indicating possible problems in the Polarstern's SST data. Figure 2.1 (B) shows the OI SST interpolated to the sounding launch time vs. a centered 6-hour average of the ship-sensor SST record. The standard error is somewhat reduced, but the outliers persist, since the typical time scale of the suspect SSTs reported by the Polarstern is about 3 hours. Nonetheless, the overall good agreement between the IO SST and the SST reported by the ships indicates that they are equally useful for calculating LHF over the world's oceans. Note however the cut-off of the OI SST at a maximum tem-

perature. The comparison SSTs here are from the R/V Moana Wave, with a few points from the Hakuho Mara (see Section 2.3.4 below). The ship SST shows diurnal variation that the (weekly) OI SST does not. For comparison, Figure 2.1 (C) and (D) shows the ECMWF SST vs. the ship SST vs. the OI SST, respectively. The ECMWF data agrees nearly as well with the ship data as the OI data, with the exception of a few points from the Polarstern.

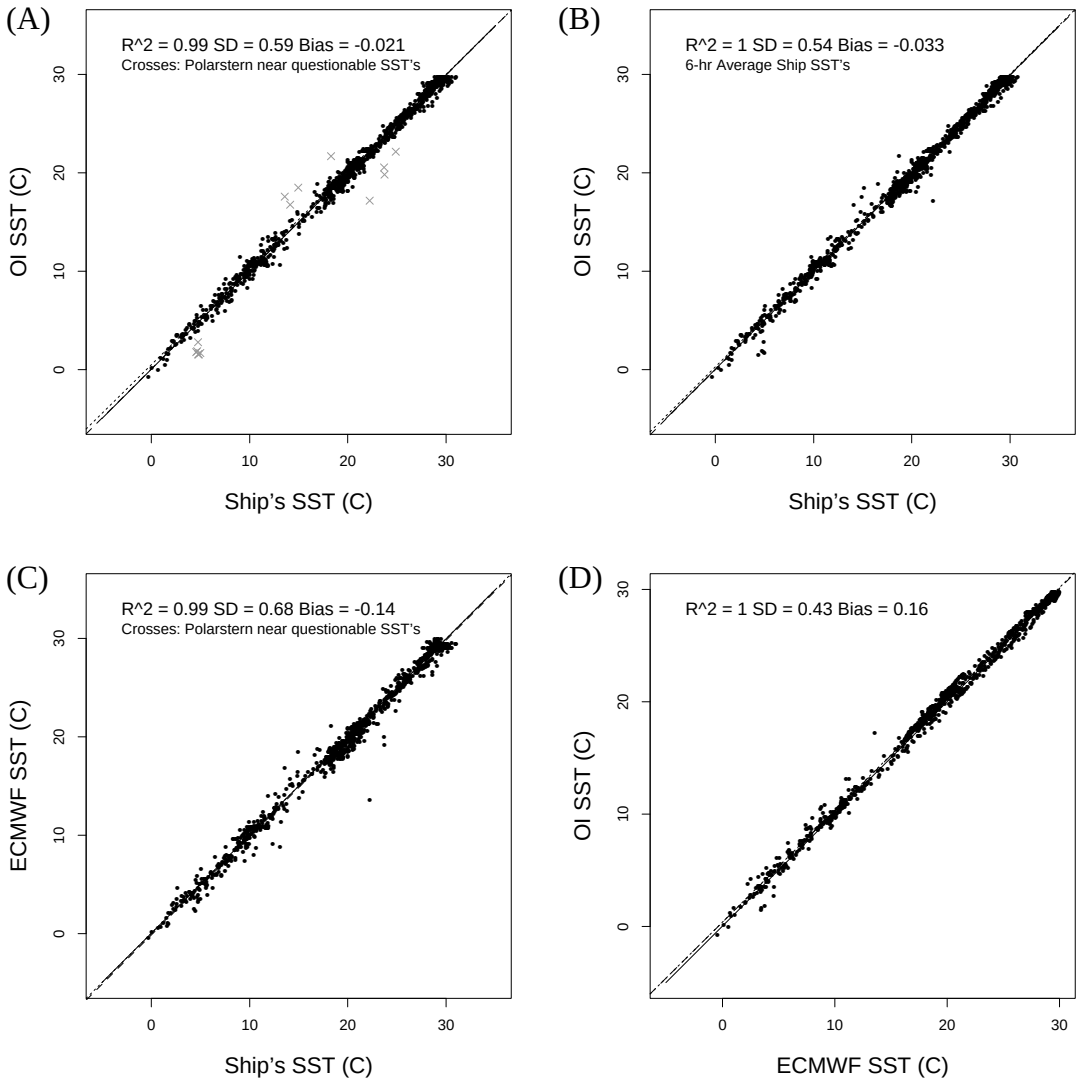

Figure 2.1 (A) Reynold's OI SST interpolated to the sounding launch times, vs. ship SST interpolated to launch times, (B) vs. 6-hour centered average of ship SST, (C) vs. ECMWF SST interpolated to launch times, and (D) ECMWF SST vs. ship SST, both interpolated to launch times.

The OI SST vs. ship-sensor SST r.m.s. scatter at the times of the SSM/I overpasses (not the same as the times of the SSM/I overpasses when a sounding was launched) is about 0.76 K. Some of this is likely due to the oceanic warm layer, mitigated by the cool skin effect. Since the SSM/I passes a particular point on the earth once at about sunrise and once at about sunset, the effect of the warm layer is smaller than if it were sampled at local noon. I assume that 0.3 K of this is due to variability in the bulk-to-skin SST difference (Schlüssel et al. 1990), leaving 0.46 K unexplained. Reynolds and Smith (1994) estimate the global average error in the OI SST analyses procedure to be 0.13 K. I take the characteristic OI SST error to be 0.5 K.

2.2) SSM/I data

Remote Sensing Systems, Inc. has made the geophysical retrievals of Wentz (1997) freely available on the internet at “ftp.ssmi.com”. The data offered spans the entire time period an SSM/I sensor has been in space, from June 1987 to the present (with a lag time of about two months). The various sensors have been cross-calibrated prior to the calculation of the geophysical parameters. I emphasize that the brightness temperature measurements are not available from Remote Sensing Systems, Inc., only the geophysical parameters retrieved via Wentz (1997). I have acquired the data from the F10, F11, F13 and F14 satellites for the time period 1992-1997. Table 2.1 shows the time coverage of each satellite. No further pre-processing was necessary.

Table 2.1 DMSP Satellite Time Coverages

Satellite	Time Coverage
F10	Jan 1991 to Nov 1997
F11	Jan 1992 to Present
F13	May 1995 to Present
F14	May 1997 to Present

2.3) Soundings and ship sensor data

Radiosondes are operationally launched from many ships and land stations around the world each day, but are usually stored only in a reduced (significant levels only) format that does not sufficiently characterize the marine mixed layer. I have therefore sought sounding data that has been archived at higher resolutions. I also decided to only seek soundings from ships and not from island stations as is commonly done by others investigating SSM/I retrievals of LHF. I feel that even relatively small islands can generate enough forced convection due to solar heating to sufficiently change the character of the

marine mixed layer, especially in the sub-tropics and tropics where most of these stations are located. In the tropics, the leading two terms that offset the incoming solar radiation are the latent heat flux and the longwave cooling. A dry land surface can not cool itself by evaporation, causing the surface temperature to rise, leading to increased convection. Often island stations are at a few hundred meters altitude, where we would not expect the marine mixed layer to exist unchanged from its basic state. I also sought ships that had high-quality coincident observations of the parameters necessary to calculate LHF from the bulk method (see section 4.3, page 59).

The Environmental Technical Laboratory (ETL) air-sea interaction group at NOAA/ETL in Boulder, CO has assembled a suite of instruments to measure direct turbulent fluxes and bulk meteorological variables from ocean-going platforms (Fairall et al. 1997). This flux/meteorological system has been deployed during several experiments since its inception in 1987. I have acquired the covariance and inertial dissipation estimates of the fluxes, along with the bulk meteorological data, from two ships, the R/V Malcolm Baldrige during ASTEX and the R/V Moana Wave during TOGA COARE. Additionally, I have acquired eddy flux data from the R/V Hakuho Maru during TOGA COARE, although this data was taken with a different system than the NOAA/ETL group's system.

2.3.1) ASTEX

I have obtained the soundings and ships sensor logs from all four of the ships that took part in the Atlantic Stratocumulus Transition Experiment (ASTEX, Albrecht et. al. 1995). The four ships were the R/V Malcolm Baldrige, the R/V Le Suroit, the R/V Valdivia, and the R/V Oceanus. Unfortunately, the Oceanus did not have a humidity sensor on board, so it's impossible to calculate the LHF from the time series. The sensor logs from the Valdivia were not posted to the Archive Center, but were available directly from Steven Klein, a student who was on board. These soundings and the rest of the ship sensor logs were obtained from the NASA Langley Research Center EOSDIS Distributed Active Archive Center (DAAC). Additionally, I obtained the eddy flux data for the Malcolm Baldrige directly from Dr. Chris Fairall, NOAA/ERL (cfairall@etl.noaa.gov).

Each of the four ships launched soundings during the experiment. These soundings have been quality controlled and interpolated to 20 m resolution prior to being posted on the DAAC (see http://eosweb.larc.nasa.gov/HPDOCS/access_data.html). Eddy flux observations when the wind was not within 90° of the bow were flagged as bad, in addition to other quality control procedures outlined by Dr. Fairall.

2.3.2) ACE-1°

During ACE-1, the Southern Hemisphere Marine Aerosol Characterization Experiment, the R/V Discoverer cruised from its home port of Seattle to the South Pacific, where it joined the R/V Southern Surveyor for the experiment. Along the way, the Discoverer launched radiosondes twice daily, resulting in a nice coverage of the Pacific ocean. Once on station south of Australia, the frequency of launches went up to 4 times per day. The soundings and ship sensor logs were obtained from the UCAR/NOAA Joint Office for Science Support (JOSS) data management system CODIAC (http://www.joss.ucar.edu/codiac/) except the Southern Surveyor sensor logs, which are not available.

2.3.3) RITS 93

The Radiatively Important Trace Species (RITS) 1993 and 1994 cruises were conducted eight months apart in order to assess regional and seasonal variations in trace gases and aerosols along the long latitudinal transect. Measurements were made aboard the NOAA ship R/V Surveyor, which departed Punta Arenas, Chile on 20 March 1993, crossed the Drake Passage to Palmer Station on the Antarctic Peninsula, continued southwest to approximately 67˚S, 140˚W, and then headed north to 57˚N, 140˚W, arriving in Seattle on 7 May 1993. The RITS 1994 cruise reversed this track, departing Seattle on 20 November 1993 and arriving in Punta Arenas, Chile on 7 January 1994. During the cruises, soundings were launched twice a day, at 0 and 12 Z. The data for RITS 93 was generously made available to me by Dr. Jim Johnson at NOAA/PMEL (johnson@pmel.noaa.gov)

2.3.4) TOGA-COARE

During the Tropical Ocean - Global Atmosphere Coupled Ocean-Atmosphere Response Experiment (TOGA-COARE, Webster and Lukas, 1992) field experiment, the R/V Hakuho Maru and the R/V Moana Wave were stationed near the equator, near 156˚E. During November 1992, the Hakuho Maru launched radiosonde 4 times daily, and took high-frequency and bulk measurement. For three separate month-long periods during November 1992 to February 1992, the Moana Wave launched radiosondes 4 times daily, and also took high-frequency and bulk measurements with the NOAA/ETL flux/meteorological system. These soundings were obtained from the UCAR/NOAA Joint Office for Science Support CODIAC system (http://www.joss.ucar.edu/codiac/). Both the Hakuho Maru and the Moana Wave's surface observations include covariance and inertial dissipation flux estimates. Observations when the wind was not coming from within 90° of the bow have been flagged as bad, in addition to other quality control procedures outlined by Fairall in the release of the data. These surface observations were obtained directly from Dr. Chris Fairall, NOAA/ERL (cfairall@etl.noaa.gov).

2.3.5) TEPPS

The Pan American Climate Studies (PACS) Program's Tropical Eastern Pacific Process Study (TEPPS, Yuter, 1998) took place in the eastern tropical and sub-tropical pacific during August to September 1997. The R/V Ron H. Brown was on station in the ITCZ near 8°N, 125°W for about 15 days, returned to San Diego, then took an 8-day cruise of the stratocumulus region commonly found off the coast of Baja California. 42 of the soundings launched during the cruise were Omega Sondes which were donated to the project after having sat on the shelf for several years. Initial analysis (see http://www.atmos.washington.edu/gcg/mg/tepps/data/sounding_data.html) showed that these sondes produced anomalous humidity readings, and are therefore not included. The surface observations were taken at the top of a 10m mast in the bow of the ship by a WHOI IMET system. I flagged observations taken when the wind was coming from +/-20 degrees of aft as bad. The soundings and ship sensor data were generously supplied to my by Dr. Sandra Yuter (yuter@atmos.washington.edu)

2.3.6) The R/V Polarstern

The R/V Polarstern is based at the Alfred Wegener Institute (AWI) for Polar and Marine Research in Bremerhaven, Germany (König-Langlo and Marx, 1997). It regularly cruises to both the Arctic and Antarctic on research and resupply missions, routinely launching radiosondes. 937 Polarstern soundings were acquired for this study, selected for their broad latitudinal coverage. Before 1994, AWI archived only the 3-hourly synoptic surface observations. After 1994 they archived the full 10-minute data. Thus 593 of the soundings have high-resolution coincident surface observations available, while 344 have only low-resolution surface observations. Initial work showed that especially when the ship was underway, conditions changed sufficiently during the 3 hours between synoptic observation times that the pre-1994 data performed significantly worse than the post-1994 data in my model. Thus only post-1994 data are used in this thesis. Ships sensors are on both the port and starboard side of the ship, at 27 m (T and q) and 37 m (U) above sea level. Data from the non-windward side has been rejected. These soundings and ship sensor logs were generously supplied to me by Dr. König-Langlo. See http://WWW.AWI-Bremerhaven.DE/MET/Polarstern/ for more information and contact points.

2.4) Sounding Processing procedure

All soundings have been visually screened, and obviously bad soundings rejected. Any sounding that had missing values in the lowest km were also rejected, since the mixed layer was not sampled well. Additionally, all soundings within 150 km of land, or with sea surface temperatures below 1.5 C were

rejected. This is to avoid advection effects when continental or polar air masses are not sufficiently in quasi-equilibrium with the ocean, and contamination of the SSM/I retrievals by land or ice.

Some of the ships used in this study had rain gauges aboard and reported rain rates or average rain amounts. Since the SSM/I retrieval of wind speed is especially sensitive to interference from raindrops, I would like to reject those soundings where rain was present. Rainy conditions often do not show the self-similar mixed-layer structure so prevalent in non-rainy conditions. I wish to only consider soundings representative of the cases where I will have valid input data, and not develop any correlations or assess my model against data where it is not applicable. I attempted to find a relationship between rain rate and some parameter derived from the sounding (e.g. average humidity in the 3 - 5 km layer, or the depth of the lowest cloud layer) but failed. I do not trust many of the ship-sensor reports of rain rates in my data set. For example, there are cases from the R/V Discoverer where the sounding showed no saturated levels yet the rain gauge reported 16 mm/hr of rain. The reported wind speed at the time was in excess of 30 knots, leading me to suspect sea spray was entering the rain gauge.

I also attempted to use an empirical method to identify rainy conditions. Any saturated layer in a sounding with a base was below 3 km and at least 2 km thick was assumed to indicate rain (Art Ragno, personal communication). Only about a dozen of my more than 1600 soundings fulfilled that requirement, and they were equally likely to be outliers as to show good agreement in the final retrievals. Thus the problem of rainy conditions introducing spurious noise was ignored.

For each sounding, the corresponding surface observations were linearly interpolated to the launch time, and the OI SST and ECMWF data were geographically and temporally interpolated to the launch time and place. The time difference between the launch of the sonde and the closest valid surface observation was 60 minutes or less (except for the SST and SLP which were allowed a 120-minute difference) or the surface observations were flagged as bad. Additionally, the surface observations could be averaged rather than sampled, for a range of averaging times. This may prove useful in that the mixed layer is thought to respond to forcing from below on time scales the order of a large eddy turn-over time, 20 to 60 minutes. Also, the SSM/I's pixel size is 25 km, which corresponds to about an hour average (assuming a wind speed of 8 m/s). Averaging may also remove spikes in the surface observations due to contamination from the ship itself, despite our best efforts to remove those effects.

Each surviving sounding was analyzed to identify the important levels: the bottom and top of the mixed layer, the bottom of any decoupled upper layer, the bottom and top of the inversion layer, etc. An objective method was used first, but each sounding was then visually inspected to assure proper identifi-

cation. Detailed definitions of each of these levels for the purposes of this thesis follow. In only 1.6% of the soundings could no mixed layer be identified.

The bottom of the mixed layer (often subscripted “mb”) is defined as the level where any questionable kinks and wobbles in the temperature or humidity due to contamination due to launch have ceased, or when the decrease of q and θ near the surface has ceased. See section 2.5, page 27, for more on the errors near the bottom of the soundings.

The top of the mixed layer is defined separately for the humidity (q), the potential temperature (θ) and the equivalent potential temperature (θ_e). In each case, it is defined as the level where the variable deviates significantly from a constant value.

The next layer above the mixed layer may be the inversion layer in the case of a single well-mixed layer, or a transition layer between the mixed layer and another more-or-less well-mixed layer below the inversion layer in the case of a deeper “decoupled” boundary layer. The top of this transition layer, synonymous with the bottom of the decoupled layer, is the layer where q, θ, or θ_e ceases to change rapidly and approaches a more constant value. Especially for θ, the decoupled layer may not be as well-mixed as the layer below, but there is often a shallow layer above the ML that is characterized by an increased temperature gradient relative to the layers above and below. This “mini inversion” can be seen very clearly in the trace of dT/dz as a layer where the lapse rate is less than the saturated adiabatic lapse rate, given by

$$\Gamma_s = \frac{-\frac{g}{C_p}\left(1 + 0.622\frac{Lp}{R_d T}\frac{e_s}{(p-e_s)^2}\right)}{1 + 0.622\frac{Lp}{C_p T}\left(\frac{L}{R_v T}\right)\frac{e}{(p-e_s)^2}} \tag{2.1}$$

all the symbols have their usual meanings. This equation is different from equation (2.70) in Wallace and Hobbs (1977) which neglects the second term in the expansion of dw_s/dz in the development of the equation:

$$\frac{dw_s}{dz} = \frac{dw_s}{dT}\frac{dT}{dz} + \frac{dw_s}{dp}\frac{dp}{dz} \tag{2.2}$$

The inversion layer is characterized by a lapse rate that is less then the saturated adiabatic lapse rate. In the sub-tropics it is usually quite strong and distinct, but in the tropics it can be hard to identify. Occasionally there are several inversions of approximately equal strength, starting with the one at the

top of the mixed layer. When this occurs, the equivalent potential temperature is used as an aid to identify the thermodynamic boundary layer, or the layer with the strongest inversion is identified as “the inversion”. The inversion base is defined as the level where the lapse rate drops below Γ_s, or the humidity suddenly drops from saturation. Occasionally, superadiabatic layers appear in the sounding just above the top of a saturated layer. This is thought to be due to evaporative cooling of the sensors aboard the sonde. Superadiabatic layers have been removed from the soundings by identifying their top and bottom and linearly interpolating the temperature across the gap. The specific humidity and saturation specific humidity are then re-calculated with this new temperature. The top of the inversion layer is defined as the level where the lapse rate once again reaches the saturated adiabatic lapse rate. Thus the inversion is defined as the layer that is most absolutely stable.

2.5) Sounding Errors

Elliott and Gaffen (1991) estimate the error in contemporary radiosonde measurements to be 0.2° C for temperature and 3.5% for relative humidity, which is close to the accuracy advertised by Vaisala, the manufacturer (05. mb for pressure, 0.2° C for *T* and <3% for RH). This translates into an accuracy for the specific humidity derived from T, RH and pressure of less than 0.5 g/kg. Averaging many individual measurements (e.g. across the mixed layer) will reduce the overall error, compared to an individual measurement (e.g. the lowest sounding level).

2.5.1) Errors in the lowest soundings level

A possible source of error in all of the statistical relations discussed in the introduction (Liu’s $W{:}Q$, Schulz’ $W_B{:}Q$, Schlüssel’s $T_b{:}Q$, and Chou’s EOF’s) is from the error in the lowest sounding level report of humidity. All of these researchers took the lowest values reported by a sonde as representative of the near-surface values, without explicitly specifying a height (thus my use of Q instead of q_{10}). Figure 2.2 shows the temperature and humidity as reported by the lowest sounding level and as reported by the independent sensors on the ships in my dataset. Care was taken to remove ship sensor data that was contaminated by maneuvering, and all data have been reduced to 10m. There is considerable scatter in the data, indicating the sonde sensors were not in equilibrium with the same air mass as the ship sensors. It is common, but not universal, practice to enter ship sensor output from a time close to the launch as the lowest sounding level. For larger ships such as the Polarstern, the temperature and humidity sensors are 27 m above sea level, and the wind sensor is 37 m above sea level. This introduces a bias of about 5%, according to my calculations.

The r.m.s. error in humidity is about the level of scatter in Schulz et al. (1993) Schlüssel et al. (1995) and Chou et al. (1995, 1997). If these soundings were used to develop a relation that used the lowest sounding level, a serious scatter would be introduced. I conclude that one cannot use the lowest sounding level of a historical sonde record to study the surface layer without introducing serious errors, unless independent sensors can be used to verify the quality of the lowest sounding level.

2.5.2) Errors in the lowest ~100 meters

Figure 2.3 shows samples of soundings with questionable data near the surface. The two soundings were launched from the Le Suroit at 10:56 Z on 4 June 1992 at 36.16° N, 335.54° E; and from the Polarstern at 09:56 Z on 1 June 1995 at 23.17° N, 331.17° E. The analyzed heights of the mixed layer, the inversion layer, and the bottom of the mixed layer are indicated with horizontal lines. The small vertical line near the surface in (B) and (D) indicates the virtual potential temperature of the surface. The deficit in humidity in the lowest few hundred meters is fairly common, and is found in soundings launched from all the ships used in this study. These anomalously dry layers are often the result of heating of the sonde sensor relative to the ambient temperature prior to launch (Cole, 1993). The relaxation distance (time) for the TEPPS data has been calculated to be about 50m (8 sec.) (see http://www.atmos.washington.edu/gcg/MG/tepps/DATA/sounding_data.html). These examples further underscore my conclusion that soundings are not a very good tool for studying the atmospheric surface layer. Soundings can be used to study the mixed layer, but independent surface layer measurements must be used to relate the mixed layer variables to the surface fluxes.

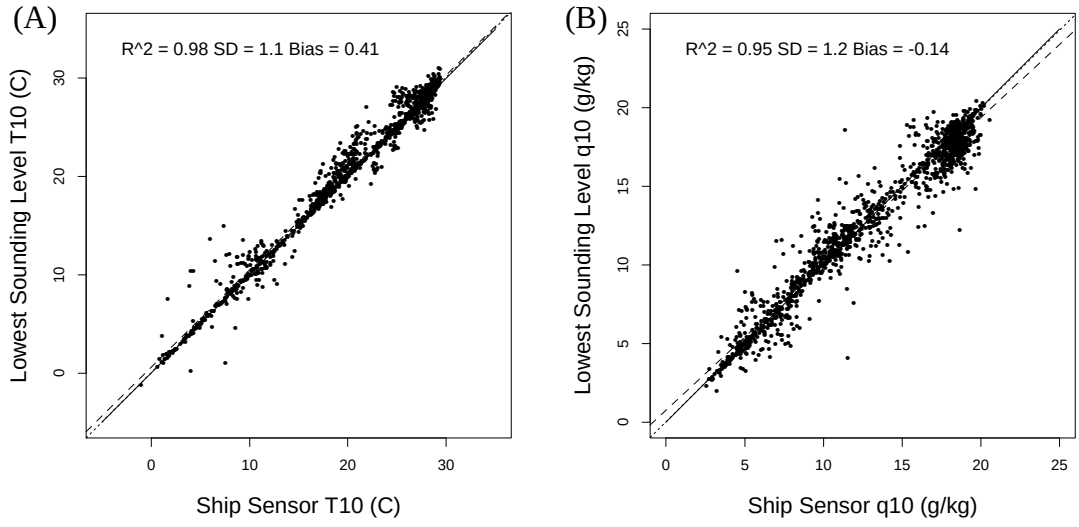

Figure 2.2 The lowest sounding level report vs. the ship sensor report for (a) temperature and (b) specific humidity for all ships.

2.6) SSM/I collocation

At various stages in this work, it will be necessary to collocate SSM/I observations with conventional observations, either soundings or surface observations. In an ideal world, for every observation there would be an SSM/I fly-by within the auto-correlation time of the variable in question, and we could match each observation to a single SSM/I pixel. However, since the DMSP satellites are in sun-synchronous near-polar orbits, and since the width of the SSM/I swath is smaller than the distance it precesses each orbit, these perfect match-ups are uncommon. The sounding-SSM/I collocation problem is further confounded by the fact that the SSM/I flies over a point on the earth's surface once in the

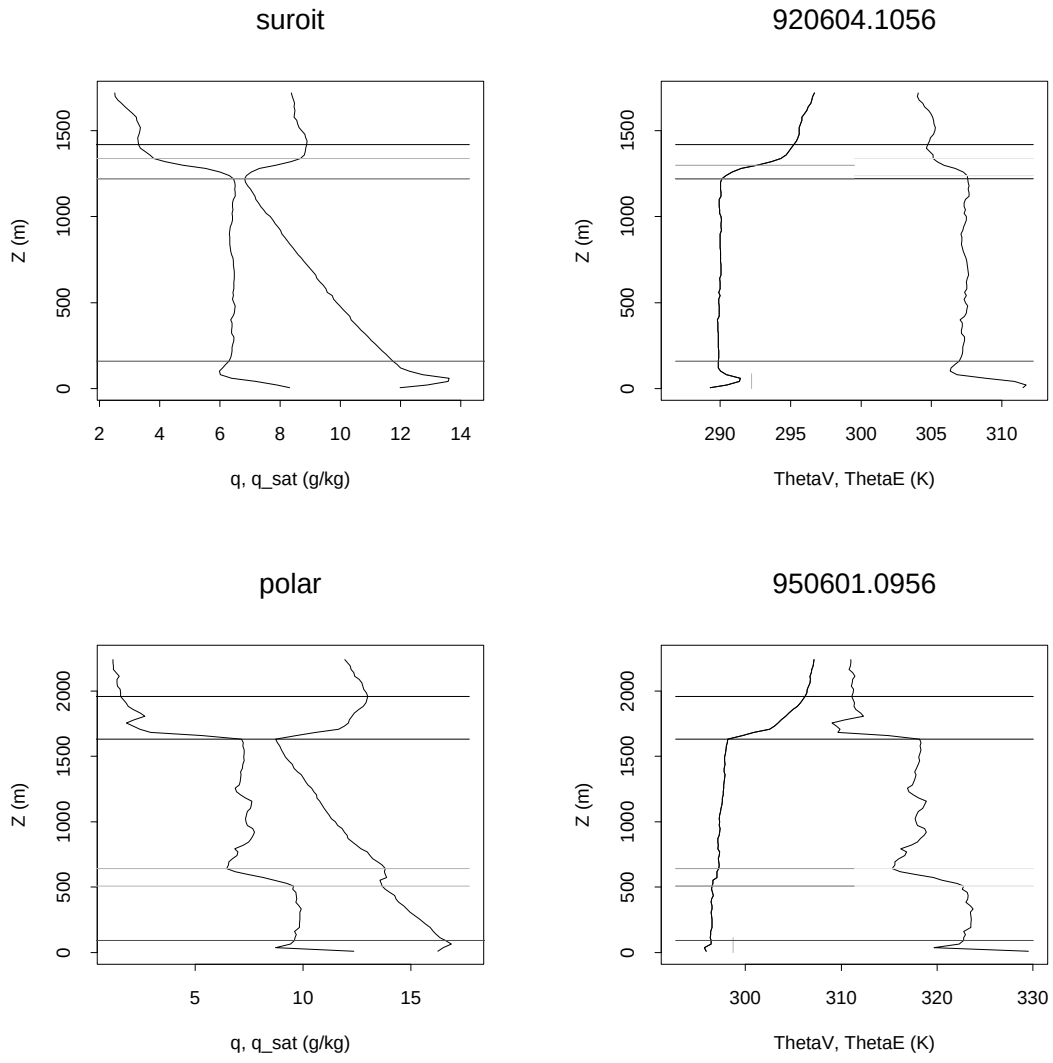

Figure 2.3 Soundings launched from the Le Suroit (A) - (B) and from the Polarstern (C) - (D). See text for explanation

morning and once in the evening unless the point falls within the gap between swaths for that day. For instance, soundings launched at 0Z and 12Z will only have a perfectly matched SSM/I pixel if they were launched at longitudes near 0° and 180°. Similarly, only soundings near 90° and 270° E at 6Z and 18Z would have perfect match-ups. There may also be problems comparing a point measurement such as a surface observation to an area-averaged observation such as an SSM/I pixel. This section attempts to quantify the error involved in collocation of SSM/I and conventional data.

The time and space differences allowed between an SSM/I pixel and a conventional observation in the literature varies. Chou et al. (1995) used 1.5 hours and 100 km, Wentz (1997) used 6 hours and 60 km, Schulz et al. (1993) used 3 hours and 0.5° latitude or longitude. Each of these was an attempt to optimize the trade-off of accuracy versus total number of collocations.

I chose to calculate a single match-up between a sounding/observation and an SSM/I swath, rather than the multiple match-ups between one sounding and the nearest 5 or 6 SSM/I pixels allowed by Wentz (1997). I calculate the value of the SSM/I data using a scheme that weights SSM/I pixels by their distance and time difference from the sounding/observation:

$$W = \frac{\sum_i \left(\frac{D_0}{D_i}\right)^2 \left(\frac{T_0}{T_i}\right)^2 W_i}{\sum_i \left(\frac{D_0}{D_i}\right)^2 \left(\frac{T_0}{T_i}\right)^2} \tag{2.3}$$

where I require all pixels within distance D_0 and time difference T_0 have weight 1 by using

$$D_i = max(D_i, D_0) \text{ and } T_i = max(T_i, T_0) \tag{2.4}$$

I take D_0 to be the pixel size of the SSM/I, 25 km, and take T_0 to be a typical eddy-turnover timescale for the mixed layer, 30 minutes.

In order to guide my selection of match-up criteria, I have calculated the correlation, standard deviation, and mean bias between the SSM/I retrievals of W and U_{10} the ship measurements for a range of maximum allowed distance and time separations. The results are shown in Figure 2.4.

2.7) Summary

The work described in this thesis requires a large amount of data from several sources. ECMWF analyses of sea surface temperature and near-surface air temperature, humidity and sea level pressure

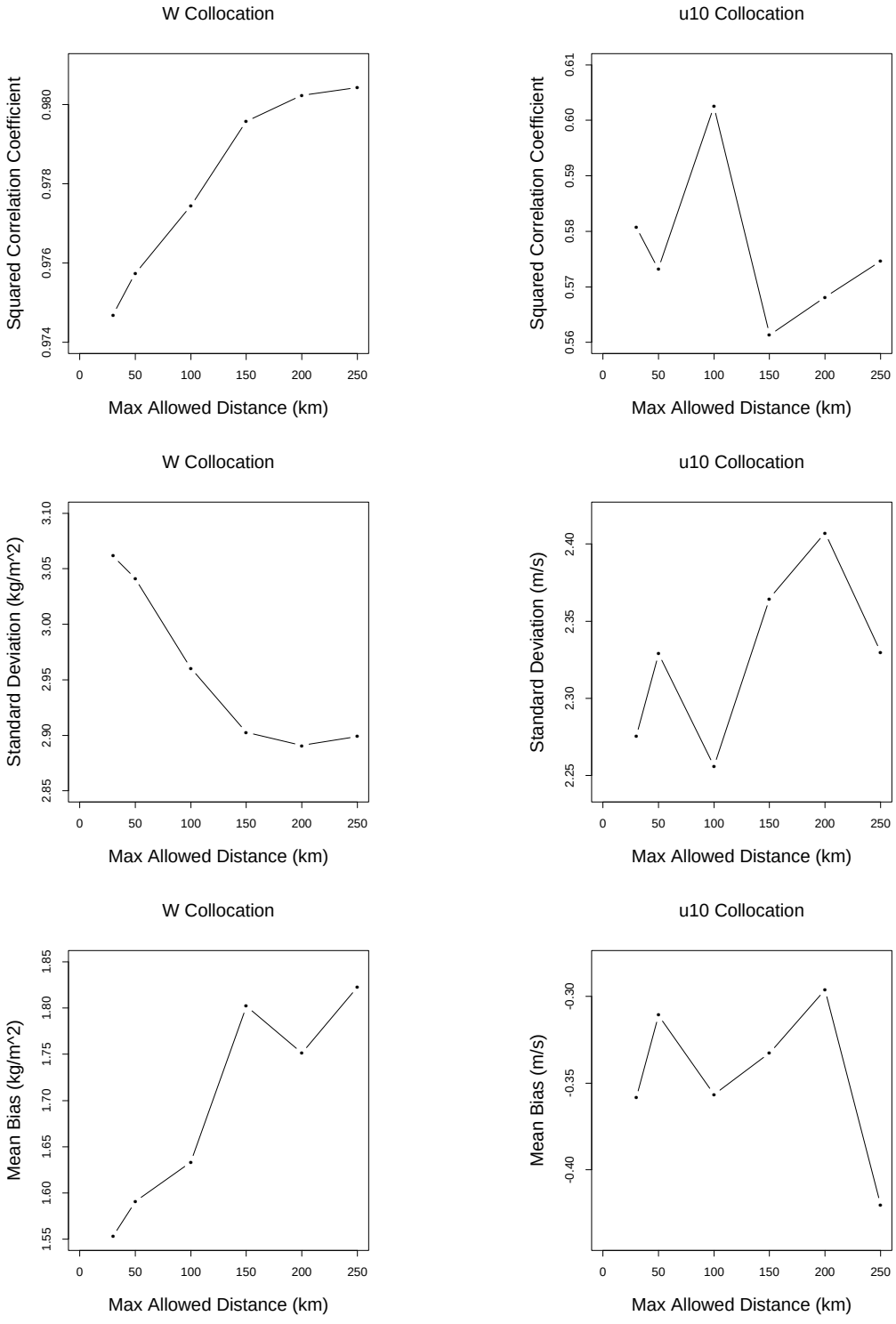

Figure 2.4 Squared correlation coefficient, standard deviation, and bias vs. sonde-SSM/I pixel separation distance for (A-C) *W* and (D-F) U_{10}.

are needed to run PBL-LIB to calculate a climatology of latent heat flux. A large and geographically widespread collection of high-resolution soundings launched from ships is needed, along with each ship's time series of sea surface temperature and near-surface temperature, humidity and wind, to develop and validate the model. Several year's of SSM/I retrievals of total integrated water vapor (W) and wind speed (U_{10}), along with the corresponding time period's optimal interpolation SSTs (OI SST), are needed to calculate an SSM/I latent heat flux climatology.

Table 2.2 shows the total number of soundings from each ship, the number that survived the processing procedure, the approximate height resolution, and the latitude and longitude ranges. The names

Table 2.2 Summary of Soundings

Ship Name	Total Soundings	Surviving Soundings	Height Resolution	Min Lat	Max Lat	Min Lon	Max Lon
Malbal	133	119	20 m	27.31	37.29	332.12	338.08
Suroit	68	69	20 m	34.5	37.7	333.64	336.92
Valdiv	152	149	20 m	27.1	46.01	334.33	348.08
Oceans	74	74	20 m	32.7	41.17	334.11	338.91
Disco	180	161	40 m	-54.51	47.64	134.99	233.95
Survey	46	38	50 m	-53.3	-40.74	139.9	151.9
RITS93	63	53	40m	-67.23	52.22	210.46	296.14
Hakuho	148	148	10 m	-13.78	24.5	142.59	156.1
Moana	261	237	40 m	-1.88	0.22	154.98	156.14
TEPPS	253	195	10 m	7.1	32.2	231.4	277.4
Polar	937	440	40 m	-62.5	77.1	0.5	359.97
TOTAL	**2274**	**1683**	**-**	**-62.5**	**77.1**	**0.5**	**359.97**

have been abbreviated to the codes that will be used throughout this thesis, and are hopefully obvious. Figure 2.5 shows the geographical distribution of the 1631 soundings.

Soundings close to land and the ice edge, and those with obvious errors or with too much missing data in the mixed layer have been culled from the dataset. The soundings have been analyzed to identify the bottom and top of the surface mixed layer, the top and bottom of any decoupled layer, and the top and bottom of the inversion layer. Errors in the soundings have been discussed, and the collocation procedure used in later chapters has been explained.

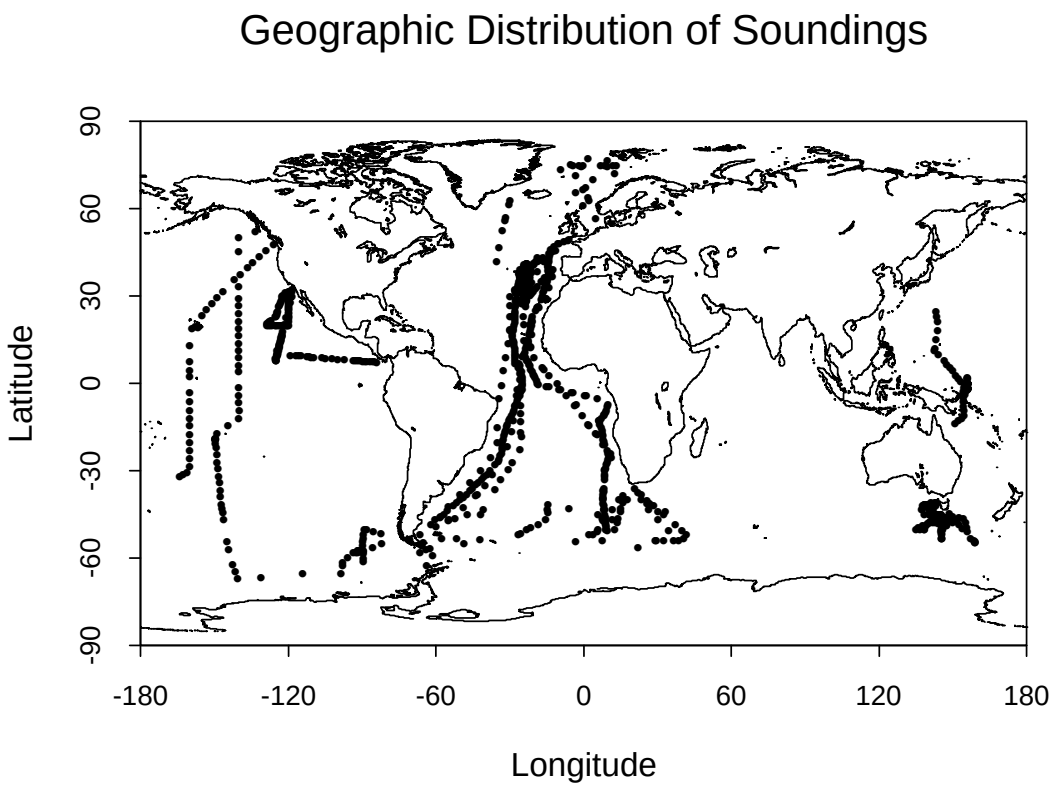

Figure 2.5 The geographical distribution of the soundings used in this study

Chapter 3

Statistical Retrievals from SSM/I Measurements

The needed geophysical parameters that can be retrieved from the SSM/I are U_{10}, the wind speed at 10 m; and *W*, the total integrated water vapor defined as

$$W \equiv \int_0^\infty q(z)\rho(z)dz \tag{3.1}$$

where q is water vapor mixing ratio, ρ is density and z is height. *L*, the total integrated liquid water is defined as

$$L \equiv \int_0^\infty q_l(z)\rho(z)dz \tag{3.2}$$

where q_l is the liquid water mixing ratio.

Other interesting geophysical retrievals exist, including detection of sea ice and the ice edge, precipitation rates, land use types, etc., but we restrict our attention to those parameters relevant to the open non-frozen ocean.

3.1) Wentz (1997)

Wentz (1997) is the latest of a series of retrieval algorithms developed for the SSM/I. He solves a set of four simultaneous equations for the antenna temperatures of the channels 19V, 22V, 37V, and 37H (where V is vertical and H is horizontal polarization) for U_{10}, *W*, *L* and the "line-of-sight" wind $U_{10}\cos(\phi)$, a parameter which is then used to reduce the error in the retrievals of the first three parameters. The accuracies of the retrievals are 0.9 m/s, 1.2 kg/m^2, and 0.025 kg/m^2, respectively. Since the method solves for the set of four variables simultaneously it is not possible to extract the explicit dependence of each parameter on specific input brightness temperature channels.

However, in Technical Report 063097-V (Wentz and Smith, 1997) he gives an algorithm that "has essentially the same performance" as Wentz (1997) that does show the explicit dependence of the *W*-retrieval on the brightness temperatures:

$$W = 359.661 + 0.279816(T_{19V} - 150) + 0.266168(T_{19H} - 150) \quad (3.3)$$
$$+ 82.002\ln(290 - T_{22V}) - 0.439158(T_{37V} - 150) - 0.17517(T_{37H} - 150)$$
$$- 0.0112846(T_{19V} - 150)^2 + 0.00202513(T_{19H} - 150)^2$$
$$+ 1.93046\ln(290 - T_{22V})^2 + 0.0048304(T_{37V} - 150)^2 - 0.00124045(T_{37H} - 150)^2$$

Note that this retrieval uses all five of the lower frequency channels (excludes only the 85 GHz channels), and includes both linear and quadratic terms. Most other retrievals attempt to exclude those channels that do not add significantly to the final retrieval, but this “kitchen sink” method produces the best result, both in terms of lowest r.m.s. and in terms of “cross talk” (changes in one parameter affecting the error of another parameter).

Wentz has made the retrievals of U_{10}, W, L, Ice amount, precipitation rate, and the time each measurement (pixel) occurred available through his company, Remote Sensing Systems of Santa Rosa, CA. The data are available free of charge via the Internet at www.ssmi.com or via anonymous ftp at ftp.ssmi.com. The original brightness temperatures are not available, as it would be a rather large amount of data and would require that the user re-do the inter-satellite cross calibration that Remote Sensing Systems has done prior to calculating their geophysical retrievals.

3.2) Alishouse et al. (1990)

Alishouse et al. (1990) tested three competing retrieval algorithms as part of the Calibration/Validation effort the for the first SSM/I aboard the DMSP F8. It was found that the best fit to the data is obtained with a nonlinear global algorithm. Linear segmented and linear global algorithms give higher r.m.s. differences. The “winning” algorithm, which enjoyed widespread popularity in the following years, is

$$W = 232.89393 + 0.148596T_{19V} + 1.828125T_{22V} + 0.006193T_{22V}^2 + 0.36954T_{37V} \quad (3.4)$$

The r.m.s. error of this retrieval is 2.0 kg/m^2, but it was found to have biases at very low (< 5 kg/m^2) and very high (> 60 kg/m^2) values of W (Petty 1990).

3.3) Liu and Niiler (1984) and Liu (1986)

Liu and Niiler (1984) and Liu (1986) investigated the determination of monthly-mean surface latent heat flux from monthly-mean estimates of wind speed and near-surface air humidity (Q). They derived a

5th-order polynomial fit of Q against W measured by a large collection of radiosondes (17 years of soundings from 49 mid-ocean stations at small islands and weather ships). Their regression is

$$Q = 3.819W + 0.1897W^2 + 0.1892W^3 - 7.549 \times 10^{-2}W^4 + 6.0882 \times 10^{-3}W^5 \quad (3.5)$$

with an estimated standard error of 0.8 g/kg for monthly means. They did not apply any radiometer data, but Gautier et al. (1988) found discrepancies when compared to climatological values of 50-90 W/m^2 in the Arabian Sea and as high as 190 W/m^2 south of India.

Liu's method was perhaps not so successful itself, but it spawned a whole host of journal articles, leading eventually to this thesis.

3.4) Schulz et al. (1993, 1997)

Schulz et al. (1993) presented a retrieval and a statistical regression of geophysical parameters needed for the application of the bulk aerodynamic equation for LHF using SSM/I measurements as input. He derived an equation relating the "bottom layer" integrated water vapor, defined as

$$W_B \equiv \int_0^{500m} q(z)\rho(z)dz \quad (3.6)$$

with my substitution of W_B for his w_l for clarity of terminology.

The W_B retrieval uses the 19V, 19H, 22V, and 37V channels of the SSM/I:

$$W_B = -5.9339 + 0.03697T_{19V} - 0.02390T_{19H} + 0.01559T_{22V} - 0.00497T_{37V} \quad (3.7)$$

The theoretical standard error derived by Schulz is 0.6 kg/m^2, but when he tested this against an independent set of 166 globally distributed radiosonde flights the actual standard error was found to be 0.9 kg/m^2.

Additionally, Schulz found a linear relationship between W_B and the near-surface specific humidity Q (the height of Q was not specified):

$$Q = a_0 + a_1 W_B \quad (3.8)$$

This relation had a standard error of 0.80 g/kg when W_B was directly integrated from each sounding, and 1.2 g/kg when W_B was from collocated SSM/I data (the coefficients a_0 and a_1 are slightly different for the two cases). Comparison between the satellite-derived Q (via equation (3.8)) and the near-surface specific humidity at 10 m normalized from the lowest reported level of 166 radiosondes ascents yielded an r.m.s. difference of 1.5 g/kg. Schulz notes that this is probably due to retrieval errors, errors in the *in situ* measurements, and temporal and spatial variability in the collocations, and concludes that the overall method when applied to real satellite data incurs an r.m.s. Q-error of 1.2 g/kg.

The criteria for identifying collocations between the sounding and an SSM/I pixel was +/- 3 hours and 0.5 degrees latitude and longitude. Note that using latitude and longitude rather than actual distance has the effect of allowing more collocations in the tropics than near the poles, since the size of the SSM/I pixels is independent of latitude. Schlüssel et al. (1995) found that although Schulz' method for estimating Q has smaller standard deviations at high latitudes (~1.2 g/kg), it has a significant bias in the high Southern latitudes (see his Table 2) with an overall standard deviation of 1.73 g/kg. Chou et al. (1995) found similar results using soundings from 28 island and atoll stations, using the collocation criteria of +/- 1.5 hours and 100 km. She found r.m.s. differences between Schulz' W_B retrieval and those obtained by direct integration from the soundings to be 0.91 kg/m^2, and between Q derived using equation (3.8) and the lowest sonde level to be 1.88 g/kg. She also found W_B is underestimated for the wintertime extratropics (as pointed out by Schulz et al. 1993) by about 0.75 g/kg.

Table 3.1 lists the standard errors of Schulz' regressions, both with simulated and collocated SSM/I data, along with similar assessments from Schlüssel et at. (1995) and Chou et al. (1995).

Table 3.1 Standard Errors of the Regressions from Schulz et al. (1993)

	W_B	Q	Notes
Schulz et al. (1993)	0.6 kg/m^2	0.88 g/kg	W_B from ship-launched sondes
Schulz et al. (1993)	0.9 kg/m^2	1.5 g/kg	Real SSM/I data, ship-launched sondes
Schlüssel et al. (1995)		1.73 g/kg	Real SSM/I data, volunteer ships
Chou et al. (1995)	0.91 kg/m^2	1.88 g/kg	Real SSM/I data, island stations

Schulz et al (1997) was a larger study that used merchant ships and weathership M in the North Atlantic. They found the r.m.s. error in the retrieved q_{10} to be 1.6 g/kg, and the r.m.s. error in derived LHF to be 50 W/m^2. Their Figure 4 shows a distinct turning of the cloud of points near LHF = 0, where the SSM/I method predicts large negative values.

3.5) Schlüssel et al. (1995)

Schlüssel et al. (1995) recognized that the two-step process used by Schulz et. al (1993) where Q is statistically derived from W_B which is itself statistically derived from the SSM/I brightness temperature measurements is more complicated than need be. He derived a retrieval of Q (again, no height specified) directly from the SSM/I measurements:

$$Q = -80.23 + 0.6295T_{19V} - 0.1655T_{19H} + 0.1495T_{22V} - 0.1553T_{37V} - 06695T_{37H} \qquad (3.9)$$

The source of the *in situ* data that he used to assess the accuracy of this regression is unclear, but Schlüssel appears to have used soundings from both island stations and ships, as well as ships of opportunity to conclude that his method has a slight improvement over Schulz et al. (1993) with a standard error of 1.61 g/kg.

3.6) Miller (1990), Miller and Katsaros (1992)

Miller (1990) attempted to retrieve Q statistically from a third-order fit to W, as opposed to Liu's 5th-order fit. He used one year's worth of soundings from 4 weather ships and one island station in the North and West Atlantic, again taking the lowest sounding level to be representative of the near-surface humidity. The best fit resulted from taking data from only the month of January, with an r.m.s. error of 1.256 g/kg. However, when he used real SSM/I data to assess the performance of the regression, he found 130 match-ups between the SSM/I and ship/island stations gave an r.m.s. error of 2.609 g/kg.

In an attempt to improve the retrieval accuracy, he included SST as analyzed by NOAA and AVHRR to the retrieval. His retrieval is of the form

$$(q_0 - Q) = -0.11676W - 9.7811 \times 10^{-4}W^2 + 0.33441SST + 5.6958 \times 10^{-3}SST^2 \qquad (3.10)$$

q_0, the specific humidity at the surface, is often taken to be 0.98 q_s(SLP, SST), where q_s is the saturation specific humidity over fresh water (a function of pressure and temperature only) and the 98% factor is to account for the salinity of sea water. Since SLP varies by about 1.5% over the globe (r.m.s. ~ 13 mb, mean ~ 1009) q_0 can be adequately predicted by a regression on SST and could be separated from a regression of Q on W and SST.

The data were all from 20° to 50° N and from 55° to 85° W, where the SSM/I passes close to 0 and 12 Z, and resulted in an r.m.s. difference between ships of opportunity/island stations of about 2 g/kg.

3.7) Clayson and Curry (1996)

Following Miller and Katsaros (1992), Clayson and Curry (1996) derived a retrieval for the Western Equatorial Pacific of the form

$$(q_0 - Q) = 3.572W - 0.298W^2 + 6.315SST - 0.129SST^2 - 0.017U_{10} \quad (3.11)$$

They included wind speed U_{10} in the regression, but note that the coefficient is smallest by an order of magnitude, indicating it did not decrease the r.m.s. variability by much. Also note the much larger values of the coefficients for TOGA-COARE, which leads to the conclusion that this type of regression is not 'portable' from one geographic location to another. They derived the coefficients from data from the R/V Franklin during TOGA-COARE, and assessed its performance against the R/V Moana Wave, showing an r.m.s. error of 0.63 g/kg and a correlation of 0.49.

3.8) Chou et al. (1995, 1997)

Chou et al. (1995) developed a technique to estimate the near-surface specific humidity using an empirical orthogonal functions (EOF) technique that uses satellite retrievals of both W and W_B. The technique uses six W-based categories of coefficients in an attempt to make it globally applicable, rather than regional EOF's or global EOF's. As such, it inherits the drawbacks of the retrievals of both W and W_B, including the bias in the wintertime extratropics that Schulz et. al. (1995) found. Chou et al. (1996) attempts to redress this deficiency by placing less weight on W_B in these cases, assuming that the retrieved W is more accurate and more highly correlated with Q.

Chou et al. (1995) calculated the standard error of the retrieval of Q from both simulated SSM/I data (directly integrated from a collection of soundings, using equations (3.1) and (3.6)) and using real SSM/I data collocated within 1.5 hours and 100 km of each sounding. They found the standard error to be 0.75 g/kg for the soundings and 1.70 g/kg using real SSM/I data. In addition, she calculated the standard error of her retrieval using simulated SSM/I products but with random errors approximately equivalent to the r.m.s. accuracies of the W and W_B retrievals, and found the standard error in Q increased from 0.75 to only 1.16 g/kg. Thus it seems that collocation errors account for about half the increase in standard error when using real SSM/I data.

Chou et al. (1997) used a larger set of *in situ* data along with a slightly more complicated scheme that requires ECMWF air-sea temperature differences, and found the standard error of the Q-retrieval compared with 28 globally distributed small island stations for all of 1993 was 1.83 g/kg. Match-ups

with the Moana Wave during TOGA-COARE showed an r.m.s. scatter in the LHF of 29 W/m^2 and a correlation of 0.83.

3.9) Summary of Satellite Retrievals of LHF

As a summation of the previous sections, Table 3.2 lists the channels of the SSM/I used by each of the various retrievals, and Table 3.3 lists the standard errors associated with each of the water vapor related regressions/retrievals when real SSM/I data is compared with *in situ* data.

Table 3.2 SSM/I Retrieval Algorithm Dependencies

	Parameter(s)	SSM/I Channels Used
Wentz (1997)	U_{10}, W, L	19V, 22V, 37V, 37H
Wentz and Smith (1997)	W	19V, 19H, 22V, 37V, 37H
Alishouse et al. (1990)	W	19V, 22V, 37V
Schulz et al. (1993)	W_B	19V, 19H, 22V, 37V
Schlüssel et al. (1995)	q_{10}	19V, 19H, 22V, 37V, 37H

Table 3.3 Standard Errors of Retrievals/Regressions

	Parameter	Typical Range	Error	Comment
Schulz et al. (1993)	q_{10}	1 - 20 g/kg	1.88 g/kg	Global
Schlüssel et al. (1995)	q_{10}		1.61 g/kg	Global
Chou et al. (1995)	q_{10}		1.83 g/kg	Global
Miller and Katsaros (1992)	q_{10}		2.0 g/kg	Northeastern Atlantic
Clayson and Curry (1996)	q_{10}		0.63 g/kg	Western Equatorial Pacific
Schulz et al. (1993, 1997)	LHF	0 - 300 W/m^2	30 W/m^2	Global
Schlüssel et al. (1995)	LHF		30 W/m^2	Global
Chou et al. (1995)	LHF		29 W/m^2	Global
Miller and Katsaros (1992)	LHF		20 - 30%	Northeastern Atlantic
Clayson and Curry (1996)	LHF		53 W/m^2	Western Equatorial Pacific

Schulz' retrieval has not been widely accepted by the general SSM/I community. It has been claimed that it does no better, or even slightly worse, than a purely statistical regression (Frank Wentz, personal communication). Following Wentz's suggestion, I embarked upon an attempt to derive a statistical regression using the sounding data described in Chapter 2.

3.10) Proposed New Retrieval

I chose to use a double approach where both W_B and q_m (the mixed-layer specific humidity) regressions are developed simultaneously. For reasons that will become clear in Chapter 5, I used q_m (the mixed-layer humidity) instead of q_{10} (the humidity at 10 meters) as Schlüssel et al. (1995) did.

The regressions were derived using the "lsfit" and "lmsreg" built-in functions in Splus, a statistical program from MathSoft Inc. These subroutine fit the response variable to a linear combination of the explanatory variables by minimizing the square of the residuals or the median of the square of the residuals, respectively. This "least-squares" fitting is technically guaranteed to be correct only if the distributions are gaussian, but in practice it is widely applied. I also performed regressions using the "ltsreg" and "l1fit" functions (least trimmed squares robust method, and minimum absolute residual) but found only very small differences in the results.

Figure 3.1 shows the relation of W_B and q_m to the total integrated water vapor W, and sea surface temperature (SST). W and W_B are each integrated from the soundings, q_m is analyzed from the soundings, and the SST is obtained from the ship sensor at the time of each sounding flight. Figure 3.1 (A) and (B) are similar to Figure 5 of Liu (1986). There exists significant correlation between the variables. However, there are trends and digressions that suggest there is room for improvement. In (B) and (D), we see the effect of the Claussius-Clapeyron equation, since the air humidity is usually about 70 - 80% of the saturation humidity at the sea surface temperature. The *departures* from this general tendency are of interest.

For $W < 40$ kg/m^2, and for SST < 290 K there exist linear relationships. However, for $W > 40$ kg/m^2 the "bent over" shape of the cloud of points indicates that at some point (in the deep tropics, with a few cases in mid-latitudes) the total water vapor in the atmosphere continues to increase without a corresponding increase in the mixed-layer humidity. The processes controlling the amount of water vapor in the upper troposphere become increasingly independent of the processes controlling the mixed-layer water vapor. For these points, W_B and SST are essentially not correlated, but W_B and W have a correlation of 0.32, indicating some residual skill. For these same points, q_m and W have a correlation of 0.40, and q_m and SST have correlation of 0.36. However, while q_0 - q_m and W are not correlated, q_0 - q_m and SST have a correlation of 0.69, indicating a q_m-retrieval should still possess skill at predicting the LHF. Doing a piece-wise fit above and below $W = 40$ kg/m^2 does not help the regression for either piece significantly. The skill of either the local or full W_B (q_m) regression in the high-W range is low, with R^2 = 22% (58%), but the standard error is the same as the full regression and the low-W regression.

Motivated by the shapes of the clouds of points in this figure, linear and quadratic terms for each of these variables (*W,* SST) are included in the regressions. Figure 3.2 shows the statistically predicted vs. observed retrievals of W_B (calculated from the soundings) for increasingly complex lists of dependent parameters, along with the squared correlation coefficient (R^2), standard deviation (SD) and overall average bias of a least-squares linear fit to the data. There are two lines fit to the data in each graph, a standard least-squares fit (dashed) and robust trimmed least squares fit (dotted) to give an indication of how robust each regression is. Note that a second-order regression on *W* results in almost the same standard error as a second-order regression on SST. One can also see the effect of the imperfect sampling of

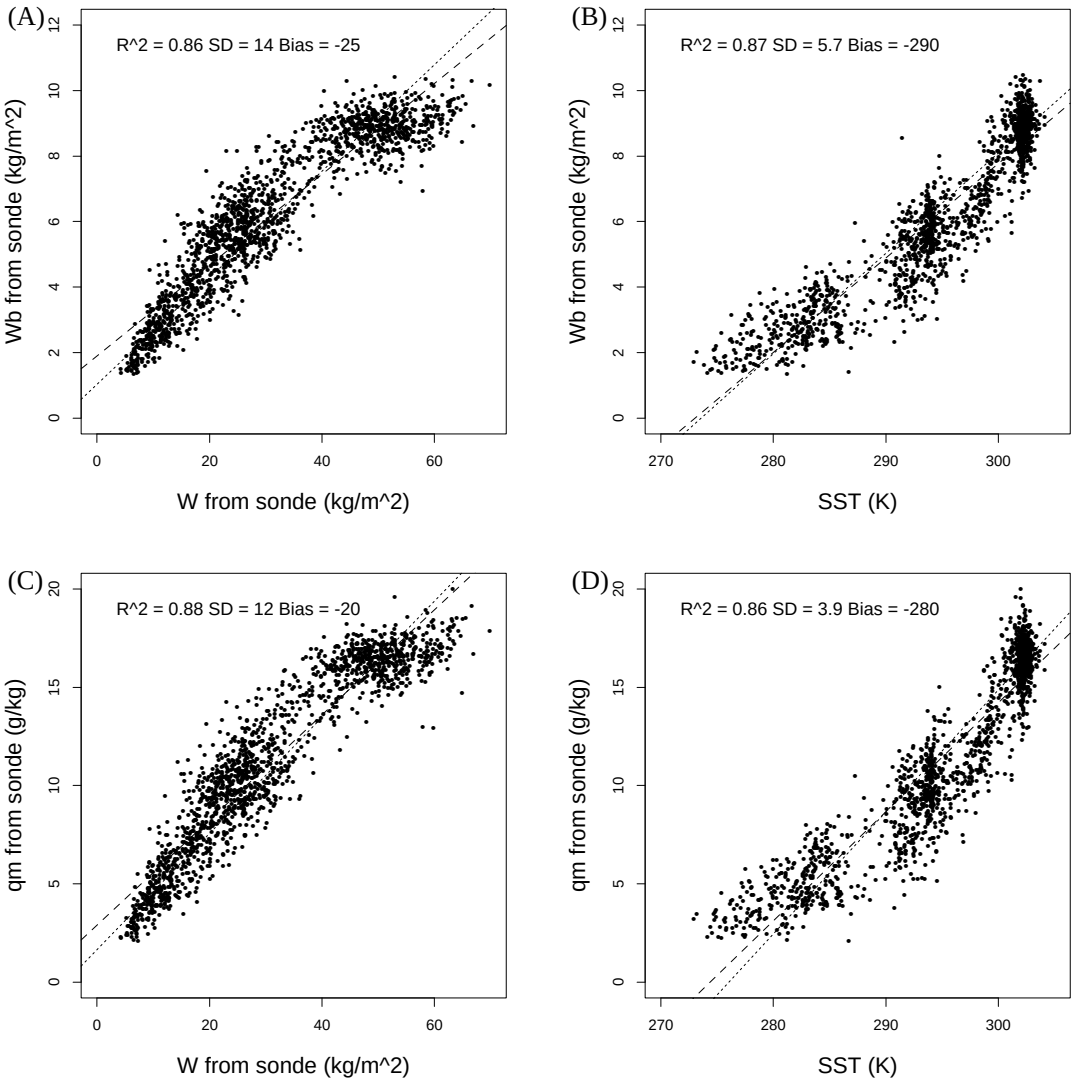

Figure 3.1 W_B as a function of (A) *W*, and (B) SST, and q_m as a function of (C) *W* and (D) SST.

global conditions by the ships (panel C) in the uneven distribution of SST. Adding other parameters such as U_{10} and L, the integrated liquid water as measured by the SSM/I, did not yield any increased predictability to the regressions. The standard error of Figure 3.2 (D), 0.52 kg/m^2, is better than the initial estimated standard error of Schulz et al. (1993), 0.6 kg/m^2, and much better than the error he found using collocated SSM/I data (0.91 kg/m^2).

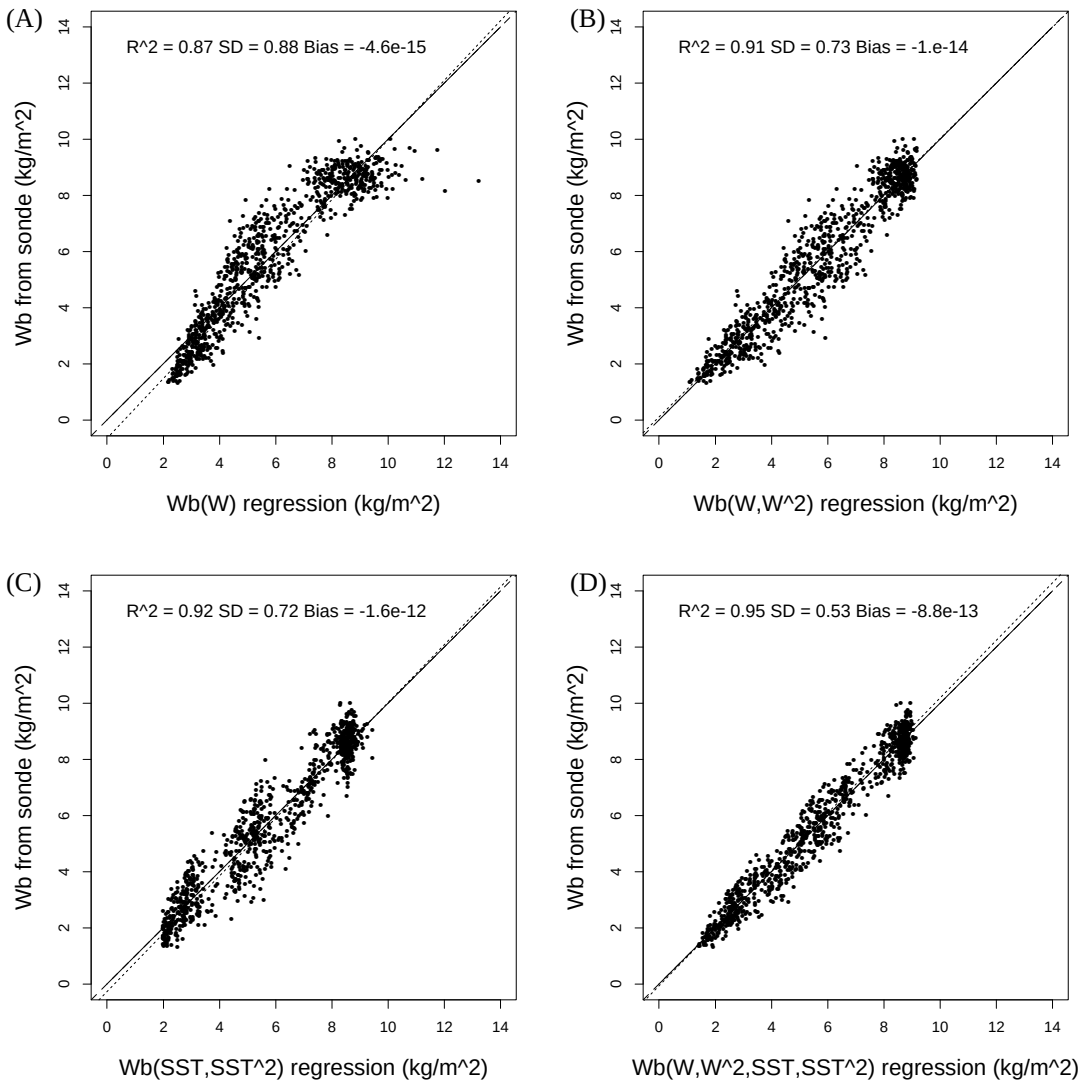

Figure 3.2 The performance of various W_B statistical regressions of increasing complexity.

In section 5.1.1, page 75, I show that using the ideal gas law and the hydrostatic assumption, one can integrate equation (3.6) for a mixed layer (constant θ, constant q), yielding the following relation between q_m and W_B:

$$q_m = \frac{gW_B}{P_0}\left[1 - \left(1 - \frac{500g}{c_p\theta_m}\right)^{\frac{c_p}{R_d}}\right]^{-1} \tag{3.12}$$

If the assumptions used in deriving this equation are implicit in the statistical regression of W_B by the choice of dependent parameters, then finding q_m from a regression will yield results as good as those of finding W_B from a regression and then applying this equation. As an added bonus, using q_m from a direct regression instead of q_m calculated via equation (3.12) from a regression of W_B avoids violating the assumption that the mixed layer is at least 500 m deep.

In analogy with Figure 3.2, Figure 3.3 shows the statistically predicted vs. observed retrievals of q_m for an increasingly complex lists of dependent parameters, along with the squared correlation coefficient (R^2), standard deviation (SD) and overall average bias of a least-squares linear fit to the data. The variation in q_m that is purely due to variation in SST has been removed from this figure by plotting the air-sea humidity difference q_0-q_m instead of q_m. There are two lines fit to each graph, a standard least-squares fit (dashed) and a robust trimmed least squares fit (dotted) to give an indication of how robust each regression is. Again, the second-order regression on W produces almost the same standard deviation as does the second-order regression on SST, but in this case the correlation coefficient is significantly worse for the SST fit. Adding other parameters, such as U_{10} and L, did not yield any increased predictability, just as with the W_B regression. The standard error of the best fit, Figure 3.3 D), is 0.9 g/kg, is larger than the estimated standard error of Chou et al. (1995) of 0.75 g/kg.

Table 3.4 lists the parameters included in most of the various regressions I have performed, along with the standard error of each regression. Note that only W_B and q_m are directly regressed; the middle column lists the results of applying equation (3.12) to W_B, and is included for comparison with the last column. Adding SLP had the same (negligible) effect as adding U_{10}, and regressions of $\Delta q = q_0 - q_m$ produced the same results as regressions of q_m. Including or excluding a constant term in the regressions had little effect, except when attempting to retrieve Δq where it degraded the result considerably (*c.f.* Miller and Katsaros (1992)). Adding T_{10} - SST, although it didn't decrease the overall r.m.s. error, helped bring the medians of the error in various range bins closer to zero. Without it, the residual is weakly correlated with air-sea temperature difference.

In this table, we start with the simplest regression, W_B and q_m regressed on *W*, and add terms. Note that using only SST gives about the same results as using only *W*, and that adding U_{10} does not reduce the standard error. The last row shows the parameters used by Liu and Niiler (1984) and Liu (1986) to derive their $q_{10}(W)$ fifth order regression for monthly mean data. We see that it does no better for these

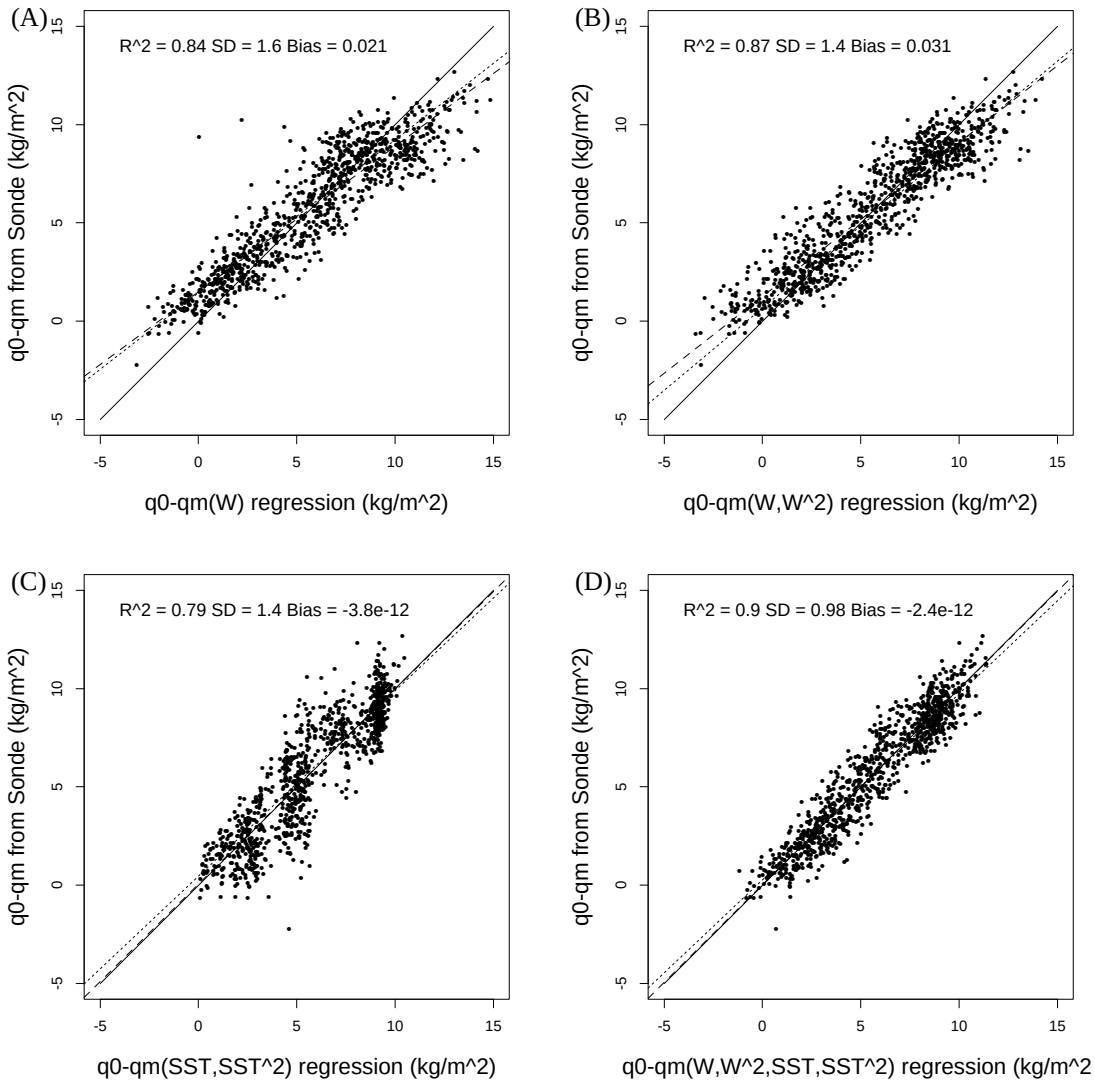

Figure 3.3 The performance of various q_m statistical regressions of increasing complexity.

retrievals than using no SSM/I parameters at all and using only SST, or using only the linear and quadratic terms.

Table 3.4 Standard Deviations of Statistical Regressions

Parameters included in retrieval	W_B(Stats)	$q_m(W_B(\text{Stats}))$	q_m(Stats)
W	0.88 kg/m^2	1.6 g/kg	1.6 g/kg
W, W^2	0.73 kg/m^2	1.4 g/kg	1.4 g/kg
SST, SST^2	0.71 kg/m^2	1.5 g/kg	1.4 g/kg
W, W^2, SST	0.57 kg/m^2	1.1 g/kg	1.1 g/kg
W, W^2, SST, SST^2	0.55 kg/m^2	1.1 g/kg	0.91 g/kg
W, W^2, U_{10}	0.73 kg/m^2	1.4 g/kg	1.4 g/kg
W, W^2, SST, SST^2, U_{10}	0.52 kg/m^2	1.1 g/kg	0.91 g/kg
W, W^2, SST, SST^2, (T_{10} -SST)	0.55 kg/m^2	1.1 g/kg	0.91 g/kg
W, W^2, W^3, W^4, W^5	0.73 kg/m^2	1.4 g/kg	1.4 g/kg

It is difficult to pick one parameter to retrieve using such statistical methods, as W_B, q_m and q_{10} are all highly correlated. Table 3.5 shows the squared correlation coefficients and standard deviations between these three parameters. It is not surprising that the correlations are so high, since we have an equation relating W_B to q_m, and can relate q_m to q_{10} via the LKB equations. Schlüssel chose to retrieve q_{10}, Schulz chose W_B, but I think the most relevant and fundamental geophysical parameter is q_m, the average humidity in the mixed layer.

Table 3.5 The R^2 and SD between W_B, q_m and q_{10}

	W_B	q_m	q_{10}
W_B		$R^2 = 0.99$	$R^2 = 0.97$
q_m	SD = 2.4		$R^2 = 0.98$
q_{10}	SD = 2.9	SD = 0.94	

The two statistical regressions' parameter values are given in Table 3.6, where the coefficients are defined by

$$W_B = a + bW + cW^2 + dSST + eSST^2 \tag{3.13}$$

and

$$q_m = a + bW + cW^2 + dSST + eSST^2 + f(T_{10} - \mathrm{SST}) \quad (3.14)$$

The regression can be performed with either the SST measured by the ship, or the OI SST interpolated to the ship's position and time.

Table 3.6 Regression coefficients

Using	Regression	a	b (W)	c (W^2)	d (SST)	e (SST^2)	f (T_{10}-SST)
SST	W_B	322.771	0.158031	-1.2337e-3	-2.35677	4.3109e-3	-
	q_m	922.493	0.175997	-1.0039e-3	-6.64644	1.2010e-3	0.39117
OI SST	W_B	348.437	0.163496	-1.3718e-3	-2.54151	4.6427e-3	-
	q_m	117.123	0.266108	-1.2916e-3	-0.99471	2.0784e-3	8.98421e-2

3.10.1) Regression performance

Figure 3.4 shows the performance of the W_B and q_m regression using both W integrated directly from the soundings and real collocated SSM/I data, compared to the values calculated from the soundings. The sample size of the real collocated data is much smaller due to the collocation requirements, as explained in section 2.6, page 29, but the standard error of the W_B regression only increased from 0.555 to 0.565 kg/m^2 when using real SSM/I data, not nearly as much as the 50% increase from 0.6 kg/m^2 to 0.9 kg/m^2 of Schulz et al. (1993). The increase in the r.m.s. of the q_m regression from 0.907 to 909 g/kg is indistinguishable due to the low number of SSM/I-sounding match-ups. The increase in the scatter of q_m from simulated to real data is smaller than the increase in r.m.s. that Chou et al. (1995) exhibits (from 0.75 to 1.83 g/kg) or the increase (from 0.88 to 1.5 g/kg) of Schulz et al. (1993), and better than the 1.61 g/kg r.m.s. of Schlüssel et al. (1995).

Since we observe higher water vapor amounts in the total atmosphere near the tropics where the sea surface temperature is higher, W is highly correlated to SST. To show that the addition of W as a parameter in the retrievals adds new information beyond the correlation between W and SST, Figure 3.5 shows normalized W_B and air-sea humidity difference as a function of normalized W. To do this, each of W,W_B,and q_m was first regressed against SST with a second-order fit. The sonde-measured data was then normalized by the statistical prediction to remove the overall variation due to SST and plotted. The graphs show a tight cluster of points and a good correlation, considering that half the variability (that due to SST) has been removed. The q_0 - q_m plot is especially tightly clustered. The tail of points near x=0.5 are all soundings taken by the Polarstern, at 50 - 60 °S and have observed SSTs only a few degrees C. These points indicate conditions where the whole atmosphere is much dryer than normal for

that SST, and the boundary layer air is *even more* dry compared with average conditions for that SST. It is therefore likely that these soundings were influenced by advection of dry air across the ice edge, and the ice-detection scheme I used to reject soundings (section 2.4, page 24) was not quite adequate to remove these.

Finally, the regression was tested for robustness by using various subsets of the soundings to develop the regression and the remaining soundings to assess the r.m.s. scatter and bias. Only small differences in the coefficients and evaluation parameters were found. We also note that there is little differ-

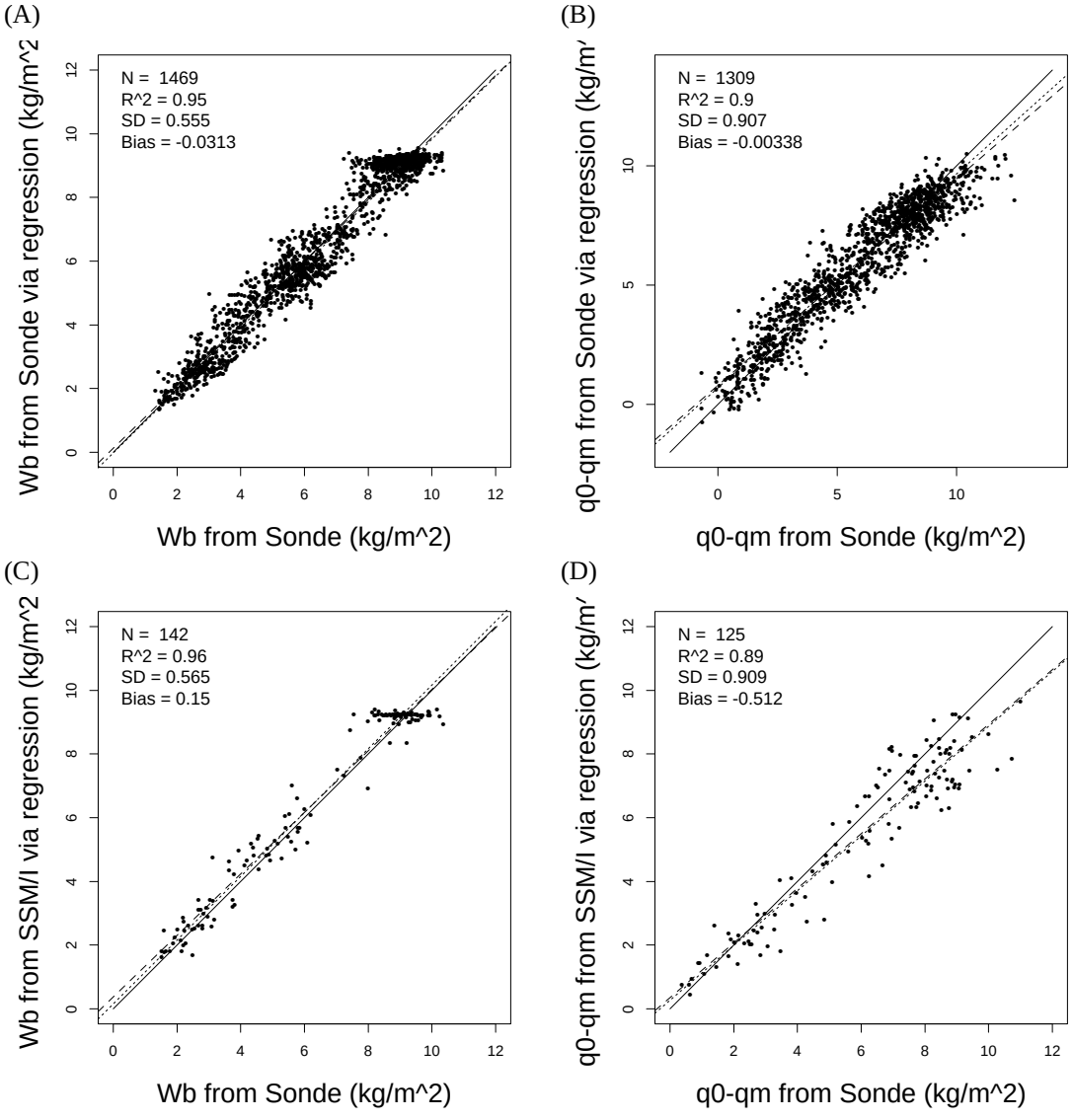

Figure 3.4 The W_B (A and C) and q_m (B and D) statistical regressions' performance, using (A and B) *W* from the soundings, and (C and D) *W* from collocated SSM/I data, compared with radiosonde data.

ence between the regression using SST measured by the ship, and the regression using the OI SST interpolated to the ship's position and time.

Figure 3.6 shows box plots of the retrieval of q_m vs. the surface to mixed layer humidity difference as measured by the radiosondes. This regression was based on minimizing the median of the squares of the residual, which is not the method that produces the lowest standard error. Several other methods produce standard errors of about 0.90 g/kg, but have more bin-by-bin median errors. They produce good overall agreement while still under-predicting q_m at low q_m values and over-predicting it at high values. This regression still underpredicts the air-sea humidity difference at high values (representative of tropical conditions) by about 0.5 g/kg. As will be shown in section 4.7, page 69, this will lead to an underpredicting of the latent heat flux by about 10 W/m^2. Fortunately, the expected value of LHF for these conditions is greater than 200 W/m^2, such that the calculated LHF will be about 5% low.

Figure 3.7 shows a similar plot, but for the statistical retrieval of W_B as a function of sonde-measured W_B. There is more scatter, a significant deviation in the 8 kg/m^2 range, and a trend toward underprediction at high values. Adding ΔT to the regression yields only a slightly different distribution of error. Based on the performance of the two regressions, I tend to favor the q_m regression both due to its better and more consistent performance and because it is a more fundamental (c.f. the arbitrary 500 m depth of W_B) geophysical parameter.

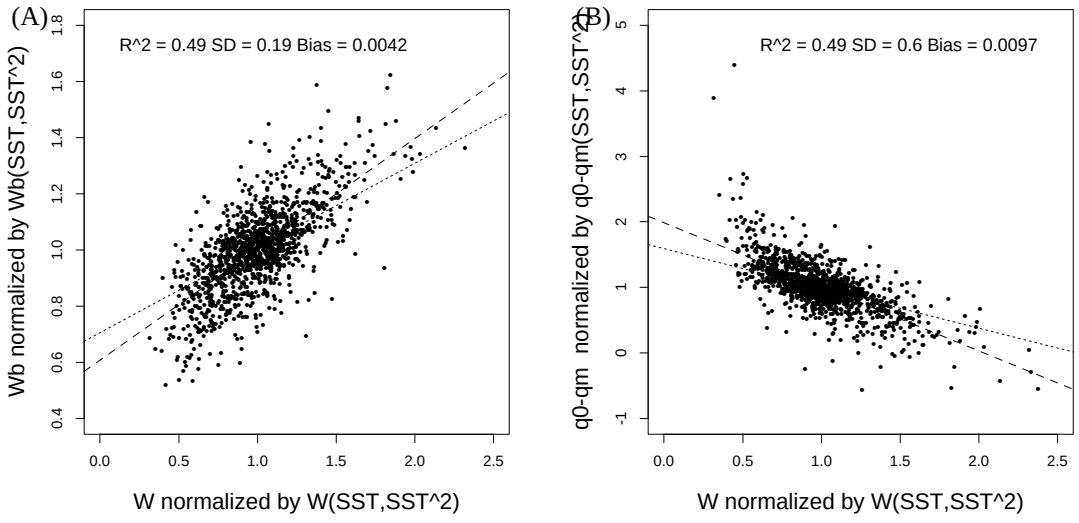

Figure 3.5 (A) W_B and (B) q_0 - q_m normalized by their respective SST regressions, vs. W normalized by its SST regression.

3.10.2) Retrieval error analysis

It is useful to estimate how much of the observed scatter in the two retrievals is due to measurement errors in the input data and how much is due to physical processes that are not accounted for in the model. The major sources of uncertainty in the measurements are 3% due to radiosonde humidity accuracy, SST uncertainty, and uncertainty in the ECMWF T_{10} - SST predictions. I will take the error in W_B and W to be 3% of their average values of 6.4 and 23 kg/m^2, or 0.19 and 0.69 kg/m^2, respectively. The characteristic error of the OI SST is taken to be 0.7 K (see section 2.1, page 19). The errors in the r.m.s. scatter at the time of the SSM/I overpasses between the ECMWF and ship sensor air-sea temperature difference is 1.0 K. About 0.3 K of this can be attributed to differences between bulk and skin temperatures.

Wentz (1997) gives the r.m.s. accuracy of the W SSM/I retrieval as 1.2 kg/m^2. By contrast, my collocations show a standard error of 3.04 kg/m^2, but this includes collocation errors as well as random retrieval errors. Wentz (1997) gives an error budget (his Table 3) that indicates the sampling mismatch is

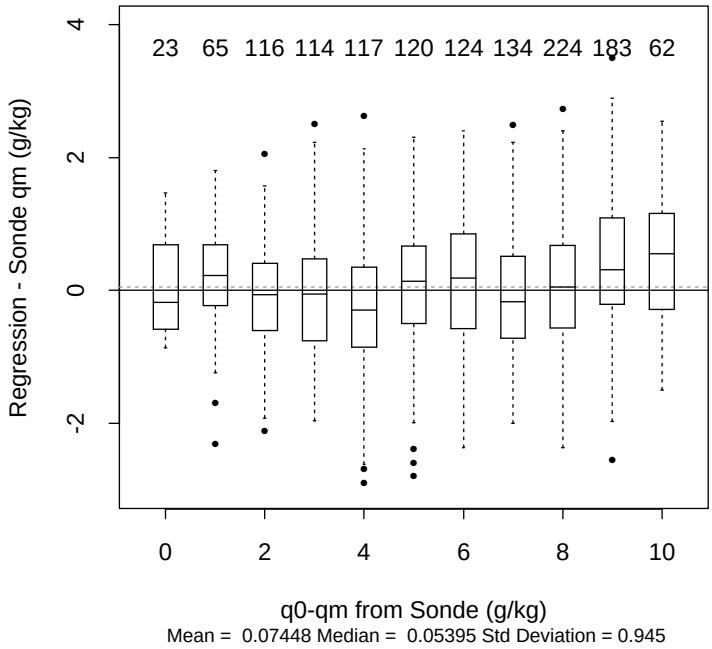

Figure 3.6 The difference between the statistical prediction of $q_m(W, \mathrm{SST}, \Delta T)$ and q_m measured by the sondes, as a function of surface-ML q difference.

3.68 kg/m^2 for a time window of 6 hours and a radius of 60 km for sonde and SSM/I match-ups. I used a much smaller time window of 60 minutes but a larger radius of 150 km as my criteria. Using my observed variance and Wentz's stated accuracy, I deduce the collocation error to be 2.79 kg/m^2. This can then be multiplied by the sensitivity of each of the methods to give the uncertainty due to collocation errors.

For the sensitivity of the retrievals to their input parameters, I evaluated the functions at the standard (global mean) values of the input variables and with the deviations listed above. The estimated variance budget due to uncertainty in the measurements of the input variables is given in Table 3.7. The estimated collocation errors are listed for reference. The observed variance minus the total of the mea-

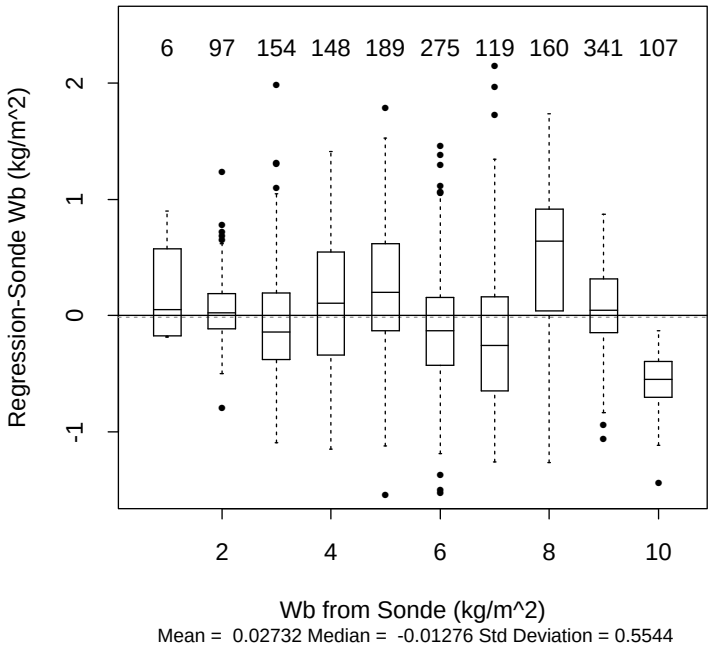

Figure 3.7 The difference between the statistical prediction for $W_B(W, \mathrm{SST})$ and W_B measured by the sondes, as a function of measured W_B

surement errors is listed as the residual. These values represent the physics that has not been accounted for in the regressions.

Table 3.7 Variance budget for the statistical retrievals

	q_m retrieval	W_B retrieval
Error in sonde W (0.69 kg/m^2)	0.08 g/kg	0.07 kg/m^2
Error in OI SST (0.5 K)	0.32 g/kg	0.06 kg/m^2
Error in T_{10} - SST (0.7 K)	0.27 g/kg	-
Total Measurement Error	0.43 g/kg	0.09 kg/m^2
Collocation Error	0.52 g/kg	0.32 kg/m^2
Observed variance	0.91 g/kg	0.56 kg/m^2
Residual	0.61 g/kg (2.1% of 11 g/kg)	0.33 kg/m^2 (5.2% of 6.4 kg/m^2)

3.10.3) Dependence on brightness temperature channels

It is of interest to examine the dependence of the new W_B regression on the SSM/I's brightness temperature channels. The new regression is intended to be used with Wentz's (1997) retrieval of W, but the dependence of W on the brightness temperatures cannot be explicitly separated from the retrievals of the other parameters. Instead, I examine the retrieval presented in Wentz and Smith (1997) which behaves very much like Wentz (1997). Calculating and showing the formula for the new retrieval would as likely obscure as elucidate the point, since Wentz and Smith (1997) includes quadratic terms and the new retrieval then squares that, yielding a mess of cross terms with no easy way to sort out the leading terms.

To find the dependencies of the various retrievals and regressions on each channel of the SSM/I, I first chose "basic state" values for each channel and then separately varied each one through the observed range for that channel. The "basic state" was chosen as the observations taken by the F11 SSM/I at 38° N, 215° E at 02:18 Z on 18 July, 1992, and is listed in Table 3.8, along with the range of

each channel. Also listed is the SST from the ECWMF analysis for 0 Z on the same day and an appropriate range. Note that the SSM/I cannot retrieve SST, since it lacks a channel below 10 GHz.

Table 3.8 Basic State" brightness temperature values and ranges.

Parameter	Value (K)	Range (K)
T_{19V}	198.1181	170 - 222
T_{19H}	133.2547	95 - 160
T_{22V}	227.5652	175 - 250
T_{37V}	216.0752	205 - 240
T_{37H}	157.2748	120 - 170
SST	292.0577	274 - 304

Figure 3.8 through Figure 3.13 shows the functional dependence of the four retrievals by Wentz, Alishouse, Schulz, and the current statistical regression on the lower five SSM/I channels and SST (Schulz and statistical regression only). Of the three channels that Wentz and Alishouse share, it is remarkable how different their responses are to changes in the brightness temperature. The behave similarly for the 22 GHz channel, commonly referred to as the water vapor channel due to the strong water vapor absorption line near there. Their slopes are rather different for 19V, and are even reversed in sign for 37V, yet they produce a *W* within 0.87% of each other for the basic state.

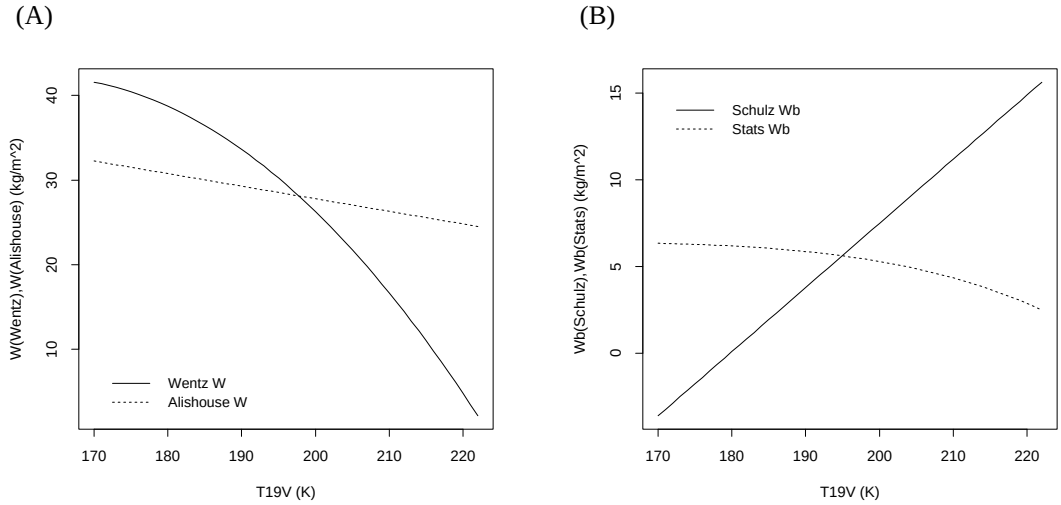

Figure 3.8 (A) *W* and (B) W_B vs. T_{19V} for the various retrievals.

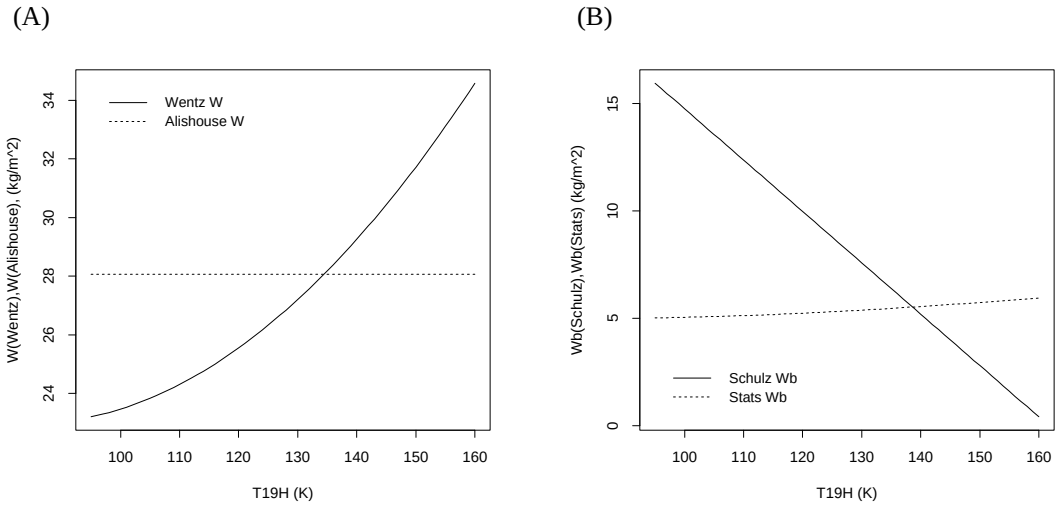

Figure 3.9 As in Figure 3.8, but for T_{19H}.

Schulz' retrieval and the statistical regression share all but two input parameters: Schulz does not use 37H or the SST. Of the remaining channels, only the 22V (the water vapor channel) shows similarity of their dependencies, as with Wentz and Alishouse. Note also the reversed slope of the other channels, and the diminished slope of the statistical regression compared to Schulz. The sensitivity to each of the channels of the statistical regression must be diminished to "leave room" for variability to be explained by the SST 'channel'. We trade sensitivity to the SSM/I channels for sensitivity to SST.

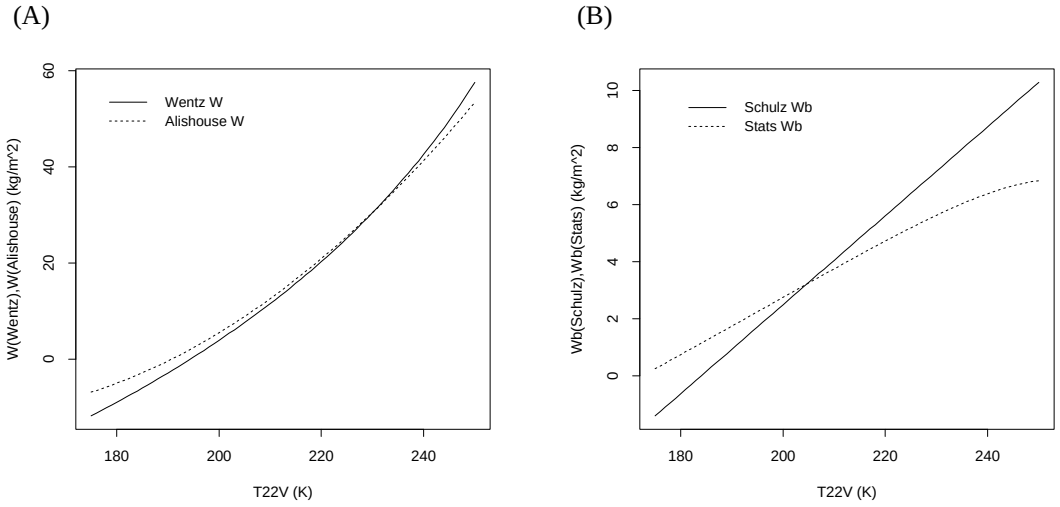

Figure 3.10As in Figure 3.8, but for T_{22V}.

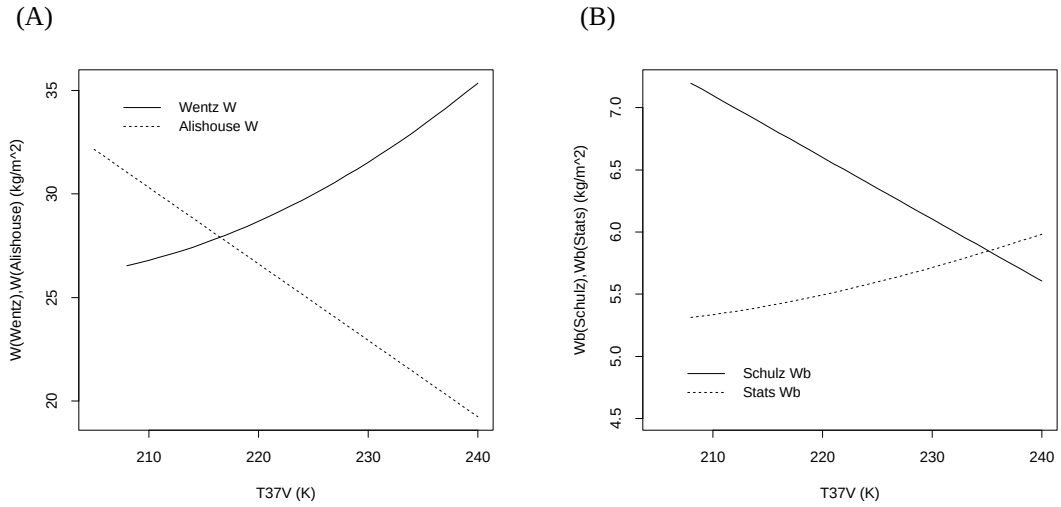

Figure 3.11As in Figure 3.8, but for T_{37V}.

Note also that Schulz' retrieval can produce unphysical values ($W_B < 0$) for 19V and 22V at the extremes of the ranges of these observed brightness temperatures. The statistical regression always produces acceptable values, even at the highest sea surface temperatures (SST > 29°C). It is unknown what fraction of real SSM/I observations produce these erroneous values in Schulz' retrieval, as one must first eliminate ice- and rain-contaminated pixels.

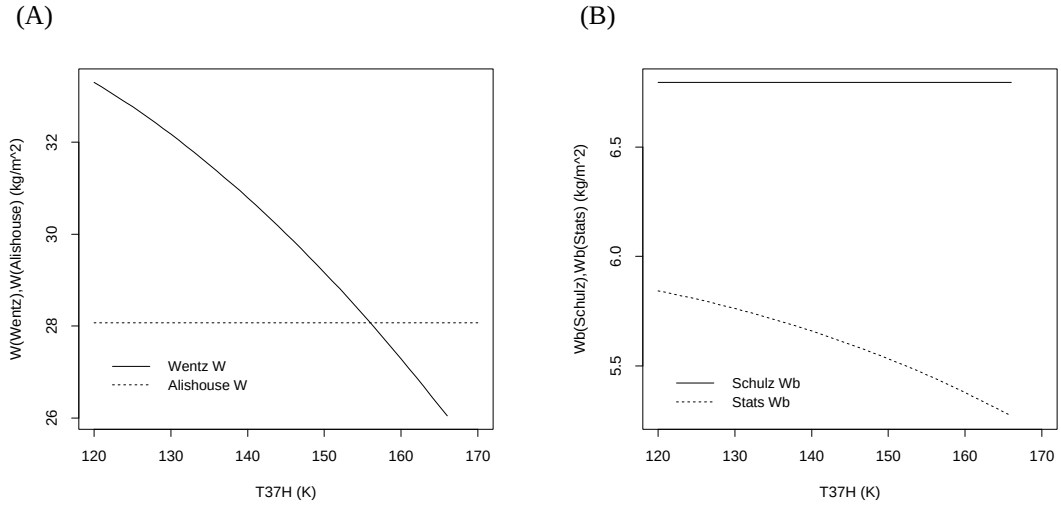

Figure 3.12As in Figure 3.8, but for T_{37H}.

3.11) Summary

This chapter discussed some of the most popular and relevant geophysical parameters retrieved from SSM/I measurements, including Wentz (1997), Alishouse et al. (1990), Schulz et al. (1993), Schlüssel et al. (1995) and Chou et al. (1995, 1997). The performance of each of the retrievals was discussed, along with some of the shortcomings and biases of each of the methods.

Due to the general lack of acceptance of Schulz' results and motivated by Wentz' comments, I developed statistical methods of retrieving both W_B and q_m from the widely accepted and readily available retrieval of total integrated water vapor W and externally (non-SSM/I) supplied sea surface temperature SST. Various combinations of regression parameters were tried and assessed, and a final format settled upon: linear and quadratic terms of both W and SST. The standard error of the regressions were estimated from the regression data and from real collocated SSM/I data. Wentz' suspicions that Schulz' method gave results equivalent or slightly worse than pure statistics turned out to be true, in that the standard error of both the W_B and the q_m regressions is less than the various assessments of Schulz et al. (1993), Schlüssel et al. (1995) and Chou et al. (1995, 1997). The estimated error (standard error of the original regressions) and actual error (assessed using real collocated SSM/I data) of the various competing methods are listed in Table 3.9.

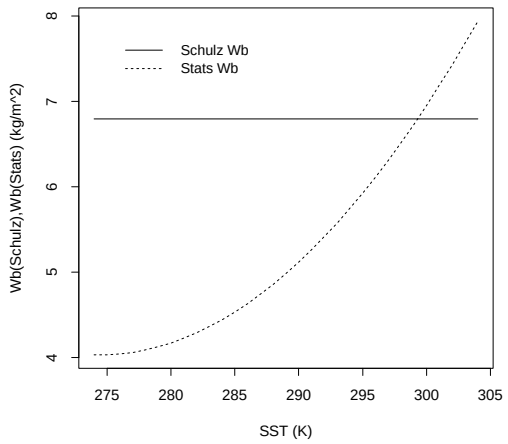

Figure 3.13W_B vs. SST for the Schulz and the statistical retrievals

An error analysis of the retrievals was performed, and the errors due to imperfect measurements was assessed. An error budget was constructed, and it was found that even without taking into account SSM/I - sounding collocation error (sample mismatch) most of the observed variance was explained.

Table 3.9 Standard Errors of Retrievals

	Parameter Retrieved	Method Used	Estimated Error	Real Error
Schulz et al. (1993)	W_B	Schulz	0.6 kg/m^2	0.9 kg/m^2
Chou et al. (1995)	W_B	Schulz		0.91 kg/m^2
Current Work	$\mathbf{W_B}$	**Current**	**0.55 kg/m^2**	**0.56 kg/m^2**
Schulz et al. (1993)	q	Schulz	0.88 g/kg	1.5 g/kg
Schlüssel et al. (1995)	q	Schulz		1.73 g/kg
Chou et al. (1995)	q	Schulz		1.88 g/kg
Schlüssel et al. (1995)	q	Schlüssel		1.61 g/kg
Chou et al. (1997)	q	Chou	0.75 g/kg	1.83 g/kg
Current Work	$\boldsymbol{q_m}$	**Current**	**0.91 g/kg**	**0.91 g/kg**

Finally, the dependencies on each of the brightness temperature channels and SST of the retrievals of Wentz, Alishouse, Schulz, and the current work were examined. The new statistical regressions were found to be well behaved for the full range of observed brightness temperatures and sea surface temperatures, unlike some of the other retrievals.

Chapter 4

The Calculation of Latent Heat Flux

4.1) Latent Heat Flux Methods

There exists four common ways to estimate latent heat flux:

1. The covariance or ‘eddy correlation’ technique uses direct high-frequency measurements of the 3-component velocity fluctuations and humidity fluctuations. This is the only “true” or direct measure of the flux.
2. The inertial dissipation technique also uses direct high-frequency measurements of the vertical velocity fluctuations and the humidity fluctuations, but converts these to spectral measurements and uses the Kolmogorov hypothesis of the existence of an inertial subrange to infer the flux. It is hoped that flow distortions around the measurement platform have little effect on the high frequency measurements.
3. Bulk parameterizations use time-averaged measurements and relations that are the result of either dimensional analysis or basic physics. Two bulk parameterization methods will be further explained below.
4. Profile-fitting uses time-averaged measurements at multiple heights in the surface layer. They are fit to the expected profiles (see the section on the surface layer below) to find the parameters used to calculate the flux. This is the crudest of the methods.

The first two require fast-response instruments capable of directly measuring the turbulent fluctuations. Such instruments are often hard to operate at sea, since they tend to become dirtied by sea spray and drizzle, as well as being affected by any rolling of the platform. Thus they are seldom deployed, and then only on research ships during specific experiments for short time periods. The latter two require only time-average measurements, which are much easier to obtain, and are routinely produced by buoys, commercial ships, research ships, etc.

4.2) The bulk aerodynamic method

A common method used to estimate fluxes is to use the bulk-aerodynamic formulae. They are the result of dimensional analysis, and one of the oldest methods used in meteorology to estimate fluxes and drag. The bulk-aerodynamic formula for latent heat flux is

$$E = \rho L_v C_E U_{10}(q_0 - q_{10}) \tag{4.1}$$

where ρ is air density, L_v is the latent heat of vaporization, C_E is a transfer coefficient, U_{10} is the wind speed at 10 m, q_0 is the surface specific humidity, and q_{10} is the specific humidity at 10m.

U_{10} can be estimated from any one of several satellite measurements (e.g. SSM/I, ERS-1, NSCAT). q_0 is usually taken to be 98% of the saturation specific humidity at the SST (Kraus, 1972) which can also be obtained from satellites (e.g. AVHRR). Density can be calculated from analyses of sea level pressure and temperature. C_E, the transfer coefficient, must be either experimentally determined or predicted from a surface-layer model. Several large experiments were performed to establish its value between 1.1 x 10^{-3} to 1.3 x 10^{-3}, with a small dependence on stratification. Measurements of q_{10}, however, are generally not available over large portions of the world's oceans.

4.3) The LKB bulk method

Liu et al. (1979, hereafter referred to as LKB) postulated that based on Monin-Obukhov similarity theory arguments (e.g. Businger 1973a) the mean diabatic profiles of wind speed (u), potential temperature (θ) and specific humidity (q) in the surface layer may be expressed as:

$$u(z) = \frac{u_*}{k}\left[\ln\left(\frac{z}{z_0}\right) - \Psi\left(\frac{z}{L}\right)\right] \tag{4.2}$$

$$\theta(z) = \theta_0 + \frac{T_*}{k_T}\left[\ln\left(\frac{z}{z_{0T}}\right) - \Psi_T\left(\frac{z}{L}\right)\right] \tag{4.3}$$

$$q(z) = q_0 + \frac{q_*}{k_q}\left[\ln\left(\frac{z}{z_{0q}}\right) - \Psi_q\left(\frac{z}{L}\right)\right] \tag{4.4}$$

$$L^{-1} = \frac{gk}{\theta_v u_*^2}(T_*(1 + 0.61q) + 0.61\theta q_*) \tag{4.5}$$

k, k_T and k_q are von Karmen's constant and the temperature and humidity equivalents, z_0, z_{0T} and z_{0q} are the roughness lengths, and u_*, T_*, and q_* are the Monin-Obukhov scaling parameters for momentum, temperature and humidity, respectively. L is the Monin-Obukhov length taking into account the buoyancy of water vapor. Ψ, Ψ_T and Ψ_q are the stratification corrections to the neutral 'log-laws', and are related to the dimensionless gradients Φ, Φ_T and Φ_q by

$$\Psi\left(\frac{z}{L}\right) = \int (1-\Phi)d\ln\left(\frac{z}{L}\right) \tag{4.6}$$

They are generally given for unstable stratification as

$$\Psi = 2\ln[(1+\Phi^{-1})/2] + \ln[(1+\Phi^{-2})/2] - 2\operatorname{atan}\Phi^{-1} + \frac{\pi}{2} \tag{4.7}$$

$$\Psi_T = \Psi_q = 2\ln[(1+\Phi_T{}^{-1})/2] \tag{4.8}$$

with

$$\Phi = \left(1 - a_u\frac{z}{L}\right)^{-1/4} \text{ and } \Phi_T = \Phi_q = \left(1 - a_T\frac{z}{L}\right)^{-1/2} \tag{4.9}$$

and for stable stratification, as

$$\Psi = -B_u\frac{z}{L} \text{ and } \Psi_T = \Psi_q = -B_T\frac{z}{L} \tag{4.10}$$

where a_u, a_T, B_u and B_T must be determined experimentally. Many sets have been presented in the literature. (e.g. Businger et al. 1971, Dyer 1974, Kondo 1975, Francey and Garratt 1981, Dyer and Bradley 1982, Högström 1988).

Contained in equation (4.2) is what essentially amounts to choosing the form of the drag coefficient, in the choice of the parameterization of z_0 as a function of u_* (e.g. Kondo 1975, Smith 1988, Large et al. 1995, Chou et al. 1995). The most common formula is

$$z_0 = \alpha\frac{u_*^2}{g} + 0.11\frac{\nu}{u_*} \tag{4.11}$$

where ν is the kinematic viscosity of air. The first term is following Charnock (1955) and is valid for rough flow (U_{10} > 8 m/s). The parameter α is the “Charnock constant”. The second term is from LKB and is valid for smooth flow (U_{10} < 2 m/s) where the roughness Reynolds number, defined as $R_r = z_0 u_*/\nu$, approaches a constant value of about 0.11.

Figure 4.1 shows the drag coefficient (C_D) vs. 10-m wind speed that result from choosing the parameterizations of $z_0(u_*)$ from Kondo (1975) as extended by Smith (1989), Fairall et al. (1996) and

Large et. al. (1995). Each fits the experimental scatter about equally well, but they are rather different. PBL-LIB uses the Kondo/Smith parameterization.

The values of z_{0T} and z_{0q} are determined from the viscous sub-layer model of LKB. They are power-law curve fits to the roughness Reynolds number:

$$\frac{z_{0T}u_*}{\nu} = a_1\left(\frac{z_0 u_*}{\nu}\right)^{b_1} \tag{4.12}$$

$$\frac{z_{0q}u_*}{\nu} = a_2\left(\frac{z_0 u_*}{\nu}\right)^{b_2} \tag{4.13}$$

where the values of a_1, a_2, b_1 and b_2 are given in Table 1 of LKB.

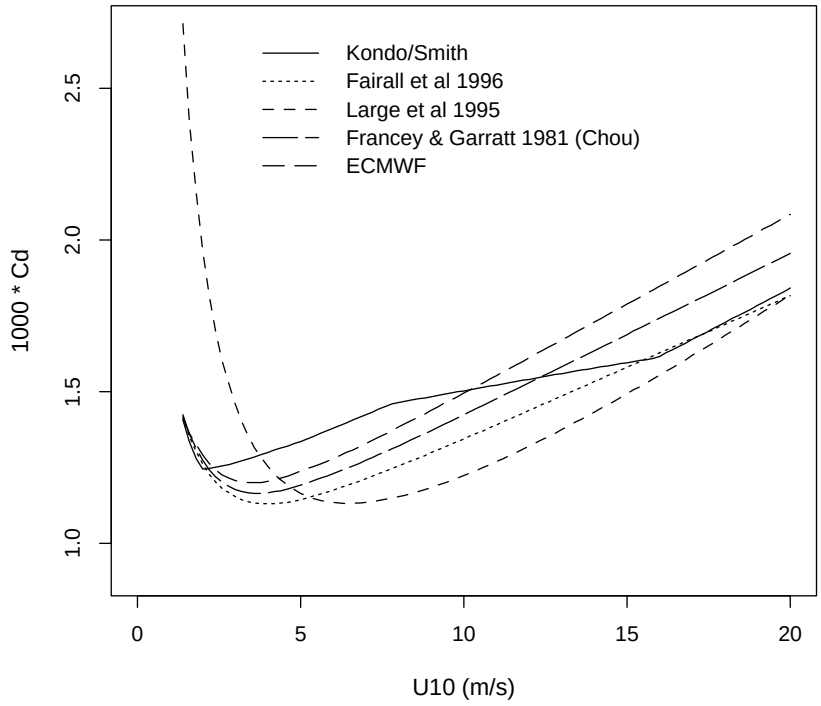

Figure 4.1 The drag coefficient parameterizations of Kondo (1975) as extended by Smith (1989), Fairall et al. (1996), Large et al. (1995), Miller et al. (1991), and Francey and Garratt (1981) which was used by Chou et al. (1995, 1997).

This framework has the important feature of defining transfer coefficients that depend on height, wind speed and stratification. We can see this by substituting Equations (4.4) and (4.2) into (4.1), leading to

$$C_E = \frac{k}{\ln\left(\frac{z}{z_0}\right) - \Psi\left(\frac{z}{L}\right)} \cdot \frac{k_q}{\ln\left(\frac{z}{z_{0q}}\right) - \Psi_q\left(\frac{z}{L}\right)} \tag{4.14}$$

The height and stratification dependence is explicit (z and the Ψ's) but the wind speed dependence is implicitly contained in both the Obukhov length (L) and the roughness length (z_0 and z_{0q}) parameterizations.

We can transform the bulk aerodynamic framework to the LKB formulation of LHF by substituting equations (4.2), (4.4) and (4.14) into equation (4.1), yielding

$$E = -\rho L_v u_* q_* \tag{4.15}$$

The above system of equations (4.2) to (4.13) is non-linear and must be solved iteratively. Required inputs are the surface temperature and one measurement of u, T and q at any height. The bulk aerodynamic formula for LHF is a linearization of the system with a constant z, L, z_0, z_{0T}, and z_{0q}, yielding a constant C_E (equation (4.14)).

It is important to note that (q_0 - q_{10}) and q_* contain the same information. Given two measurements, one can calculate q_*. Given q_* and q_0, one can calculate q_{10}, or q at any other height in the surface layer. In the same way, U_{10} and u_* contain the same information. In fact, since the SSM/I delivers the neutral-equivalent wind speed ($\Psi = 0$) it's even easier to convert to u_*, requiring only an iteration on $z_0(u_*)$.

Note also that as the vector-averaged wind speed approaches zero, the LKB model predicts $u_* \rightarrow 0$ and E $\rightarrow 0$. Consider the case of the wind blowing at 2 m/s for 30 minutes from the West, and then for 30 minutes from the East. Obviously, the LHF in this situation is the same as if it had blown for an hour from the West, not zero as the LKB model predicts. Care must be taken to use the correctly averaged wind speed, especially in conditions of no mean wind but gustiness due to convection above the surface layer, in the mixed layer.

4.4) Gustiness parameterization

The LKB model has the problem that as the mean wind speed falls to zero, it predicts zero flux, contrary to observations. Stated another way, it assumes all the turbulence is generated by near-surface shear, while in conditions of zero mean wind the turbulence is in fact generated mostly by buoyancy. This reflects the fact that even in conditions with no mean wind, there can still be considerable gustiness due to convective processes.

Following Godfrey and Beljaars (1991) a gustiness velocity is combined with the (vector) averaged wind speeds (reported by the ship) to place a lower bound on wind speed:

$$S^2 = u^2 + W_g^2 \tag{4.16}$$

The gustiness velocity is defined as

$$W_g \equiv \beta w_* \tag{4.17}$$

where $\beta^2 = (\sigma_u{}^2 + \sigma_v{}^2) / w_*{}^2$ is a factor to account for averaging times and w_* is the Deardorff (1970) convective velocity scale:

$$w_*^3 = -\frac{g z_i}{\theta_v}(u_* T_* + 0.61\theta u_* q_*) \tag{4.18}$$

where z_i is the inversion height. S is then the speed used in Equation (4.2) in place of *u(z)*. Applying a little algebra shows us that as $U \rightarrow 0$, $S \rightarrow W_g$, which when applied to Equations (4.2)-(4.5) will yield a result equivalent to Stull (1994).

This extension to the LKB parameterization is also used in Fairall et al. (1996), which presented the COARE 2.0 bulk flux algorithm. It is based on the LKB model, but on the basis of several recent experiments including TOGA-COARE, they adjusted some of the empirical constants and added additional physics, including the gustiness velocity correction, an altered form of the stratification corrections to the logarithmic profiles in highly unstable conditions (the Ψ's in Equations (4.2)-(4.4)), a cool-skin and warm layer correction for non-radiative SST measurements, the "Webb" correction to account for the buoyancy of water vapor, and the precipitation sensible heat flux.

Chou et al. (1997) also included this gustiness velocity correction, but found it had a negligible effect on the monthly-average latent heat flux for January 1993, increased by only 1.5 W/m^2. For daily

flux comparisons with the R/V Moana Wave during TOGA COARE, it increased the bias and the r.m.s. difference between the SSM/I LHF and the covariance fluxes by 0.88 and 0.36 W/m^2, respectively. This result is mainly because the SSM/I retrieved wind speed is very seldom less then 1 m/s. Typically, W_g is on the order of 0.5 m/s. Thus its inclusion adds only a small amount to a very small number of daily estimates of LHF, which has a negligible impact on the monthly average.

4.5) Choice of empirical constants

This bulk model framework, often referred to as the LKB model" has many free parameters (empirical constants). We must specify the gustiness parameterization (β and z_i), the 'drag coefficient' model (z_0 as a function of u_*), the parameterization of z_{0q} and z_{0T}, and seven more free parameters (k, k_H, k_E, a_u, a_T, B_u and B_T).

In Chapter 5, I will force this model with the mixed-layer average specific humidity and ECMWF air-sea temperature differences. Therefore, I must pick values of the free parameters that best minimize the r.m.s. differences when using ECMWF air-sea temperature differences, not the ship-sensor T_{10} - SST, compared to the turbulence data. The reason lies in the ECMWF surface layer parameterization. The T_{10} - SST it finds will be based on a certain value of k_H. If I select a different value, I will calculate the wrong T_* and z/L which will result in a flux bias. The value of k_H that minimized the error using ship-sensor data is of no use to my model, since I won't have measured data to input. Therefore, the value I select for k_H should not be used with other than ECMWF temperature data, as it is not the best value to use with "real" data.

There are many proposed sets of constants presented in the literature, each derived from different sets of turbulence measurements through the years. The LKB framework is most sensitive to the choice of k, k_H, and k_E. The other stratification correction constants, and the choice of the parameterization of $z_0(u_*)$, have a second-order effect amounting to only a few W/m^2 under typical conditions. Smith's enhancement of C_D at moderate wind speeds has about a 10% effect. Moreover, the choice of the $z_0(u_*)$ function changes the LHF by a different factor at different values of LHF. The overall mean bias might not change much, as the bias at low fluxes compensates for opposite bias at high fluxes. I have performed extensive tests, evaluating five $z_0(u_*)$ functions to find the one that best fits the turbulence data at all LHF ranges, and determined that the Kondo/Smith drag coefficient with k_H = 0.45 and k_E = 0.41 and the gustiness parameterization is best for this particular application. Again, I stress that this is a special case where I blend ECMWF SST and T_{10} data with ship-sensor U_{10} and q_{10}, and my choices of parameters are only best for these conditions. For driving the LKB model with ship-sensor data alone (no ECMWF data), I found the drag coefficient of Francey and Garratt (1981) with k_H = k_E = 0.4 and no

gustiness parameterization gave the best overall fit. I also found that if using *only* ECMWF data (e.g. PBL-LIB), the best fit was with the Kondo/Smith drag coefficient, $k_H = k_E = 0.45$ and no gustiness parameterization.

Table 4.1 lists the values of Von Karman's constant and its analogs for heat and moisture from various papers, along with the results of comparing the output from the bulk model with the turbulence data from the three ships where it is available. There were 1140 ~1 hour average inertial dissipation estimates and 1041 eddy covariance measurements available. The empirical constants are from Liu et al, (LBK, 1979), Francey and Garratt (FG, 1981), Dyer (D74, 1974), Dyer and Bradley (DB, 1982) and Fairall et al. (F96, 1996). ECMWF T_{10} -SST were used, and only data in the 50 - 150 W/m^2 range only were compared as there are not enough points outside this range to give stable statistics. The error from using the LKB values but with the gustiness parameterization turned off is also listed, for comparison.

Table 4.1 The mean and median errors of the bulk model compared to turbulence data, for various choices of k, k_H and k_E.

		Inertial Dissipation		Eddy Covariance	
Source	k, k_H, k_E	Mean Error	Median Error	Mean Error	Median Error
LKB	0.4, 0.45, 0.45	6.63 W/m^2	4.67 W/m^2	9.18 W/m^2	6.9 W/m^2
FG (Chou)	0.4, 0.36, 0.45	6.15 W/m^2	4.05 W/m^2	8.68 W/m^2	6.21 W/m^2
D74	0.41, 0.41, 0.41	-0.81 W/m^2	-1.17 W/m^2	2.71 W/m^2	1.58 W/m^2
DB, F96	0.4, 0.4, 0.4	-4.74 W/m^2	-5.87 W/m^2	-2.60 W/m^2	-4.34 W/m^2
LKB, no gust	0.4, 0.45, 0.45	1.61 W/m^2	-0.44 W/m^2	4.04 W/m^2	1.28 W/m^2
LKB, real ΔT	0.4, 0.45, 0.45	23.05 W/m^2	23.02 W/m^2	26.17 W/m^2	24.52 W/m^2
Best fit, EC ΔT's, with gustiness	0.4, 0.41, 0.45	-0.30 W/m^2	-1.05 W/m^2	2.64 W/m^2	2.38 W/m^2

By contrast, the model is much less sensitive to variations in a_u, a_T, B_u and B_T, the empirical constants in the stratification corrections. Table 4.2 lists the results of comparing the various sets of constants in the literature. The mean and median biases are within a few W/m^2 of each other, indicating that

the parameterizations of the diabatic corrections agree more closely with each other than the parameterizations of $z_0(u_*)$.

Table 4.2 The mean and median errors of the bulk model compared to turbulence data, for various choices a_u, a_T, B_u and B_T.

	Inertial Dissipation		Eddy Covariance	
	Mean Error	Median Error	Mean Error	Median Error
Kondo	-0.052 W/m^2	-1.62 W/m^2	2.26 W/m^2	0.41 W/m^2
Francey and Garrett (FG)	-0.052 W/m^2	-1.62 W/m^2	2.25 W/m^2	0.41 W/m^2
Dyer and Bradley (DB)	-0.54 W/m^2	-0.93 W/m^2	2.87 W/m^2	1.05 W/m^2
Dyer (D74)	-0.051 W/m^2	-1.62 W/m^2	2.26 W/m^2	0.41 W/m^2
Dyer corrected by Högström	0.23 W/m^2	-1.31 W/m^2	2.55 W/m^2	0.61 W/m^2
Businger et al.	1.35 W/m^2	-0.30 W/m^2	3.71 W/m^2	1.43 W/m^2
Businger corrected by Högström	-0.16 W/m^2	-1.68 W/m^2	2.14 W/m^2	0.14 W/m^2

Fairall et al. (1996) used $\beta = 1.25$ and z_i =600 m, based on an averages from COARE data. I have access in my data sets to the actual inversion and mixed layer heights for each case, from analyzing the soundings. I have tested the sensitivity to z_i of my augmented version of the LKB parameterization and found that knowing the real z_i makes only a small difference, and taking an average value is adequate.

I chose to prioritize matching the inertial dissipation estimates of LHF over matching the eddy correlation measurements. The former relies only the high-frequency data, which should be less susceptible to contamination by the rolling of the ship. I will take $k = 0.4$, $k_T = 0.4$, $k_q = 0.4$, $\beta = 1.25$, the Smith (1988) parameterization of z_0 as a function of u_*, $a_u = a_T = 6$ and $B_u = B_T = 16$ following Kondo (1975), and the LKB parameterizations of z_{0T} and z_{0q}. This fully specifies all the empirical constants. I will also use the same altered form of the Ψ's in the highly unstable limit as Fairall et al. (1996). I will not use any cool-skin or warm layer correction to the SST measurements nor will I include precipitation fluxes, as these are not possible to estimate from my data. The buoyancy of water vapor has already been accounted for in the LKB definition of the Monin-Obukhov length L.

4.6) Augmented LKB scheme performance

For each turbulent observation of LHF by the ship sensors in the data sets from the Moana Wave, the Hakuho Maru and the Malcolm Baldrige, the LHF was calculated using my augmented version of the LKB scheme using the ship's bulk wind speed and humidity and the ECMWF sea and air tempera-

tures as input. This combination of inputs best approximates the final model I will develop in the next chapter. Figure 4.2 shows the difference between the turbulent and bulk latent heat fluxes. Figure 4.3 shows a comparison between the two turbulent estimates of LHF.

These are ‘box plots’, where each dark box encloses the middle half of the data in that bin, the line near the middle of the box is the median for that bin, the dotted line reaches up to 2 times the inter-quartile range (which encloses 96% of a gaussian distribution), and outliers are indicated by dots. The number of points in each bin is printed near the top of the plot. The central box height is not the standard deviation of the distribution, since it encloses 50%, not 66%, of the data, but the concept is the same.

The eddy correlation and inertial dissipation agree with each other in an overall statistical sense (Figure 4.3) with a small mean and median bias. However, there is both about 17 W/m^2 of scatter overall, and systematic biases of the median error in the various range bins. At low fluxes, we expect the covariance method to have problems since small fluctuations are difficult to measure. Occurrences of very high fluxes are too rare to yield stable statistics at the high end.

The LKB bulk scheme agrees with the covariance and inertial dissipation in a statistical sense, since I chose the drag coefficient model and empirical constants such that the LKB model best matched

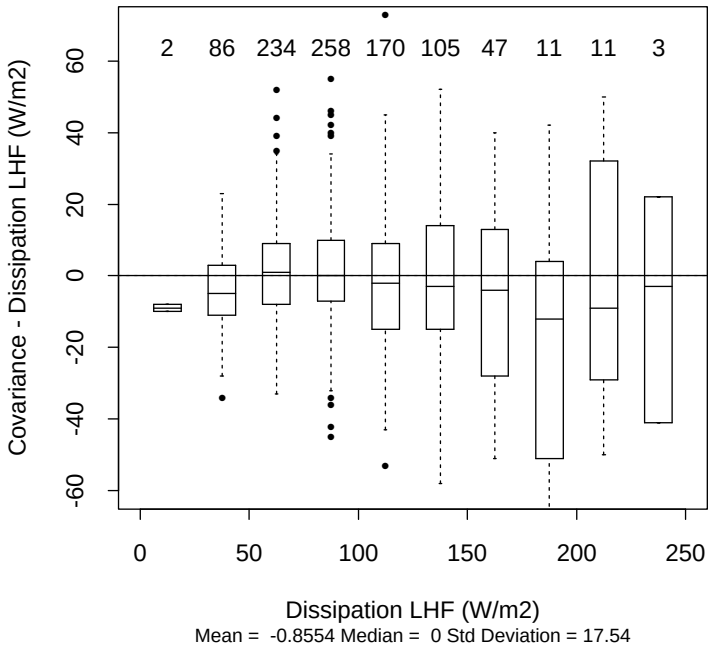

Figure 4.3 Inertial Dissipation vs. Covariance measurements of LHF.

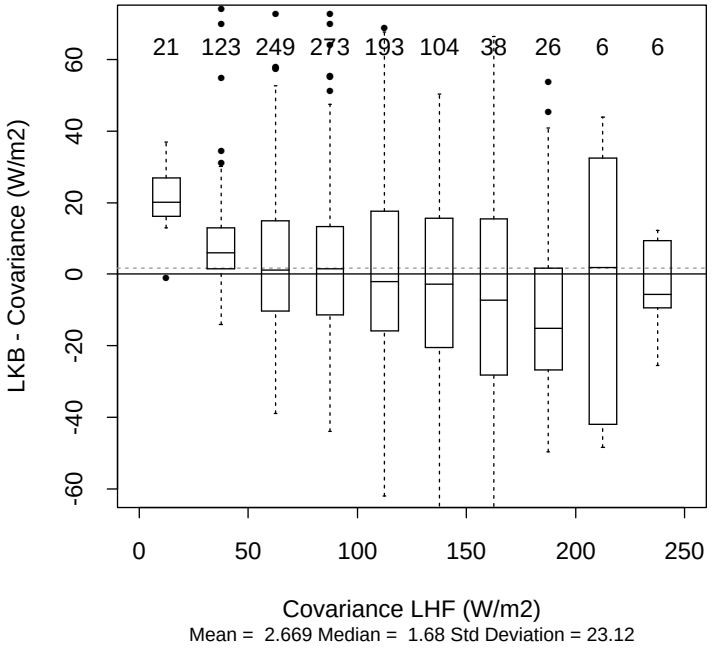

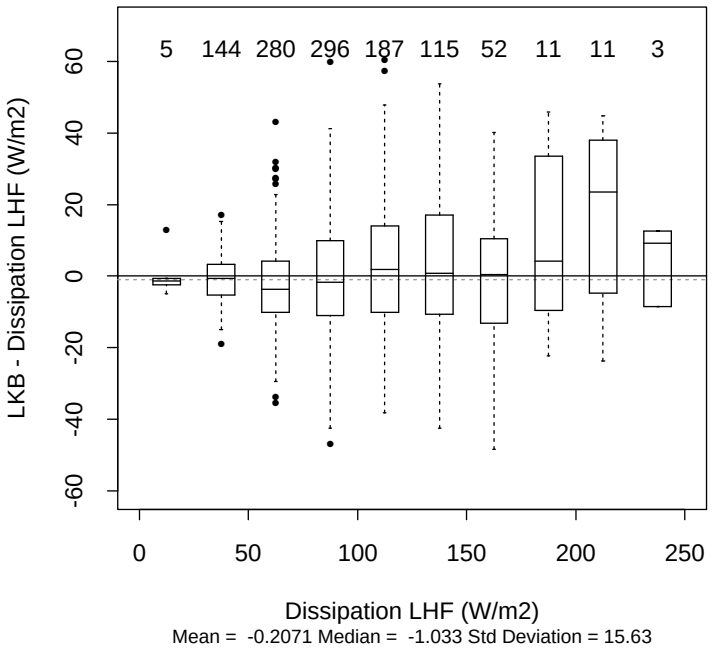

Figure 4.2 LKB bulk parameterization vs. (A) eddy covariance measurements and (B) inertial dissipation estimates of LHF.

the inertial dissipation estimates. However, there is still more than 15 W/m^2 of scatter. The comparison with the eddy covariance measurements shows even more scatter, and considerable biases at the extremes of the range. At the low extreme we don't expect the covariance method to give good results, and at the high extreme there aren't enough points to give stable statistics. In the moderate range, the agreement is reasonable, but is still plagued by large scatter. This reflects the error in measuring LHF by the various methods, and may be unavoidable given the intrinsic accuracy of the sensors and the somewhat non-stationary nature of real-world turbulent boundary layers (Blanc 1989). We would like to be able to measure LHF to within 10 W/m^2 to satisfy climate modelers and to meet the flux accuracy guidelines set by e.g. the COARE working groups (Webster and Lukas, 1992). This goal can only be met on a statistical basis, not an instantaneous one.

4.7) LKB sensitivities

Since LHF has a global mean of near 100 W/m^2 (standard deviation about 60 W/m^2), to find the LHF to within 10 W/m^2 requires at most a 10% error in any of the terms of equation (4.1), the bulk aerodynamic equation. If the errors are uncorrelated, the total variance will be the sum of the individual variances. The density ρ is not likely to be the chief source of error as an error of 10 mb or 3 K leads to only a 1% error in ρ, and analyses are probably within those errors. Similarly, L_v (units of J/kg) can be calculated from air temperature in degrees C using the expression from Bolton (1980):

$$L_v = (2.501 - 0.00237 T_c) \times 10^6 \tag{4.19}$$

to a high degree of accuracy.

Figure 4.4 shows the error due to a changes in the input variables to the LKB parameterization estimates of LHF equation for a range of SSTs and wind speeds. T_{10} was taken to be SST - 1.25 K, and q_{10} was taken as 75% of the saturation at the SST. This figure is similar to Figure 1.2, except that the air temperature is included here, since the LKB LHF is a (weak) function of air temperature while the bulk aerodynamic formula (BAF) is not. Again, the sign of the changes in the input variables were taken such that the difference in LHF was positive. The sensitivities of the LKB scheme are similar to BAF, but slightly diminished. For example, under tropical conditions (high SST, low wind speed) the error in LHF due to a 1 g/kg error in q_{10} is about 25 W/m^2. For typical midlatitude (tropical) conditions, the error in the LHF calculation due to a 1° error in SST is about 15 (30) W/m^2, indicating we need to measure SST to within 0.7 (0.3) K. This assessment agrees with the Fairall et al. (1996a) constraint of 0.2 K for the Pacific warm pool. The sensitivity to a unit error in wind speed is less, ranging from about 5 W/m^2 near the ice edge to about 20 W/m^2 in the warm pool. By contrast, the sensitivity to air tempera-

ture errors is very small, less than 6 W/m^2 for all conditions. The sensitivity to errors in sea level pressure (not shown) is a maximum of about 0.9 W/m^2/mb at low wind speeds in the tropics.

Figure 4.5 shows the effect of the choice of roughness length parameterizations (the $z_0(u_*)$ function, which essentially specifies the form of the drag coefficient). The functions are from Francey and Garratt ("FG", 1981), Miller et al. ("ECMWF", 1991), Large et al. ("Large" 1995), Fairall et al. ("Fairall" 1996) and Kondo ("Kondo/Smith" 1975). The differences due to drag coefficients at low wind speeds are all due to different choices for the "Charnock constant" α, except for Large et al. (1995)

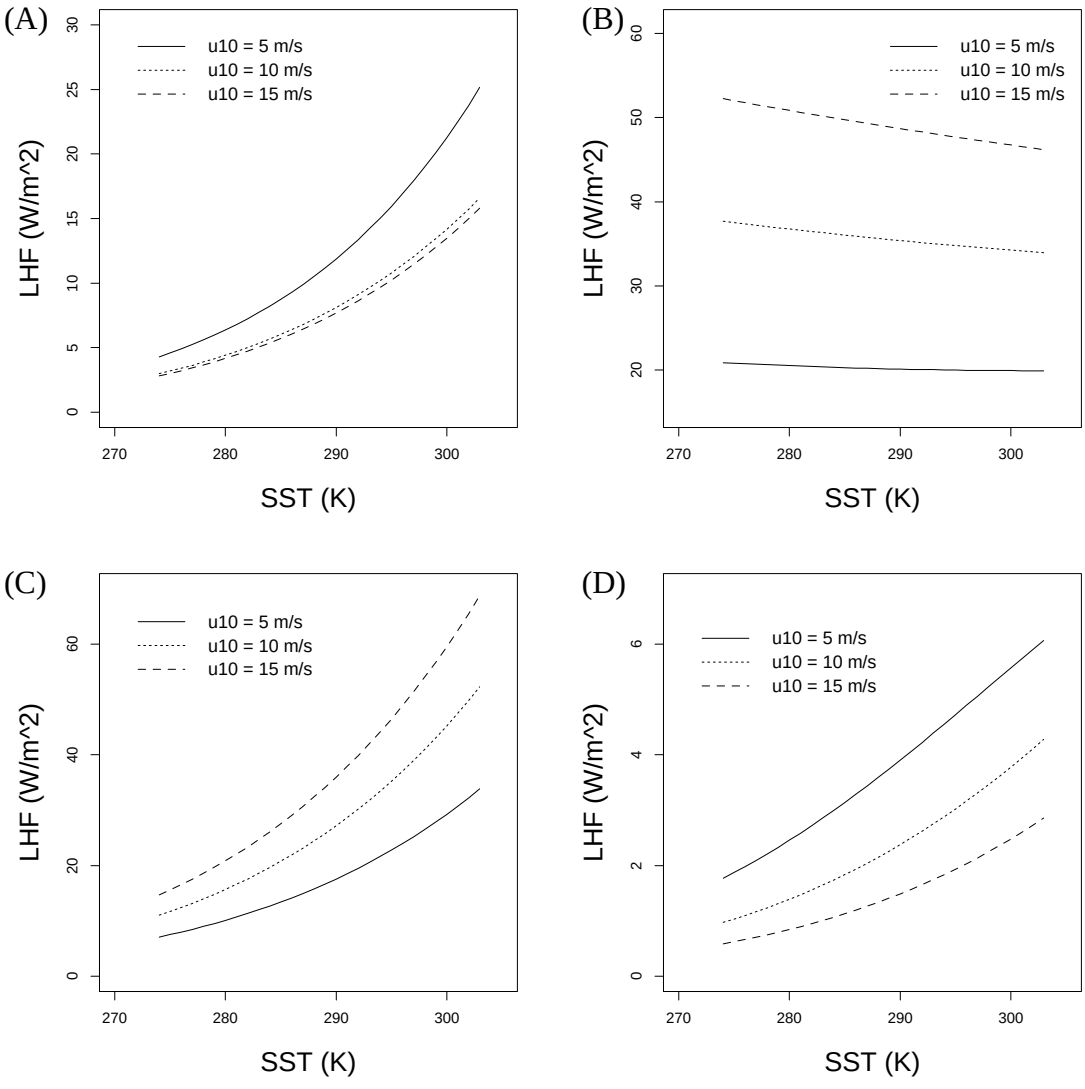

Figure 4.4 Error in LHF from the LKB parameterization, as a function of SST and wind speed, for unit errors in (A) wind speed (m/s), (B) specific humidity (g/kg), (C) sea surface temperature (K), and (D) air temperature (K).

which parameterized u_* directly in terms of a 3-term geometric series of U_{10}. At low wind speeds, it is often difficult to take reliable measurements, resulting in a larger scatter of data, such that each of the drag coefficient parameterizations fits the data equally well. Also shown in the difference in LHF calculated with two common choices for k_H and k_E (LKB used 0.45, 0.45; FG used 0.36, 0.45). Differences due to k_H are negligible, but differences due to k_E far outweigh differences in the drag coefficient, the latter being only a few W/m^2.

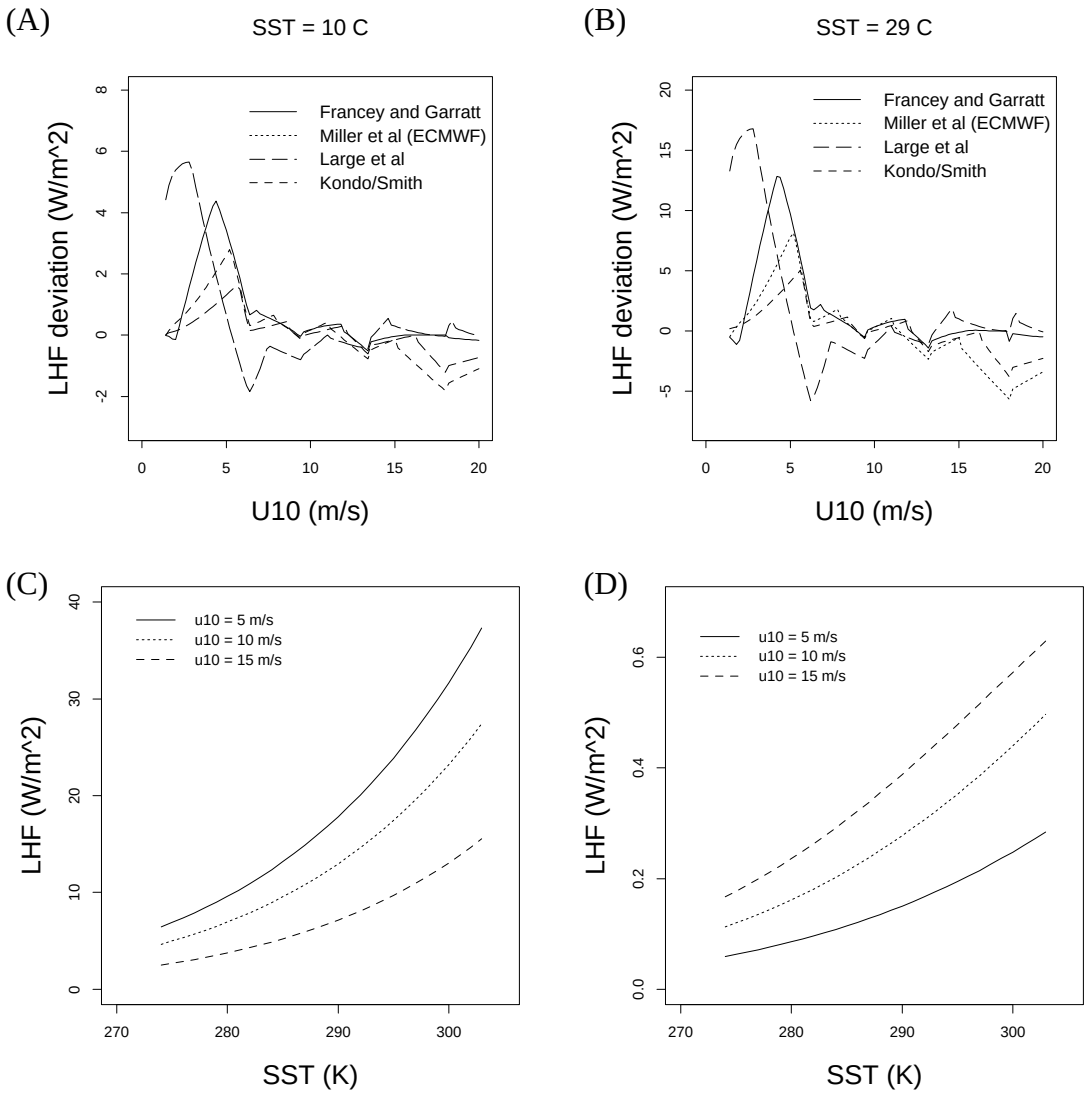

Figure 4.5 Comparison of different choices of roughness parameterization and von Karman's constant. Plotted is the difference between each LHF calculation using the stated roughness parameterization and that of Fairall et al. (1996), for (A) SST = 10° C and (B) SST = 29° C. See text for citations.

4.8) Summary

This chapter discussed a few methods of calculating latent heat flux across the air-sea boundary, and focussed more closely on two methods: the bulk aerodynamic method and the Liu-Katsaros-Businger (LKB) model. The equations that make up the LKB model were presented, and empirical constants chosen from the literature. The problem of LKB's prediction of zero fluxes at zero mean wind, contrary to observations, was resolved with a parameterization of the gustiness due to convection in the ML following Fairall et al. (1996). The performance of my augmented version of LKB was tested against eddy covariance measurements and inertial dissipation estimates of LHF taken aboard research vessels. The modified LKB scheme had a comparable standard error when compared with the other two than they have when compared to each other.

The sensitivity of the LKB model to errors in the input parameters was assessed. The impact of different choices of the Von-Karman constants, the roughness parameterization, and the stratification corrections was assessed. These sensitivities will be used in later chapters in an error budget analysis of SSM/I LHF.

For globally averaged conditions, the LKB model is most sensitive to errors in the input values for specific humidity (q_{10}), followed closely by SST. However, in the tropics the error associated with errors in SST increases while the error associated with errors in q_{10} decreases. Errors associated with unit errors in U_{10} are about 5 times smaller than q_{10} errors (unit errors are 1 m/s and 1 g/kg, respectively). Unit errors in T_{10} and especially SLP are smaller still, with a maximum of about 6 W/m^2/K and 1 W/m^2/mb, respectively. Uncertainty associated with choosing a roughness parameterization are a maximum at low wind speeds, amounting ~3 W/m^2 at SST = 10° C and ~10 W/m^2 at 29° C. At moderate wind speeds the differences are smaller, but rise again at higher wind speeds to ~2 W/m^2 at 10° C and ~8 W/m^2 at 29° C.

To use the LKB model to estimate LHF with 10 W/m^2 requires errors in SST of less then 0.3 K, errors in q_m of less than 0.3 g/kg, errors in U_{10} of less than 1.2 m/s, and correct knowledge of the von Karman constant for humidity.

Chapter 5

A Simple Model for the Lower Boundary Layer

In this chapter I will derive a simple model for the lower part of the planetary boundary layer. I will show how this model is consistent with the new statistical retrievals of W_B and q_m, and show how the latent heat flux (LHF) at the surface can be calculated from satellite data.

5.1) Model formulation

Liu (1986), Miller and Katsaros (1992), Schulz et al. (1993), Schlüssel et al. (1995), Chou et al. (1995, 1997) and Clayson and Curry (1996) have all used the lowest level of various collections of radiosonde reports to derive statistical relations to estimate the surface LHF. I have shown in Section 2.5 that serious biases and increased scatter could result from using the lowest sounding level report without first verifying its accuracy. One of the strengths of this dataset is the high-quality ship observations coincident with the soundings.

I therefore seek a relationship between the surface LHF *from ship-based observations* and a quantity that is accurately measured by *both* radiosondes and satellites, namely W_B and q_m. Rather than a statistical relationship between the two, I will use the already well-established theory for the surface layer, the Liu et al. (1979, hereafter LKB) formulation of Monin-Obukhov similarity theory, with my choice of empirical constants as outlined in Section 4.5.

A simple model for the lowest ~500 m of the boundary layer is to patch a well-mixed layer to an LKB surface layer in a continuous fashion. Profiles of specific humidity (q) and potential temperature (θ) follow the LKB profiles from the surface to the patch height Z_p and are constant above that height. A schematic of the proposed model is presented in Figure 5.1. Z_p, the "top of the log-layer", can be estimated as $\lambda\delta_{\text{Ekman}}$ from Brown and Liu (1982), or as $0.1 \bullet Z_m$ (e.g. Stull 1994), or as a function of the Obukhov length L (e.g. Stage and Businger 1981) or taken to be a constant.

In this model, the 'mixed-layer' value of humidity (q_m) and potential temperature (θ_m) can be determined by evaluating the logarithmic functions at Z_p, just as the values at 10 m can be predicted by evaluating the logarithmic functions at 10 m. The idea is that the surface layer adjusts to the forcing from

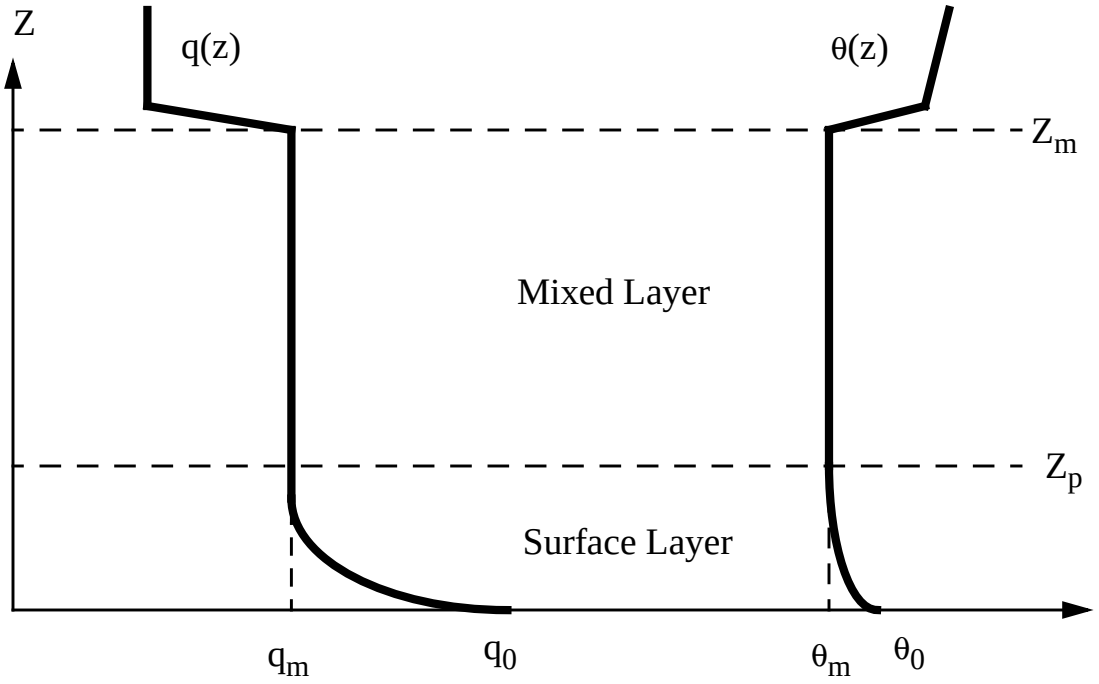

Figure 5.1 Schematic diagram of the proposed model (heights not to scale).

above and below, connecting the mixed layer to the surface values by adjusting the parameters u_*, T_* and q_* to yield a smooth profile.

Some similar models have been presented in the literature, though none have been applied to conditions other than moderate to strong convection. Leovy (1969) suggested that the sensible heat flux should be dependent on the bulk temperature difference between the mixed layer and the surface. He argued that since the height of the surface layer depends mainly on the roughness length (Z_p can move up and down without affecting θ_m) the flux should not depend explicitly on the roughness length. Stage and Businger (1981) used a very similar model to study the fluxes associated with cold-air outbreaks over the Great Lakes. They simply patched a well-mixed layer to the LKB surface layer model and assumed the height of the surface layer was Z_p= -10 L, which they felt was only justified under strongly convective conditions. Stull (1994) presented a model for surface fluxes under convective conditions that is also similar. He hypothesized that the fluxes should depend on the bulk difference of θ and q between the mixed layer and the surface, and not on the surface roughness or the height of the surface layer. He proceeded by applying similarity theory in a parallel way to Monin-Obukhov similarity theory, and derived values for his new drag coefficients from the BLX83 field experiment.

The boundary conditions to the LKB model must be specified. The LKB formulation of the surface layer equations requires specification of the set of input variables (u, T, q, SST). The SSM/I retrieves the wind at 10 m (U_{10}) which will be used directly as u. The Reynolds and Smith (1994) Optimally Interpolated sea surface temperature product (OI SST) is largely forced by AVHRR retrievals of SST and will be used. There is no global satellite retrieval of T available, but we have several options. We can take T = SST (equivalent to neglecting the sensible heat flux, $T_* = 0$), use a climatological value for the air-sea temperature difference, or use ECMWF analyzed air-sea temperature differences. The impact of various choices of T is taken up in Section 5.2.1. The remaining task is the calculation of q_*. First I will derive an analytic relationship between W_B and q_m, then I will show how to use either the retrieval of W_B or q_m from Section 3.10 to finish specifying the LKB model's boundary conditions.

5.1.1) An analytical relationship between W_B and q_m

As far as its impact on the integral W_B, the difference between $q(z)$ in the logarithmic layer and q_m is negligible above about 5-10 m, allowing the approximation in the definition of W_B

$$W_B \equiv \int_0^{500m} q(z)\rho(z)dz \;\cong\; q_m \int_0^{500m} \rho(z)dz \tag{5.1}$$

The last term can be integrated using the equation of state for an ideal gas, the hydrostatic assumption (e.g. Brown 1991) and the fact that the layer is assumed to be isentropic:

$$\int_0^{500m} \rho dz \;=\; \frac{P_0}{g}\left[1-\left(1-\frac{500g}{c_p\theta_m}\right)^{\frac{c_p}{R_d}}\right] \tag{5.2}$$

where c_p is the specific heat at constant pressure and R_d is the gas constant for dry air, g is the acceleration due to gravity, and P_0 is the surface pressure. We can now find a relationship between the mixed-layer average specific humidity (q_m) and the bottom-layer integrated water vapor (W_B) by substituting equation (5.2) into (5.1) and solving for q_m.

$$q_m \;=\; \frac{gW_B}{P_0}\left[1-\left(1-\frac{500g}{c_p\theta_m}\right)^{\frac{c_p}{R_d}}\right]^{-1} \tag{5.3}$$

Equation (5.3) relates the bottom-layer water vapor (W_B) to the mixed-layer average specific humidity (q_m). Since both W_B and q_m can be retrieved from SSM/I and SST measurements, the extra step of using equation (5.3) is only needed for one of these retrievals.

Equation (5.3) neglects the excess moisture in the surface layer, and will likely be biased low compared with real measurements of q_m. This bias should increase with increasing SST, but can be removed with a little extra computation. First, solve the LKB equations with the retrieval, such that the profile of humidity is known. Then, integrate this profile to the patch height and add the result to W_B and re-solve the LKB equations to find the LHF. Figure 5.2 shows the result of such a procedure.

5.1.2) q_* from mixed-layer values

To find the LHF, we need q_*. To do this, we simply invert the surface-layer equation for q (equation (4.4)) and evaluate it at the top of the logarithmic layer (z = Z_p)

$$q_* = \frac{k_q(q_m - q_0)}{\left[\ln\left(\frac{Z_p}{z_{0q}}\right) - \Psi\left(\frac{Z_p}{L}\right)\right]} \tag{5.4}$$

That is, q_* is calculated from the mixed-layer-to-surface humidity difference, as opposed to the more traditional 10-m-to-surface humidity difference. Of course, L and z_{0q} are both functions of u_* and T_*, so

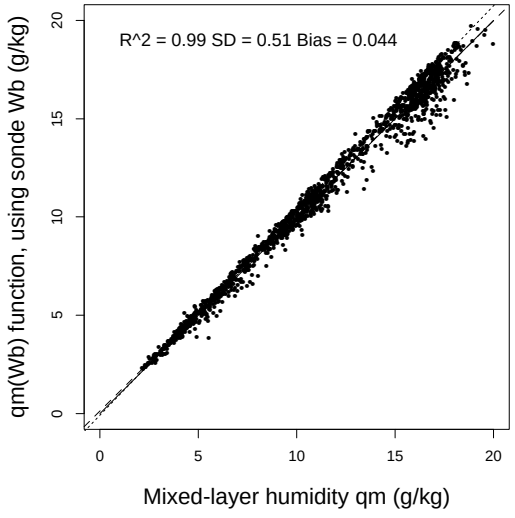

Figure 5.2 The mixed-layer average humidity (q_m) as measured by the sonde vs. as predicted by equation (5.3) corrected by integrating the surface layer humidity and summing.

we must still use an iterative method to solve for the combined input set of ($U_{SSM/I}$, T, $q_{m,SSM/I}$, $SST_{OI(AVHRR)}$). Choices for T will be discussed in Section 5.2.1.

The success of this model will depend on how closely the relationship between q_m and q_* approximates the relationship between q_{10} and q_*.

For each sounding in the data set, the time-interpolated ship-board measurements of SST, wind speed, temperature and specific humidity were used to calculate T_* and q_* using the LKB scheme. The output is labelled “Ship Sensor” in the following plots. Each sounding’s analyzed value of q_m and θ_m were then used along with the ship-board measurement of SST and wind speed to calculate T_* and q_* from the same augmented version of the LKB scheme. The output is labelled “Mixed Layer” in the following plots. A constant Z_p = 75 m was used, but the results for Z_p = 50 m are very similar (but with a slightly larger bias).

Figure 5.3 compares the results of these two calculations, along with the squared linear correlation coefficient, the standard error, and the mean bias. Since I am most interested in q_*, I am happy to note the high correlation coefficient and the general shape of the scatter in Figure 5.3 (A). The magnitude of q_* calculated from the mixed-layer averages is slightly larger than that calculated from the ship sensors, and the difference increases with increasing magnitude of q_*. Since this method essentially fits the surface-layer logarithmic profile to two points (the surface and one point at ~15 m) any error in the sensor will be amplified by extrapolating the profile to the patch height and we should expect some scatter. Fig-

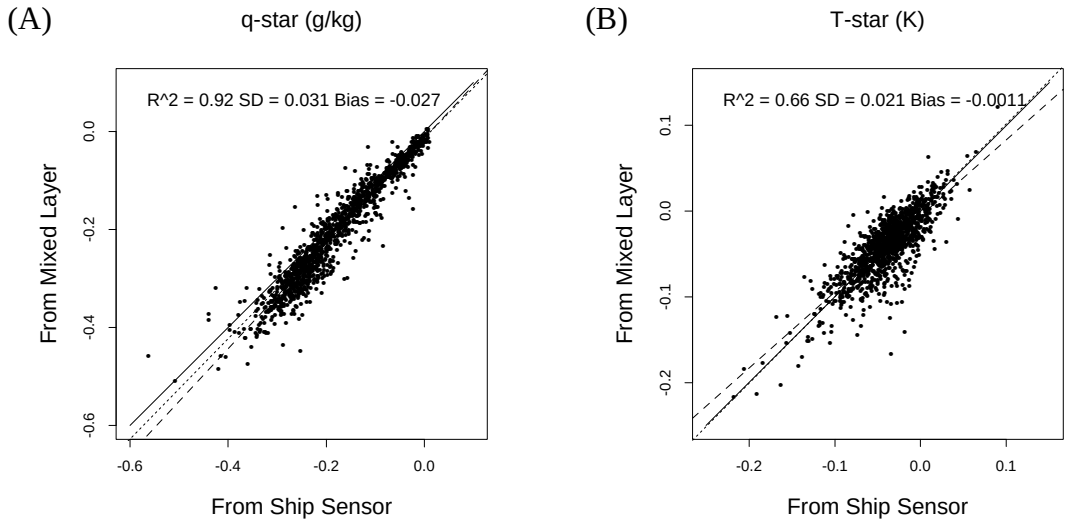

Figure 5.3 (A) q_* and (B) T_* calculated from ship-board q and T sensors vs. from mixed-layer averages, both using ship-board wind speed sensors.

ure 5.3 indicates that q_m and q_* are indeed related via the LKB surface layer equations, to within about 10%. There appears to be a systematic difference at higher $|q_*|$ values, perhaps even a regime shift. The reason for this change in behavior is not known. An equivalent test is to use the ship sensors to solve the LKB equations and then evaluate them at the patch height, yielding a prediction of q_m.

5.2) Model limitations

5.2.1) No Satellite retrieval of air temperature

There have been a few attempts to retrieve T_{10} from satellites. TOVS has a retrieval of air temperature, but it does not retrieve a value sufficiently close to the surface for the problem at hand. Clayson and Curry (1996) developed a scheme to predict T_{10} - SST based upon a correlation between a cloud classification developed specifically for TOGA-COARE and measurements aboard the Moana Wave. The standard error of their prediction was 0.6° C. Jourdan and Gautier (1995) determined T_{10} from a statistical regression on *W*, with a standard error of 1.88° C. Konda et al. (1996) predicted T_{10} from Liu's regression of q_{10} on *W* with the assumption of a constant relative humidity, with a standard error of 1.5° C. For comparison, the standard error of assuming T_{10} = SST - 1.25 for my globally distributed data is 1.0° C, and falls to 0.73° C for the Moana Wave data, as used in Clayson and Curry (1996).

Since no accurate and globally valid satellite retrieval of near-surface air temperature is available, the severity of this limitation must be assessed. I calculated q_* using (U_{ship}, T_{ship}, q_{ship}, SST_{ship}) as inputs, labelled "Ship sensors"; and using (U_{ship}, T_{ship}, $q_{m,sonde}$, SST_{ship}), labelled "Ship T_{10} - SST". The results are shown in Figure 5.4 (A).It shows that substituting T_{10} measured in the bottom of the surface layer for a temperature measured in the mixed layer (with appropriate heights input as well) produces an equivalent q_*. The simplest possible solution to our lack of a satellite temperature retrieval is to use a climatological air-sea temperature difference. Figure 5.4(B) shows the q_* calculated using the mixed layer q_m and T_{10} -SST = 1.25 K, compared with that derived from the ship sensors. The similarity to (A) is striking. Still, that may be due to a fortuitous sampling of soundings where the r.m.s. scatter about 1.25 is small. Figure 5.4(C) shows a similar plot, but using ECMWF T_{10} -SST. The persistent offset can be removed by reducing the mixed-layer $q_* < -0.2$ by 5% (dividing by 1.05), as shown in Figure 5.4(D).

5.2.2) Mixed layer depth less than 500 meters

Another problem associated with using the retrieval of W_B to find q_m (via equation (5.3)) is the arbitrary assumption that the mixed layer is at least 500 m in depth. If it is not, the assumption in Equation (5.1) is not valid, and the derived W_B:q_m relationship is suspect. Fortunately, when the mixed layer is

less than 500 m deep, the humidity above the mixed layer is usually not too different from q_m and the impact is relatively small. In these cases, W_B will be smaller, causing q_m to be smaller, which leads to a higher calculated LHF. Figure 5.5 shows LHF calculated from $W_{B,\mathrm{sonde}}$ minus LHF calculated from the ship sensors, as a function of mixed layer depth. Calculations based on the q_m SSM/I retrieval instead of the W_B retrieval are of course free from this limitation.

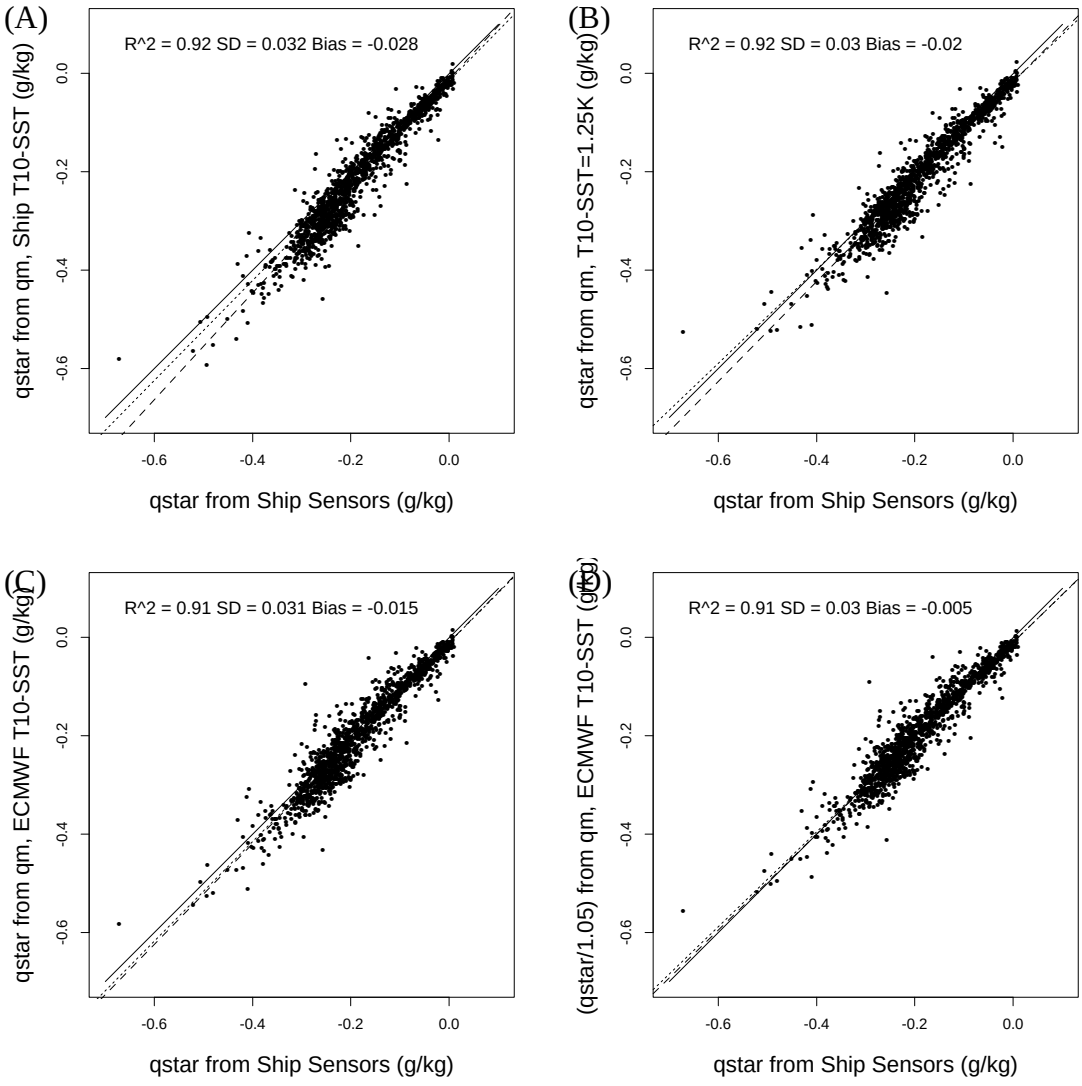

Figure 5.4 q_* calculated from ship sensors vs. from q_m with (A) ship T_{10}-SST, (B) T_{10}-SST =-1.25, (C) ECMWF T_{10}-SST, and (D) with ECMWF T_{10}-SST but reduced by 5% (q_* divided by 1.05).

5.3) Model Performance

There are 3 sources for reference LHF: eddy correlation measurements: inertial dissipation estimates, and the LKB model acting on bulk (ship sensor) data. There are two ways to force the model, with q_m, and with W_B via equation (5.3). There are also 3 sources for input data q_m and W_B: direct from the soundings, from the regressions operating on W integrated from the soundings, and from the regressions operating on W retrieved by the SSM/I. Additionally, there are two sources for SST for each calculation (ship and OI SST) and two sources for U_{10} (ship and SSM/I). That gives 72 possible combinations to assess the accuracy of the model. Obviously, I will focus only on a few combinations.

Since only 3 ships had turbulence data, certain combinations are not statistically significant and will not be shown. Additionally, the number of SSM/I-sounding pairs that met the match-up criteria is much smaller than the total number of soundings, and will not be shown. Instead, match-ups between the SSM/I and the ship-sensor time series from each ship were found, q_m and W_B were statistically derived from W and OI SST, and used to calculate LHF. This procedure led to 1415 calculations using the q_m-method, and 1454 calculations using the W_B-method.

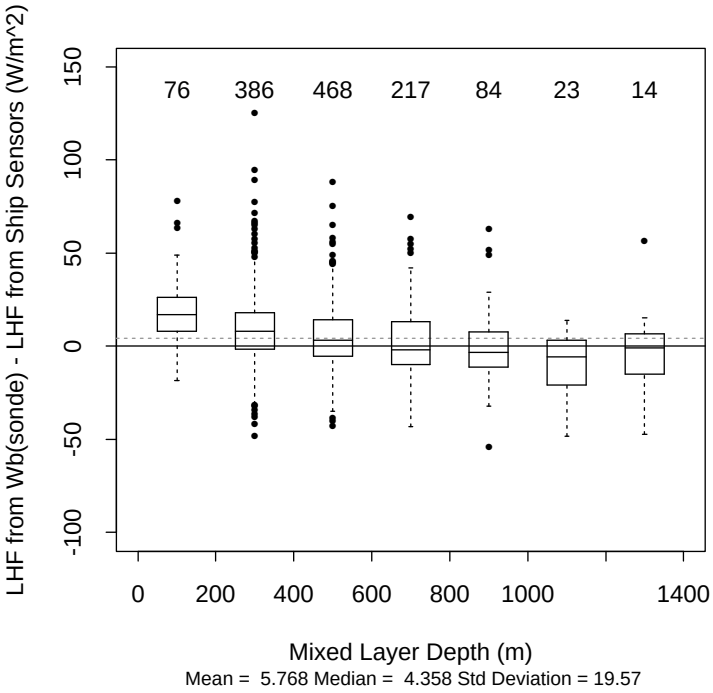

Figure 5.5 The error in LHF derived from W_B measured by the sondes as compared to LHF measured by the ship sensor, as a function of mixed-layer depth.

In the following plots, the left ones will show data using the q_m retrieval, and the right one using the W_B retrieval. All calculations were made using ECMWF air-sea temperature differences, $k_E = k_H = 0.4$, and the Kondo/Smith drag coefficient.

Figure 5.6 (A) and (B) show the LHF calculated using q_m and W_B analyzed directly from each sounding, the ship SST, T_{10} and U_{10}, vs. the LHF calculated from the LKB model using the ship sensor data. The q_m-method has a smaller scatter than the W_B-method, which has some residual high bias at low fluxes. These plots represent the minimum error of the mixed-layer method, with zero errors in

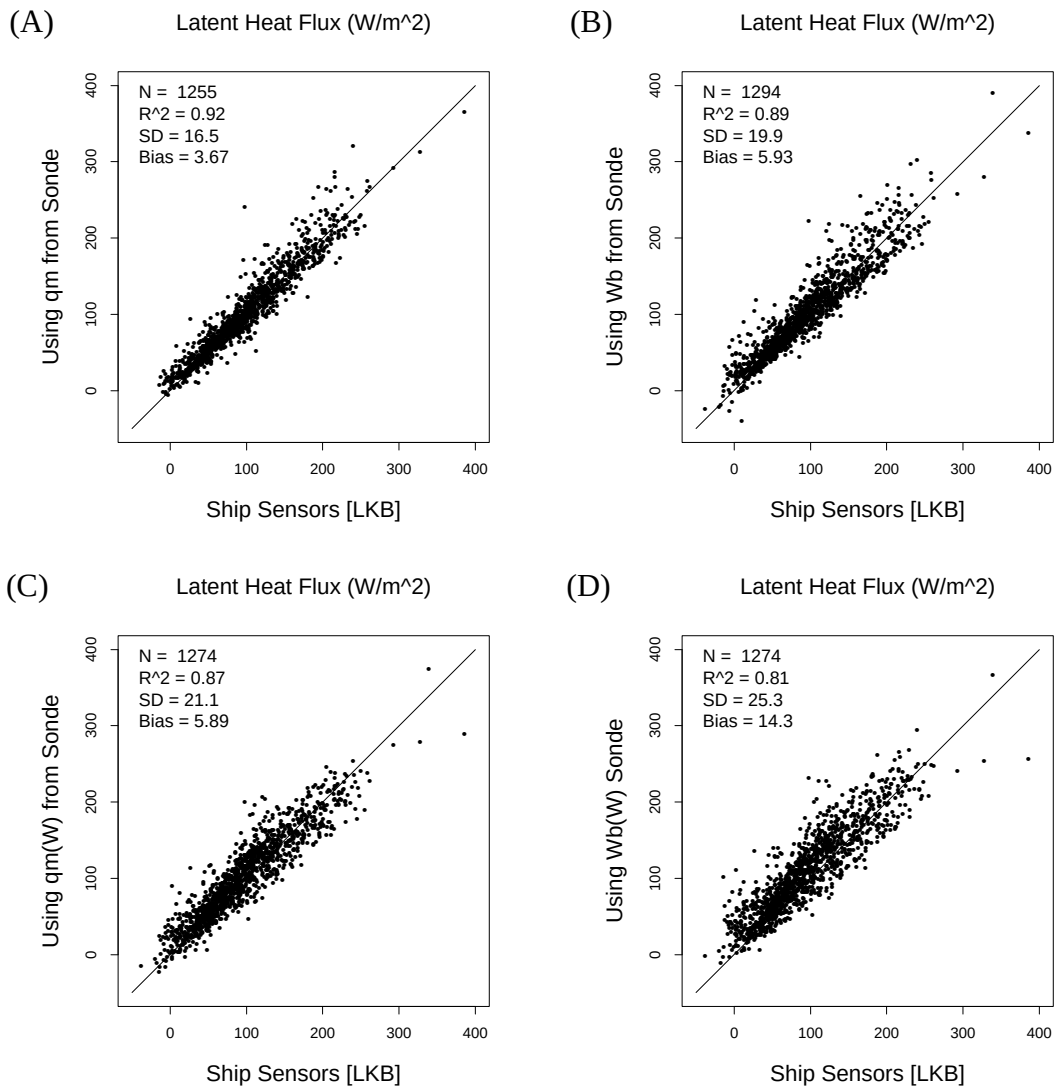

Figure 5.6 LHF from q_m (A and C) and W_B (B and D) directly analyzed from the soundings (A and B) and statistically retrieved from the soundings (C and D), vs. from the ship-board sensors (using LKB).

input variables. The scatter is about the same as the scatter of the LKB method compared with turbulence data, indicating the general success of the method. The error incurred using this method is equivalent with the inherent error in the LKB model. Some of the error in these plots is due to the sampling error of the sonde, which is a point sample of the natural variability of the mixed layer, 0.2 - 0.3 g/kg (Chris Bretherton, personal communication). This natural variability is on the same order as the error in the sonde humidity sensors (3%), leading to a calculated error (from the sensitivity of the LKB model) of 15 (6) W/m^2 at low (high) winds. The mean bias is affected by the outlying points, and is a little larger than optimal, but still acceptable.

Figure 5.6 (C) and (D) show the same comparison as (A) and (B), but using the regressions operating on *W* integrated from the soundings. The statistical retrievals of q_m and W_B add about 4 and 5 W/m^2 to the scatter, and about 2 and 8 W/m^2 to the bias, respectively. Since some of the soundings no doubt represent rainy conditions where the SSM/I retrievals are not valid, this enhances the scatter and bias to an unknown extent.

Figure 5.7 shows the LHF calculated using q_m (left panels) and W_B (right panels) from the retrieval method using *W* from collocated SSM/I retrievals. The upper panels show the LHF calculated using the ship wind speeds, and the lower panels with U_{10} retrieved by the SSM/I. OI SST's were used in all four calculations. The combined effect of the OI SST's and the SSM/I *W*'s yields another 9 (6) W/m^2 added to the scatter, but reduces the biases by 1 (16) W/m^2 for the q_m (W_B) method. The reason for the striking decrease in the bias of the W_B method is because I forced the distributions of sonde *W*'s to have zero bias compared to the collocated SSM/I *W*'s when developing the regressions by increasing the sonde *W*'s by 5.5%. Both methods have a tendency to under-predict the flux above 250 W/m^2, though the q_m method behave a bit better than the W_B method. There are no turbulence fluxes in that range of my data set, so we can't be sure the LKB method is correct either.

The lower panels of Figure 5.7 show the full model as it will be applied to calculate climatologies, compared with collocated LKB estimates of LHF. These graphs show the LHF calculated using real SSM/I retrievals of U_{10} and *W*, statistically retrieved q_m and W_B, Reynolds Optimal Interpolation SST's (largely controlled by AVHRR), ECMWF SLP and T_{10} -SST. The addition of the SSM/I U_{10} measurements adds another 7.5 (5.6) W/m^2 of scatter, and decreases the bias once again by 3 (8) W/m^2 for the q_m (W_B) method. There is a pronounced low bias of the W_B method at LHF > 200 W/m^2. For the 66 points with ship LHF > 200 W/m^2, the mean bias is -75 W/m^2 and an r.m.s. scatter of 40 W/m^2, while the rest of the points have a mean bias of -5.8 W/m^2 and an r.m.s. scatter of 32 W/m^2. The q_m method has a low bias in the high LHF range of 42 W/m^2 for this comparison. These biases stem from the error

in the statistical retrievals of q_m and W_B, in that they are biased high (low air-sea humidity difference) at high values of *W*. This is directly related to the decoupling of the upper atmosphere from the surface layer in the deep tropics, where the total water in the air column can continue to increase without changing the mixed-layer humidity. Theses changes are weakly correlated with changes in SST, as discussed in section 3.10, page 41, but not enough to greatly affect the retrieval function.

Finally, Figure 5.8 compares the eddy correlation (top panels) and inertial dissipation measurements (bottom panels) with the retrieved LHF using the full q_m (left panel) and W_B (right panel) meth-

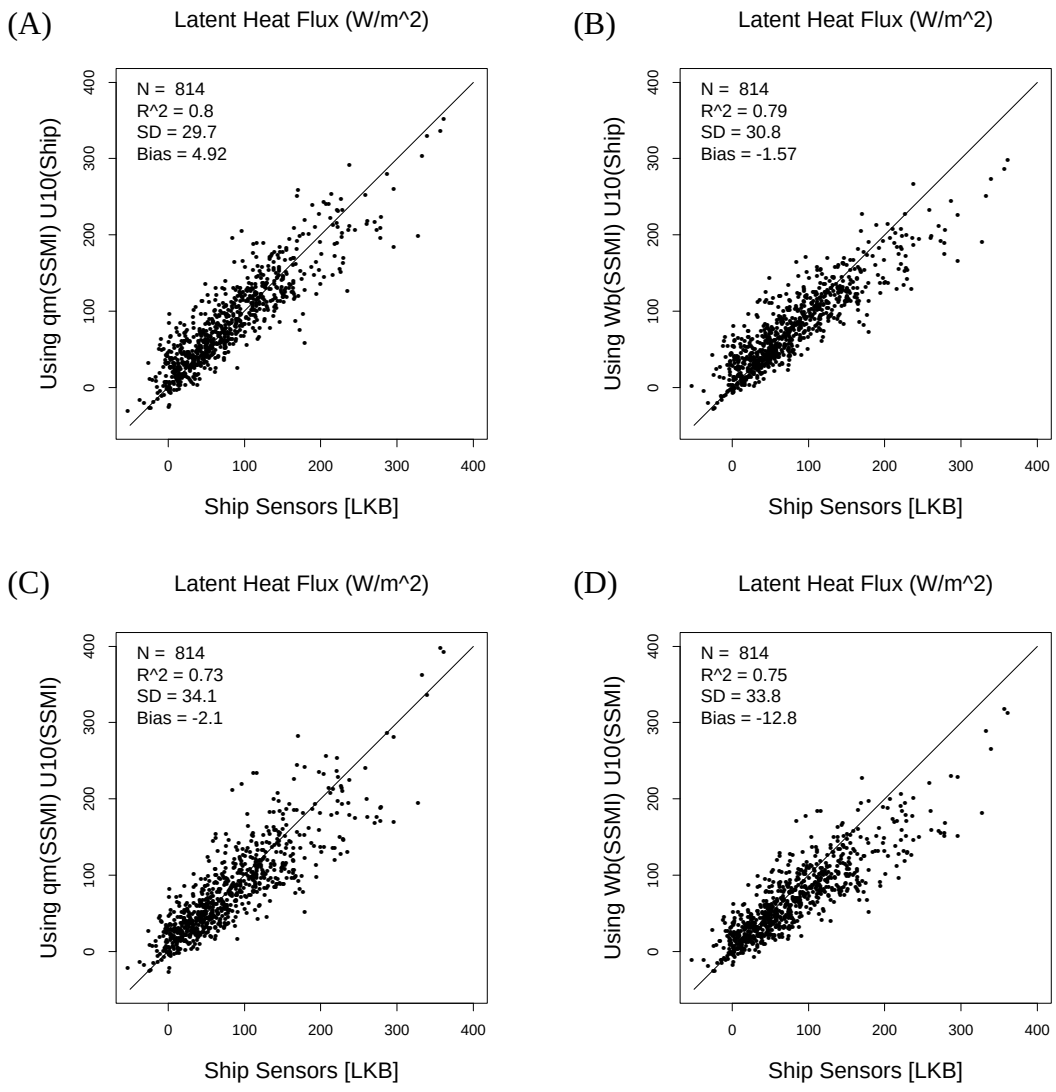

Figure 5.7 LHF from the retrievals of q_m (A and C) and W_B (B and D) using *W* directly integrated from the soundings (A and B) and retrieved by the SSM/I (C and D) vs. ship-board sensors (using LKB).

ods: U_{10} from the SSM/I, q_m and W_B statistically retrieved from SSM/I *W*, and Reynolds OI SST products. The range of the turbulence data is much smaller, and the number of collocations is also greatly reduced since only three ships had both bulk and turbulence data capabilities. The mean biases are higher than when compared with the LKB estimates, but the number of points is so low that the differences are not statistically significant.

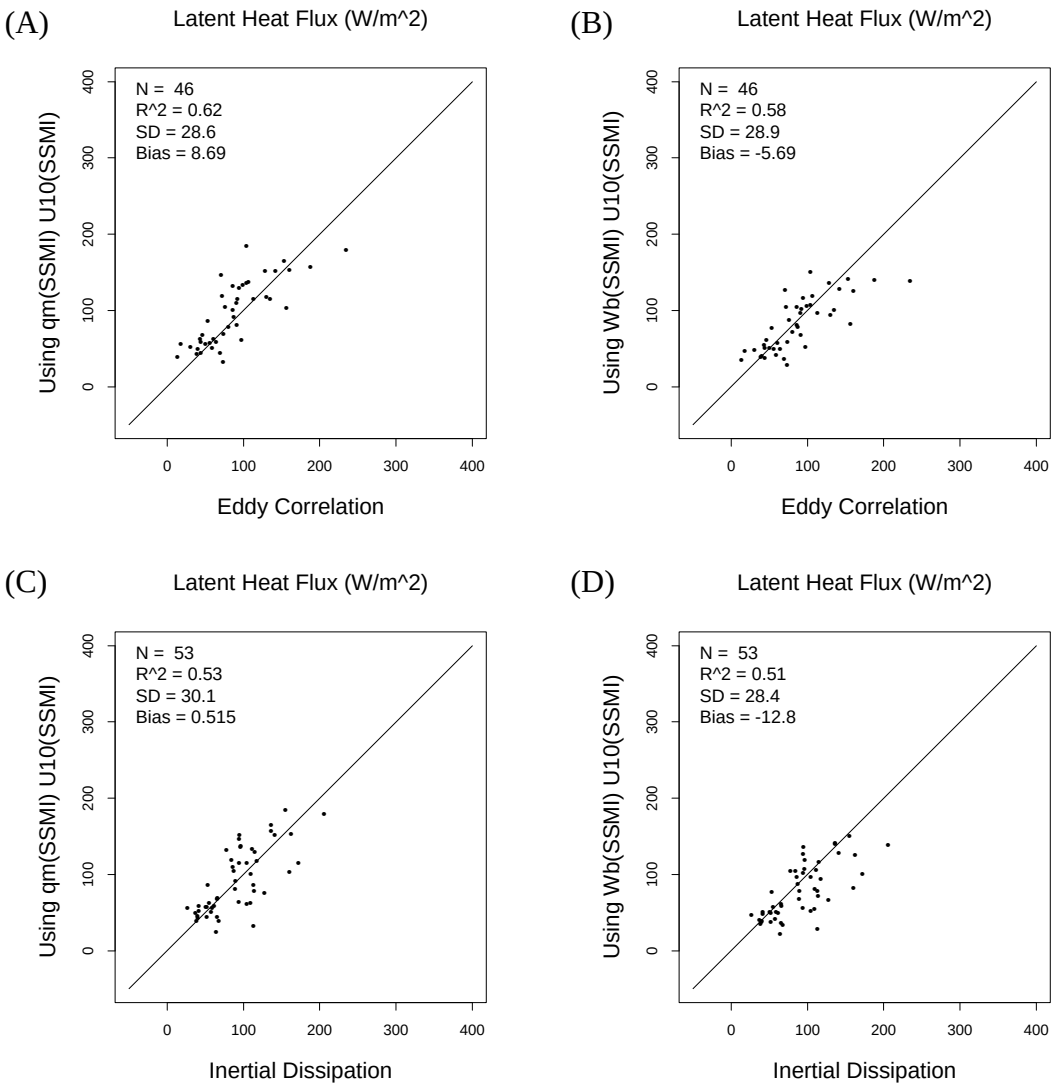

Figure 5.8 LHF from the retrievals of q_m (A and C) and W_B (B and D) using *W* integrated from the soundings, vs. eddy correlation measurements (A and B) and inertial dissipation estimates (C and D) of LHF.

5.4) Model error budget

In this section, I will identify all known sources of error in the full retrievals and attempt to quantify them. The important sources of error include

1. Ship measurements of q_{10}, T_{10}, U_{10}, and SST
2. Inherent error in the LKB method
3. Sonde measurements of humidity
4. Statistical retrievals of q_m and W_B
5. SSM/I retrievals of W and U_{10}
6. OI SST errors
7. ECMWF T_{10} - SST
8. SSM/I - ship collocation errors

Errors in the ship sensor measurements of q_{10}, T_{10}, U_{10} are about 4%, 0.2 K, and 5%, respectively. Taking mean conditions to be 10 g/kg, 15 K and 8 m/s, that translates to 16, 0.3 and 3 W/m^2 given the sensitivities discussed in section 4.7, page 69. The error in ship measurements of SST is more difficult to quantify, since a mix of near-surface and bulk temperatures exist in my data set. Some of the ships report the temperature of intake water at 2 or 4 m depths, while the Moana Wave was equipped with a floating hose fitted with a thermistor that reported temperature at 10 cm depth. Sunlight is absorbed in the upper meter or so of the ocean, tending to stabilize the oceanic mixed layer and inhibit mixing. In the oceanic molecular sub-layer, the cooling due to long wave radiation leads to a “cool skin” layer on the order of 0.1 to 0.2 K that partially offsets the warm layer effect. I will take the combined effect to be 0.4 K (Schlüssel et al. 1990) which leads to an error of 5 W/m^2 in the estimation of LHF. Thus the total uncertainty for the input data to the LKB model is 19.6 W/m^2. This is the uncertainty in the verification data, compared to some unattainable perfect measurement. It is close to the scatter between the ship-sensor estimates and the turbulence measurements of LHF (17.5 W/m^2, see Figure 4.3, page 67).

The prime inherent uncertainty in the LKB model itself is in the values of k_E and k_H. Different choices presented in the literature produce errors on the order of 15 W/m^2 for U_{10} = 8 m/s. In particular, Chou et al. (1995, 1997) used a value of 0.45 for k_E, while Fairall et al. (1996) use 0.4, as does this thesis. A secondary uncertainty comes from the choice of the drag coefficient parameterization, amounting to about 4 W/m^2. Likewise, errors in the parameterization of the stratification corrections are 1 or 2 W/m^2. Thus the total uncertainty in the LKB model is about 20 W/m^2. If we assume that the values of k_E and k_H are precisely known to be 0.4, the error in the rest of the LKB model amounts to about 5

W/m^2. These error quotes only apply to comparisons between turbulence data and the LKB model, not to the comparison between the ML method and the LKB model, since the ML method uses the same LKB model to calculate the LHF.

Radiosonde humidity sensors have an accuracy of about 3%, leading to an error in q_m and W_B of about 0.33 g/kg and 0.19 kg/m^2, respectively, given average values of 11 g/kg and 6.4 kg/m^2. It is hoped however that the errors are normally distributed through the mixed layer, and that taking an average of all points below Z_{mix} will minimize these errors. On the other hand, the variability of the structure of the mixed layer is not taken into account when a single parameter is used to characterize the whole layer. I'll take the error to be as stated.

The OI SST vs. ship-sensor SST r.m.s. scatter at the times of the SSM/I overpasses is about 0.76 K. Some of this is likely due to the warm layer, mitigated by the cool skin effect. Since the SSM/I passes a particular point on the earth once at about sunrise and once at about sunset, the effect of the warm layer is smaller than if it were sampled at local noon. We have already assumed that 0.4 K of this is due to variability in the bulk-to-skin SST difference, leaving 0.36 K unexplained. Reynolds and Smith (1994) estimate the global average error in the OI SST analyses procedure to be 0.13 K. I take the characteristic OI SST error to be 0.3 K. This error is propagated in two ways in the ML method: it affects the accuracy of the statistical retrievals, and has a direct effect on the LKB model.

Wentz (1997) gives the r.m.s. accuracy of the U_{10} and W SSM/I retrievals as 0.9 m/s and 1.2 kg/m^2, respectively. By contrast, my collocations show a standard error of 1.89 m/s and 3.04 kg/m^2, respectively, but this includes collocation errors as well as random retrieval errors. Wentz (1997) gives an error budget (his Table 3) that indicates the sampling mismatch is 0.94 m/s and 3.68 kg/m^2, for his error analysis. I take the difference between my observed variance and Wentz' published accuracies to be representative of the collocation errors in my data set.

The standard error of the q_m and W_B retrievals using sonde data is about 0.9 g/kg and 0.55 kg/m^2, respectively. This includes the uncertainty due to radiosonde measurements and the OI SST retrievals (and the ECMWF T_{10} - SST errors in the case of the q_m retrieval). The standard error of q_m calculated from W_B (equation (3.12), page 44, plus the correction for the increased humidity in the log layer) compared to the sonde value is 0.52 g/kg. The sensitivity of the statistical retrievals to their input parameters was examined in section 3.10.2, page 50. The q_m retrieval has an error of 0.61 g/kg due purely to the regression, in addition to errors due to input variables. The corresponding number for the W_B retrieval is

0.33 kg/m^2.These are multiplied by the sensitivity of the LKB model (and the sensitivity of q_m to W_B in the latter case) to yield 21.4 W/m^2 and 22.2 W/m^2, respectively.

The r.m.s. scatter between the ECMWF and ship sensor air temperatures is 1.07 K, leading to an error in the LHF of 0.9 W/m^2.

Table 5.1 summarizes the estimated error budget and compares the total with the observed error. The total estimated error without collocation errors is about 23 W/m^2 for both models.

Table 5.1 Error budget for the ML methods,

	q_m Method	W_B Method
Statistical retrieval error	21.4 W/m^2	22.2 W/m^2
W collocation error	18.2 W/m^2	18.2 W/m^2
SSM/I U_{10} error	6.8 W/m^2	6.8 W/m^2
U_{10} collocation error	12.5 W/m^2	12.5 W/m^2
OI SST error	14.0 W/m^2	14.0 W/m^2
ECMWF T_{10} - SST error	0.9 W/m^2	0.9 W/m^2
Total	34.5 W/m^2	35.0 W/m^2
Observed Error	34.1 W/m2	34.1 W/m^2
Error without collocation	**26.5 W/m^2**	**29.9 W/m^2**

5.5) An SSM/I bulk transfer coefficient method

The relatively high errors in the input variables, when translated to errors in LHF, compared to the accuracy of the LKB model itself suggests that a simpler approach is possible. Recall the bulk aerodynamic formula

$$E = \rho L_v C_E U_{10}(q_0 - q_{10}) \tag{5.5}$$

where the LKB model specifies the functional form of the transfer coefficient. In field programs designed to establish the value of C_E, there is typically close to 20% scatter of the data. Additionally, there is about a 10% difference between the average values obtained from different experiments (see the discussion in section 1.4, page 6). A much simpler method would be to derive a new drag coefficient using U_{10} from the SSM/I and the ML-surface humidity difference in place of the 10m-surface humidity difference:

$$E = \rho L_v C_E' U_{SSMI}(q_0 - q_m(W_{SSMI}, \mathrm{SST}, \Delta T)) \tag{5.6}$$

where q_m is from equation (3.14), page 47. If the LHF calculated from this method agrees with the turbulence data as well as the full ML method, then we would have a very simple way to use the SSM/I data along with the OI SST and ECMWF T_{10} -SST data, without having to iterate to solve the LKB equations. Of course, such a C_E' would be dependent on the particular turbulence data set used to derive it. Development and refinement of the method would also be dependent upon new and improved turbulence data, which is not very common over the open ocean. One would also lose the ability to calculate other variables, such as the sea-air humidity difference. It might not be widely applicable to different regimes and would have to be re-tuned for a changing climate.

Motivated by the shape of the curve in Figure 5.9 (A), I chose to fit a curve of the form

$$10^3 C_E = a\exp[b(U_{\mathrm{SSMI}} + c)] + \frac{d}{U_{\mathrm{SSMI}}} + 1 \tag{5.7}$$

The resulting fit to the turbulence data is shown in Figure 5.9 (B). The coefficients are a = -0.71536, b = -0.16719, c = -2.2876, and d = 1.9135. Given the scatter of the data, the fit seems as reasonable as assuming a constant coefficient of about 1 x 10^{-3}. However, at small U_{10} (< 2 m/s) a constant coefficient produces a 19 W/m^2 bias compared with the LKB method. This is not surprising, given the shape of the

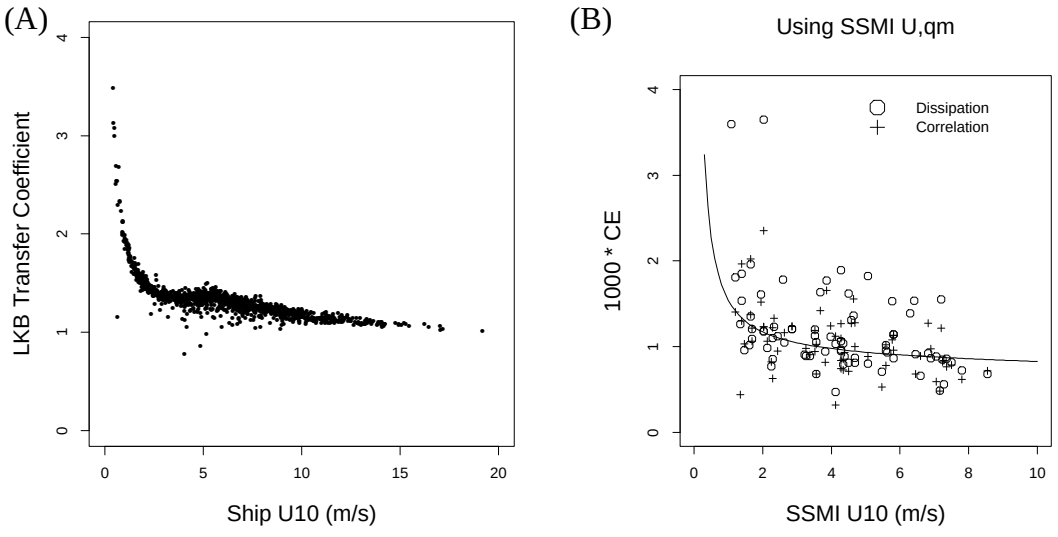

Figure 5.9 The transfer coefficients of (A) the LKB model, derived from ship data, and (B) the proposed C_E' SSM/I method derived with the turbulence data, vs. wind speed.

points in Figure 5.9 (A). There is only a small hint of such behavior in the turbulence data. The performance of C_E' compared to the LKB method is shown in Figure 5.10. The performance of the simple method is indeed as good as the performance of the more elaborate methods, indicating the results are limited by the quality of the input data, not the quality of the model.

5.6) Summary

Motivated partially by the errors in the lowest sounding level, used by almost all previous attempts to derive SSM/I LHF methods, I have assembled a collection of high-resolution soundings launched from research vessels along with coincident surface meteorological observations from which independent LHF estimates can be calculated. I then presented a very simple model for the lower part of the planetary boundary layer, designed specifically to take advantage of the error-free part of the sounding (the mixed layer average). A well-mixed layer was patched to an LKB surface layer in a continuous fashion. An analytic relation between q_m and W_B was derived as a replacement for the statistical relation developed by Schulz et al. (1993). The use of q_m - q_0 in the LKB equations was then shown to be equivalent to using q_{10} - q_0. Some of the limitations of the application of this model to the marine boundary layer were discussed, including the lack of a satellite retrieval of near-surface air temperature and the possibility that the mixed layer was less then 500 meters deep. Finally, the accuracy of the model was assessed using both *W* integrated from the soundings and retrieved by the SSM/I. The model was compared to LHF calculated from the LKB model and ship-sensor data, and to eddy correlation measurements and inertial dissipation estimates where available. An error budget was presented, an attempt was

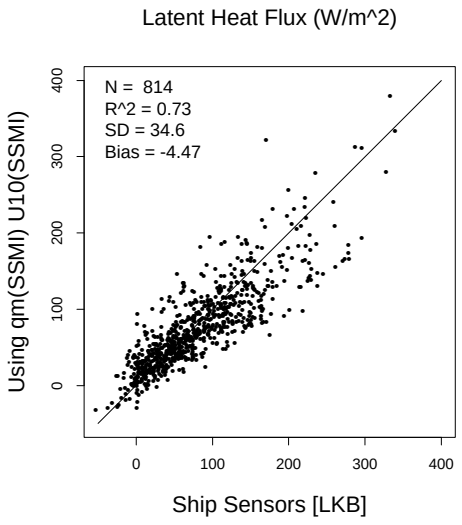

Figure 5.10Comparison between LHF predicted by the LKB model from ship sensor data and as predicted by C_E' using collocated SSM/I data.

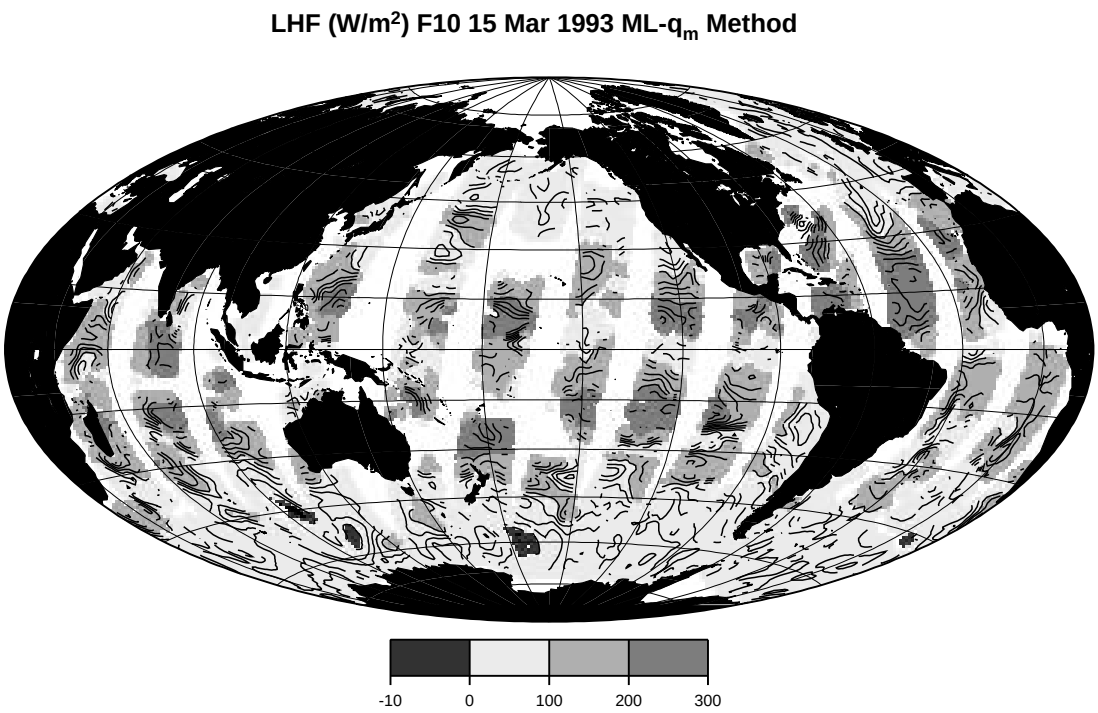

Figure 5.11Sample of LHF calculated using the ML-q_m method for 15 Mar 1993, data from the F10 DMSP satellite.

made to assess the variability of the model independent of the errors involved in collocating the SSM/I data. The r.m.s. error of the model is about 26 W/m^2, compared to the nearly identical results of Schulz et al. (1993), Schlüssel et al. (1995) and Chou et al. (1997) of 30 W/m^2. The model shows very little bias. The largest error sources are due to the statistical retrieval methods of q_m and W_B, and in the OI estimates of SST. A sample map of LHF calculated using the ML-q_m method is presented in Figure 5.11.

Chapter 6

New Climatologies from SSM/I and PBL-LIB

For each month in the period January 1992 to December 1997, all available data was used to calculate latent heat flux (LHF) in five different ways. PBL-LIB was run with and without the thermal wind correction, and the SSM/I fluxes were computed using the q_m, W_B and bulk C_E methods. I present sample months, chosen to coincide with the published results of Chou et al. (1997).

6.1) Sample monthly PBL-LIB LHF maps

PBL-LIB was run with ECMWF analysis data consisting of sea level pressure (SLP), sea surface temperature (SST), and near-surface air temperature (T_2) and humidity at 2 m. These data are available 4 times daily, at 0Z, 6 Z, 12 Z, and 18 Z. LHF was first calculated for all available times for each month (~120 total) for global grids on the native ECMWF grid (320 by 160), then the output was averaged on a grid-point by grid-point basis. The averaging scheme requires at least 25% of the data at each grid point to have good data values, or the output at that point is flagged as bad. Finally, the output for the month was interpolated to a regular grid for graphing.

Figure 6.1 shows monthly maps of PBL-LIB LHF (no thermal wind correction) for February 1993 and August 1993. There is no data between 5° N and 5° S since PBL-LIB can't find a solution there due to its dependence on the Ekman depth for the scale of the outer layer. Since the Ekman depth goes as 1/f, PBL-LIB predicts increasingly large boundary layer depths as the latitude goes to zero. The LHF generally appears similar to what we expect, with a maximum in the central pacific on the winter hemisphere side of the equator, fueled by the return branch of the Hadley circulation. There is higher LHF near the Western boundaries of the oceanic basins during Winter, due to a combination of the Southward migration of the storm track and its tendency to advect cold, dry continental air over the sea. We do not see the expected minimum over the equatorial cold tongue, or even any hint of such a structure as the cut-off limit is approached. The local minima off the West coasts of North and South America, due to low SST's, is however present.

Figure 6.2 shows the difference maps of PBL-LIB LHF without the thermal wind correction minus with thermal wind for February 1993 and August 1993. Although the same cut-off for the PBL-LIB fluxes at +/- 5° latitude still exists, the thermal wind corrected solution fails at slightly higher latitudes.

(A) **LHF (W/m^2) Feb 1992 PBL-LIB (no thermal wind)**

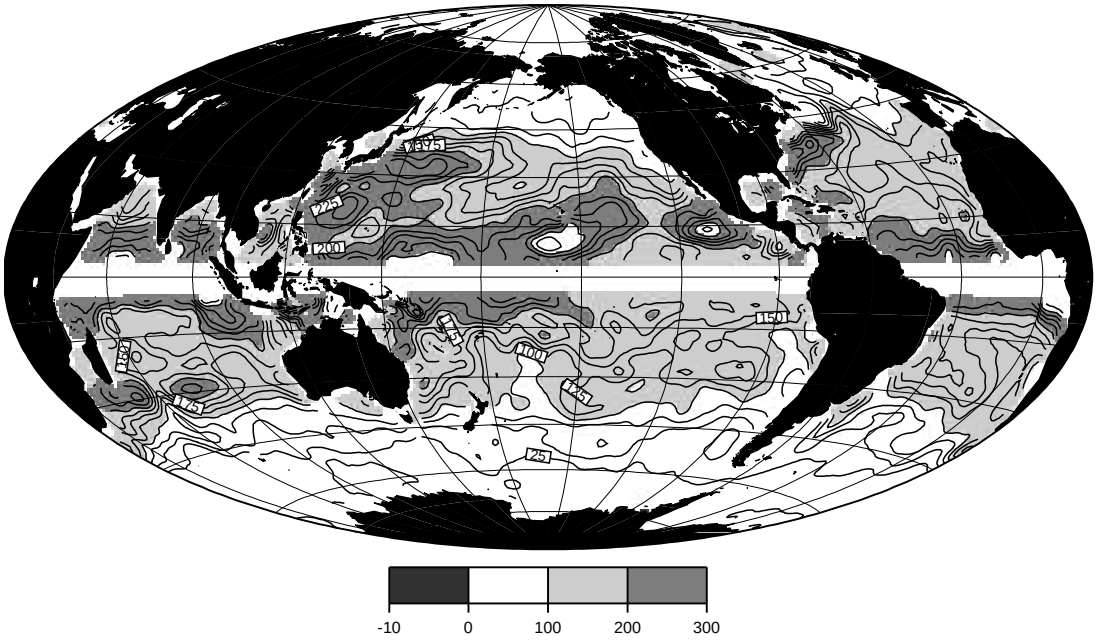

(B) **LHF (W/m^2) Aug 1992 PBL-LIB (no thermal wind)**

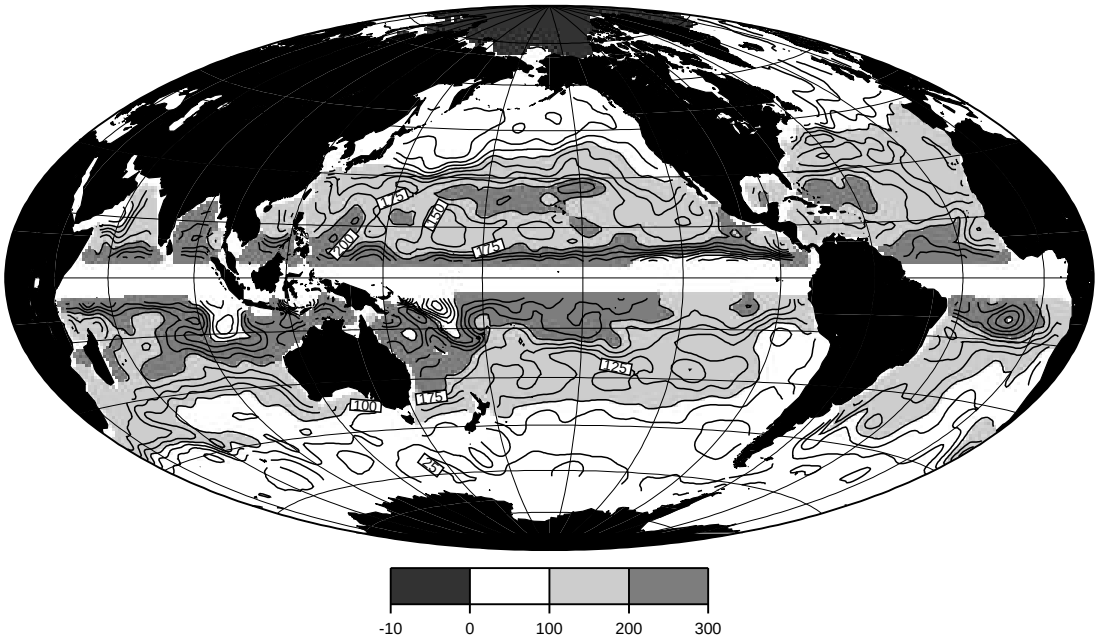

Figure 6.1 Monthly averages of 4-times-daily PBL-LIB (no thermal wind) latent heat fluxes (W/m^2) for (A) February 1993 and (B) August 1993.

(A)

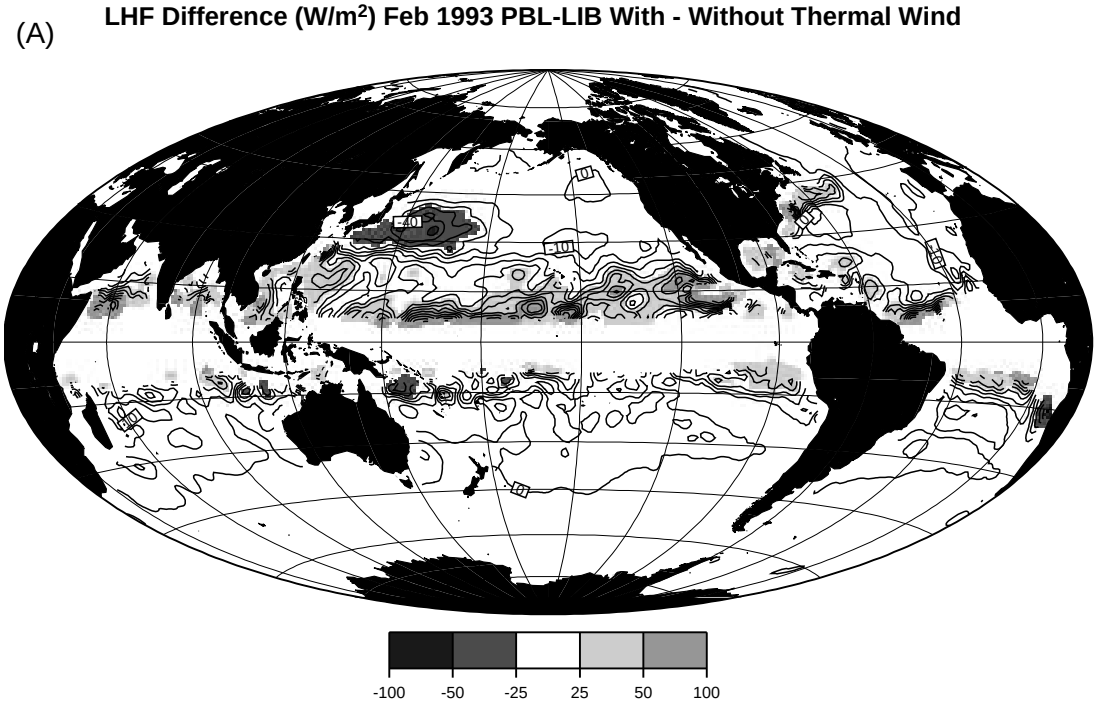

(B)

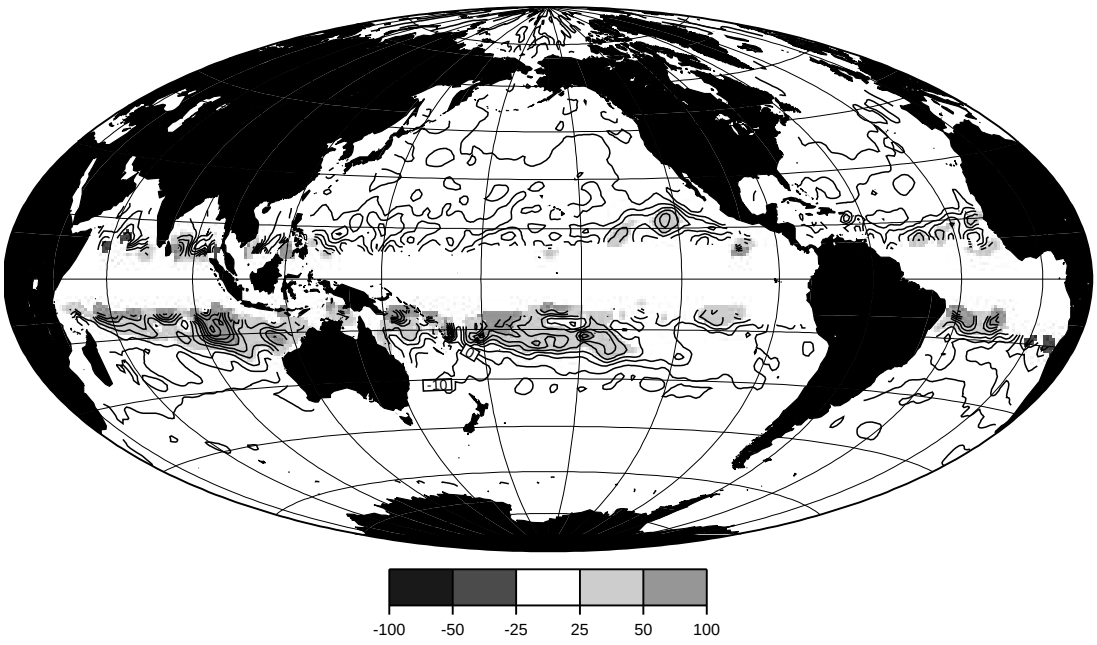

Figure 6.2 The difference between LHF using PBL-LIB without and with the thermal wind correction, for (A) Feb 1993 and (B) Aug 1993.

The predicted PBL height with the thermal wind included is larger than without, causing the iteration not to converge and the points are flagged as bad. The most striking difference between the two is in the Northern hemisphere storm track off the coast of Asia, with a smaller difference off the coast of North America. The thermal wind parameterization enhances the fluxes in these regions, about 40 W/m^2 in the Pacific. Noisy differences exist approaching the equator, but this is more likely due to problems and limitations inherent in the model than to physical processes.

6.2) Sample monthly SSM/I LHF maps

The SSM/I fluxes were computed using weekly OI SST data, daily 0Z ECMWF SLP data, daily 0Z and 12Z ECMWF SST data, and daily 0Z and 12Z ECMWF air temperature data. Since the model is not very sensitive to errors in SLP, I chose to use only one value per day. The ECMWF SST and air temperature data were used only for the air-sea temperature difference in the calculation, although the correlation between the ship sensor SST's and ECMWF SST was almost as good as between the ship sensor SST's and the OI SST. These choices are a compromise between an effort to reduce the sheer volume of data involved and the accuracy of the model.

The SSM/I data was first reduced from its native 0.25 x 0.25 degree grid to a 1 x 1 degree grid by averaging four grid boxes to one. All remaining data (ECMWF and OI SST) were linearly interpolated to the location of each SSM/I grid box, and then linearly interpolated to the time of each SSM/I pixel. The calculations were performed three times; once with the retrieval of $q_m(W, \text{SST}, \Delta T)$, once with the retrieval of $W_B(W, \text{SST})$ and the analytical relation between W_B and q_m, and once with the "bulk SSM/I" C_E method. The former two use what I have come to call the "mixed layer method," developed in Chapter 5, where the LKB model is solved using the mixed-layer value of specific humidity (q_m). U_{10} retrieved from the SSM/I was used in all three calculations, as was the ECMWF air-sea temperature difference and the OI SST product.

Figure 6.3 shows the August and February 1993 monthly maps of SSM/I LHF calculated using the mixed-layer (ML) method using retrieval of $q_m(W,\text{SST}, \Delta T)$ developed in section 3.10, page 41. All available SSM/I data were used; during this period the F10 and F11 satellites were in orbit and functional. The data are a bit noisy, likely due to the simple averaging that was done. Zeng and Levy (1995) have developed an averaging scheme that removes the commonly seen "satellite sub-tracks" in monthly mean polar orbiting satellite data. It may be useful to employ their method and re-do the averaging.

The maps shows more of the features we expect to see in a monthly climatology. 1993 was an El Niño year; a local maximum just East of the date line is seen, along the northern edge of the ITCZ,

(A)

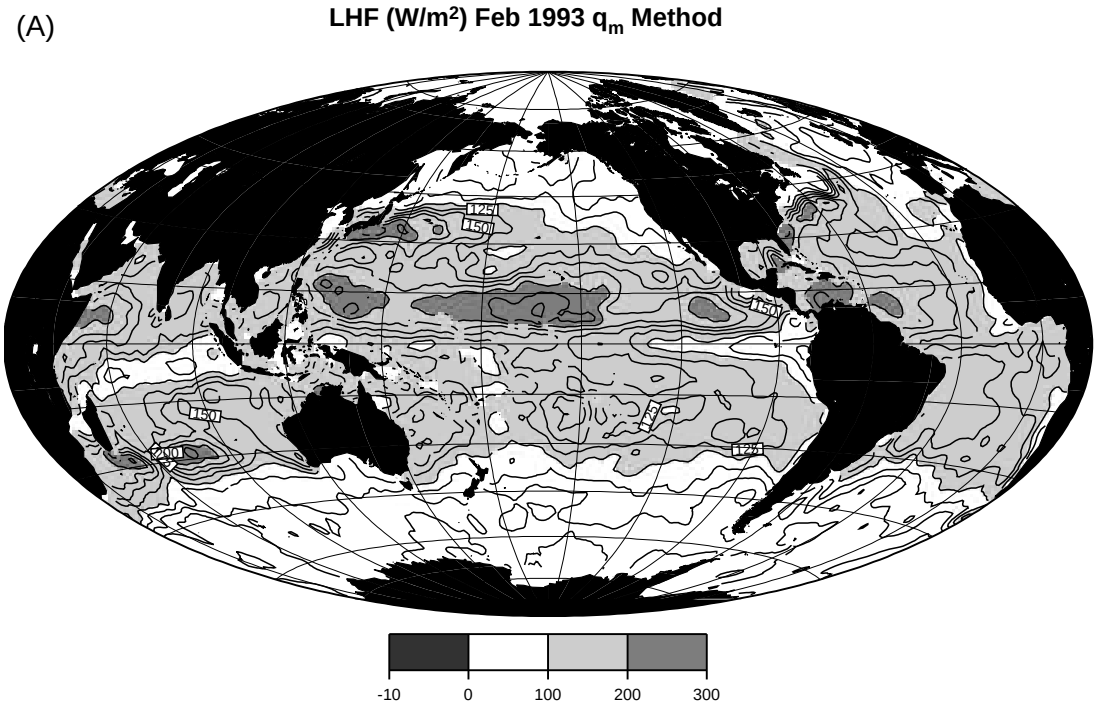

(B)

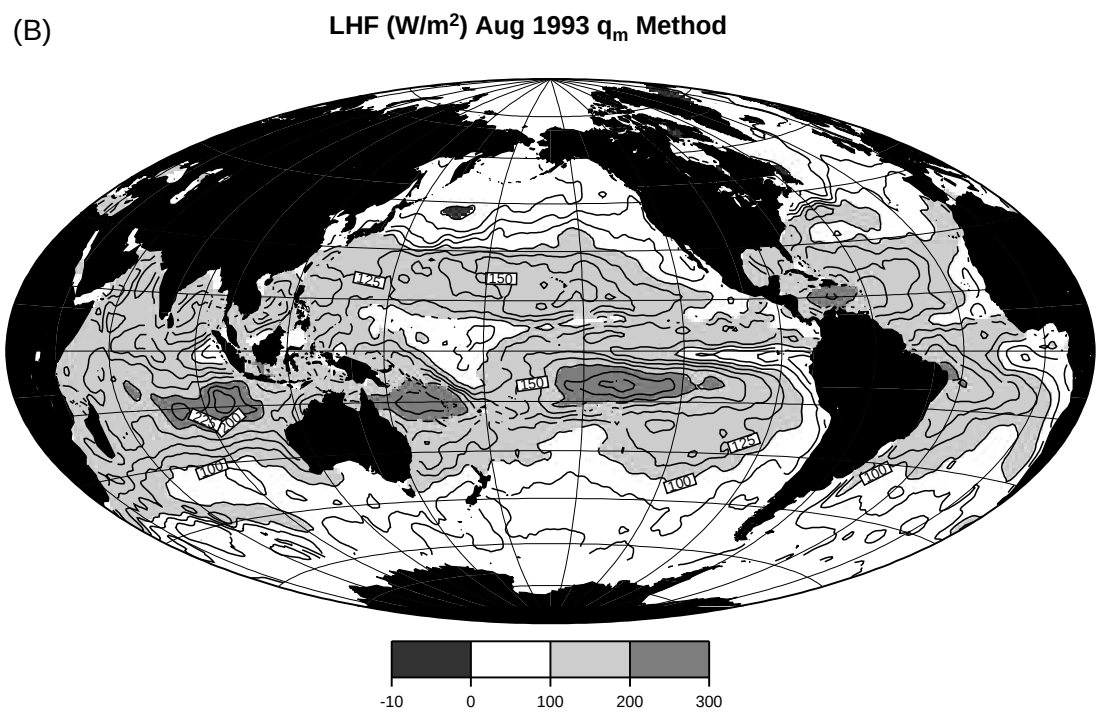

Figure 6.3 Monthly averages of all available SSM/I latent heat fluxes (W/m^2) using the ML-q_m method for (A) February 1993 and (B) August 1993.

where the SST gradient is the greatest. The minimum over the equatorial cold tongue in the Pacific is quite pronounced in both seasons, and is seen in the Atlantic in the August map. The minima along the Eastern boundaries of the basins due to the oceanic advection of cold water (along with some upwelling) are well delineated. We see the seasonal shift in the near-equatorial maxima to the winter hemisphere, with the Eastward shift of the maximum in the central Pacific to the location of the South Pacific Convergence Zone. The reflection of the maximum in the Northern edge of the West Pacific warm pool moves East of Australia in winter. The local maximum at about 15° S Southeast of Indonesia does not have a "reflection" opposite the equator, nor does the local maximum off the coast of Sudan in NH winter. The local minimum along the ITCZ in the Pacific is due to low wind speeds (see Figure 6.8) and correlates well with the highest frequency of cumulonimbus analyzed by Norris (1997). There are local maxima off the East coasts of the Northern hemisphere land masses, stronger in Winter, similar to the features seen in the PBL-LIB climatology discussed earlier. In general, the LHF is greater than 200 W/m^2 only between 30° N and S, and falls toward zero at high latitudes. There is a small region in August 1993 at about 45° N, South of Kamchatka, where the q_m method predicts a negative monthly mean LHF, which corresponds well with a maximum of frequency of sky-obscuring fog from volunteer observations (Norris, 1997). For comparison, Chou et al. (1995) showed large regions of negative LHF North of about 40°N in her August 1988 monthly mean. Chou et al. (1997) introduced the extra limitation that the EOF-retrieved q_{10} must not exceed saturation at the sea surface temperature. This forces the fluxes to be always positive. My method does have a somewhat similar requirement: the retrieved q_m is not allowed to exceed the saturation specific humidity of the mixed-layer air predicted by the LKB model (largely controlled by the ECMWF analyzed air-sea temperature differences). This still allows for positive q_m-q_0 values (negative LHF) on an instantaneous basis, but for almost all the world's oceans the monthly mean is positive.

Figure 6.4 shows the difference maps of monthly SSM/I LHF calculated using the ML-q_m method and using the retrieval of W_B(W,SST) developed in section 3.10, again using weekly OI SST data, once-daily ECMWF SLP data, and twice-daily ECMWF T_2 and SST data. In general, the differences are quite small, amounting to less than 10 W/m^2 in most regions. The W_B retrieval produces lower seasonal maximum fluxes in the near-equatorial regions compared with the q_m retrieval. The difference in the SPCZ during August is the largest anywhere either season, more than 25 W/m^2 for a large area. The SST here is still near 27°C. Recall that the W_B retrieval loses sensitivity at high SST's, and tends to over-predict the mixed-layer humidity (under-predict the fluxes). The q_m retrieval also shares this tendency, but to a lesser extent. The region South of Indonesia where the q_m retrieval produced a maximum in LHF suffers from a similar underestimation by the W_B retrieval, despite the SST being closer to 25° C

(A)

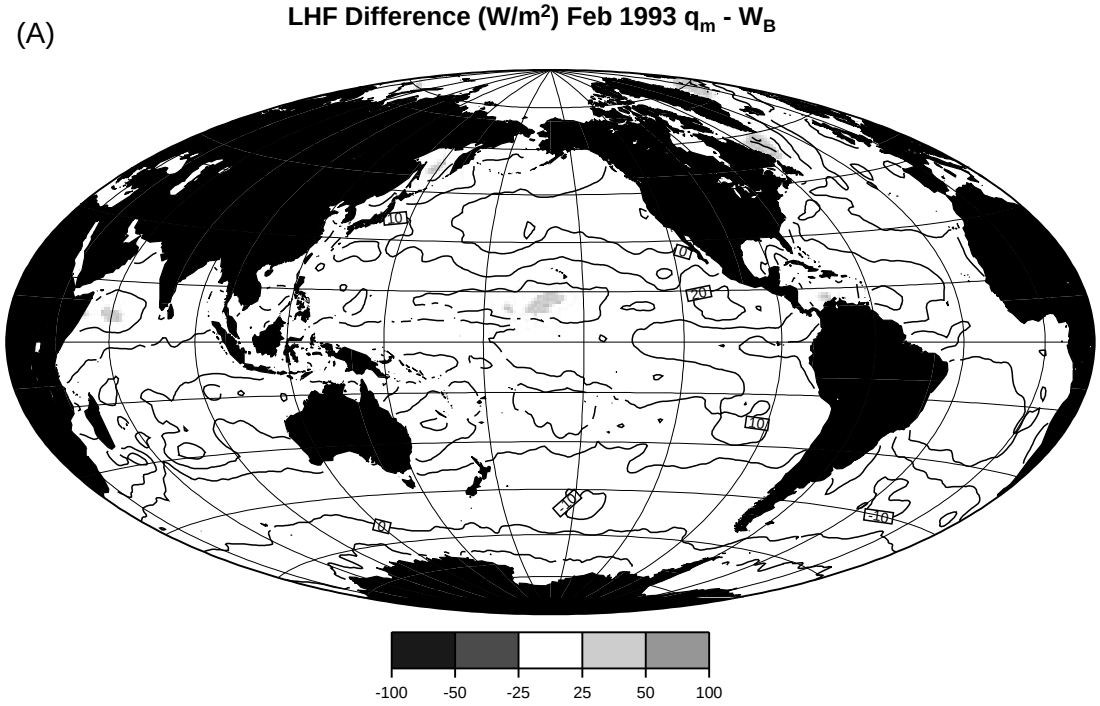

(B)

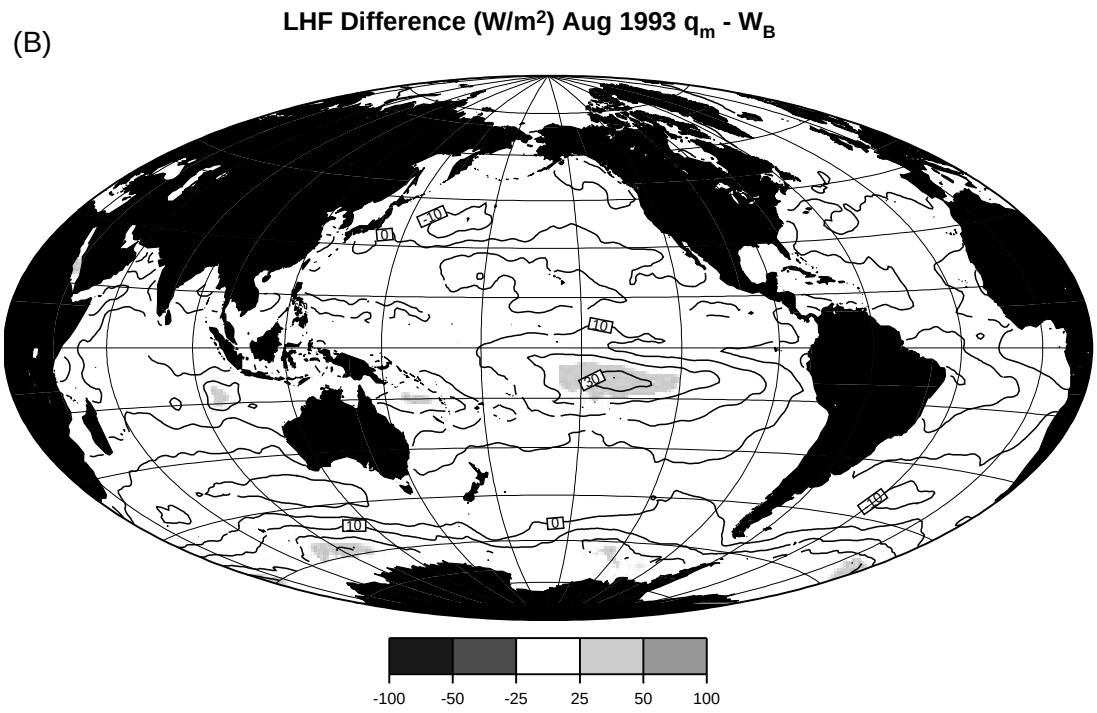

Figure 6.4 The difference between SSM/I LHF using the ML-q_m method and using the ML-W_B method, for (A) Feb 1993 and (B) Aug 1993.

than 30°. At high latitudes, the difference is nearly zonally symmetric, except for a minimum (q_m-LHF lower than W_B-LHF) at the location of the negative monthly mean flux South of Kamchatka discussed above. Since the major differences between the ML-q_m method and the ML-W_B method are limited to regions of high SST where we expect from the retrieval error analysis W_B to be erroneously high, I will focus for the comparison with other climatologies on the ML-q_m method.

Figure 6.5 shows the difference between the monthly-mean LHF calculated using the ML-q_m method and the bulk-SSM/I C_E method introduced in section 5.5, page 87. The field is rather noisy, and limited to within 10 W/m^2 in most of the extratropics. The C_E LHF is lower by 25 W/m^2 than the q_m LHF in the Western Pacific warm pool for both months, and in the SPCZ during February. It over-estimates the flux in the Atlantic ITCZ during both months, and in the Pacific ITCZ during August. There is also a hint of underestimation in the Western equatorial Indian ocean. The standard deviation between q_m-LHF and C_E-LHF for the collocated SSM/I data is about 17 W/m^2, with a bias of 2.3 W/m^2. The bulk-SSM/I C_E method is adequate for rough estimates of extratropical LHF, and is computationally quite efficient.

6.3) Comparison with other monthly climatologies

6.3.1) Single-year monthly climatologies

Figure 6.6 shows monthly maps of the difference between SSM/I LHF from the ML-q_m method and the SSM/I LHF climatology from Chou et al. (1997) for the same two months as the previous examples. They are generally in good agreement in the tropics and in the summertime extratropics, but in the mid-latitudes of the winter hemisphere the ML-q_m method LHF is significantly lower than that of Chou et al (1997). In the Western Pacific warm pool and the ITCZ regions, the ML-q_m method tends to be higher by ~25 W/m^2 during February. It also is higher over the equatorial cold tongues in both the Atlantic and Pacific during August. Figure 6.7 shows the difference in the sea-air humidity difference, normalized to 10 meters, between the two methods. On the whole, the current method predicts a larger Δq in the tropics and summertime subtropics by between 1 and 2 g/kg. Keeping in mind that 1 g/kg of change in q_0 - q_{10} produces a 20 W/m^2 (at U_{10} = 15 m/s) to 50 W/m^2 (at U_{10} = 5 m/s) difference, we would expect to see large LHF differences in the tropics where the wind speeds are generally lower than in the storm track of the winter hemisphere. With the exception of a region Southeast of Australia in August, where my Δq is 1 - 2 g/kg lower than Chou's and my LHF is ~50 W/m^2 low, this is not the case. For example, off the coast of Chilé in August and the Pacific Northwest during February, the q_m fluxes are ~40 W/m^2 lower than Chou, yet our Δq's agree very well. Since both the current method and Chou et al. (1995, 1997) use OI SST and SSM/I U_{10}, and Δq is nearly the same in these regions, we conclude differences

(A)

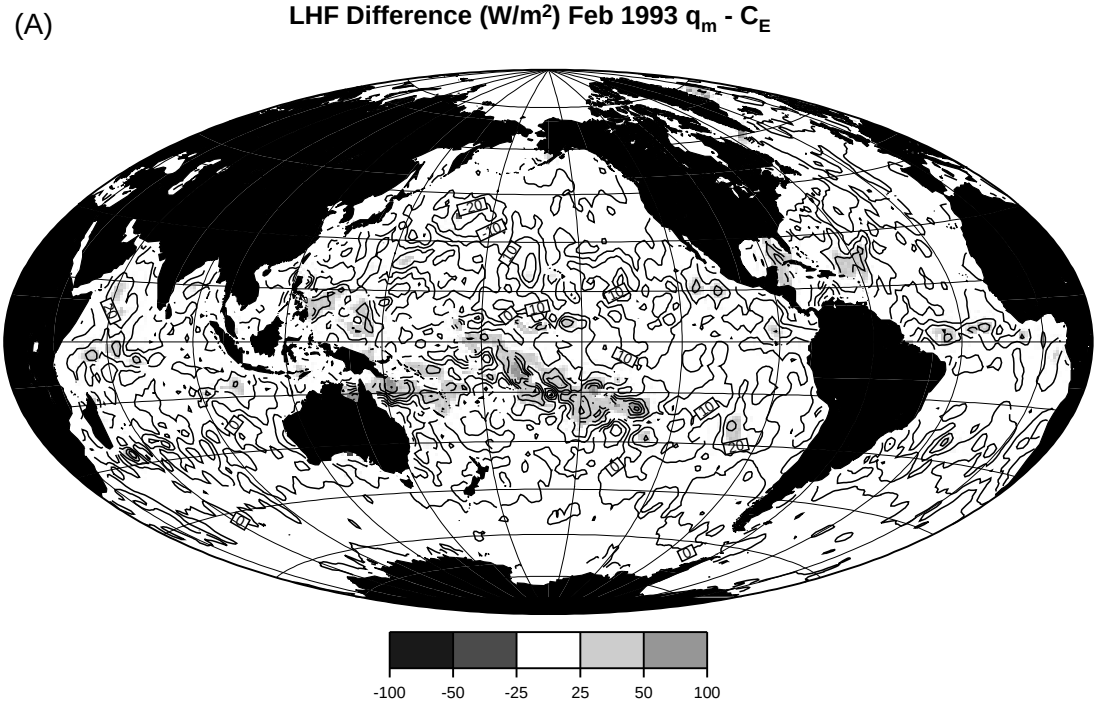

(B)

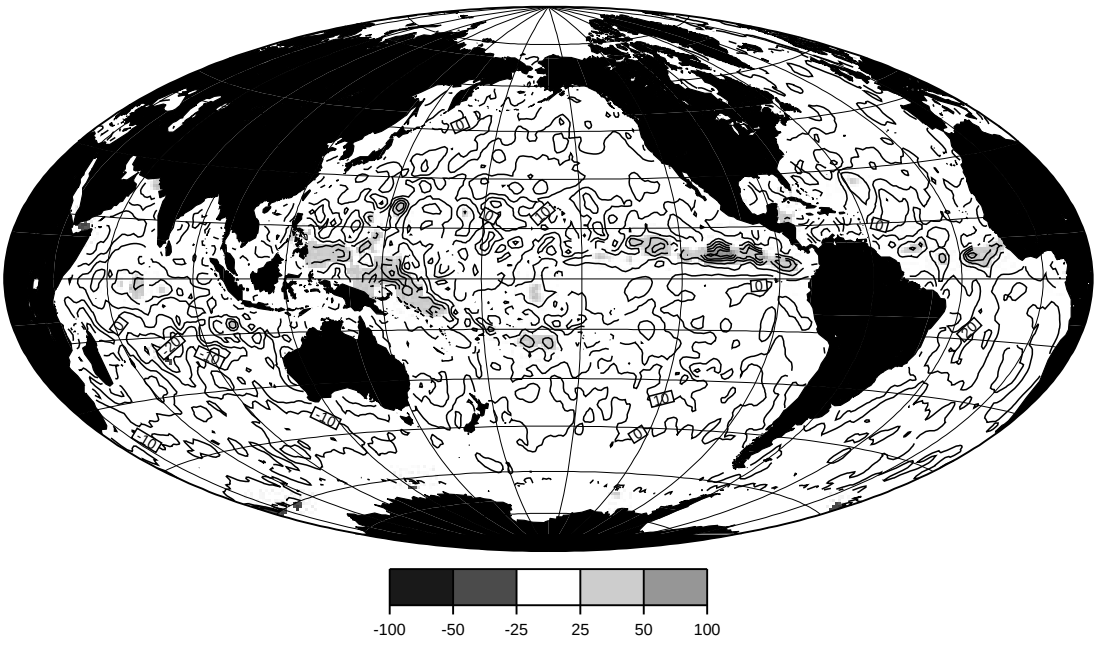

Figure 6.5 The difference between SSM/I LHF using the ML-q_m method and using the C_E (bulk SSM/I) method, for (A) Feb 1993 and (B) Aug 1993.

(A)

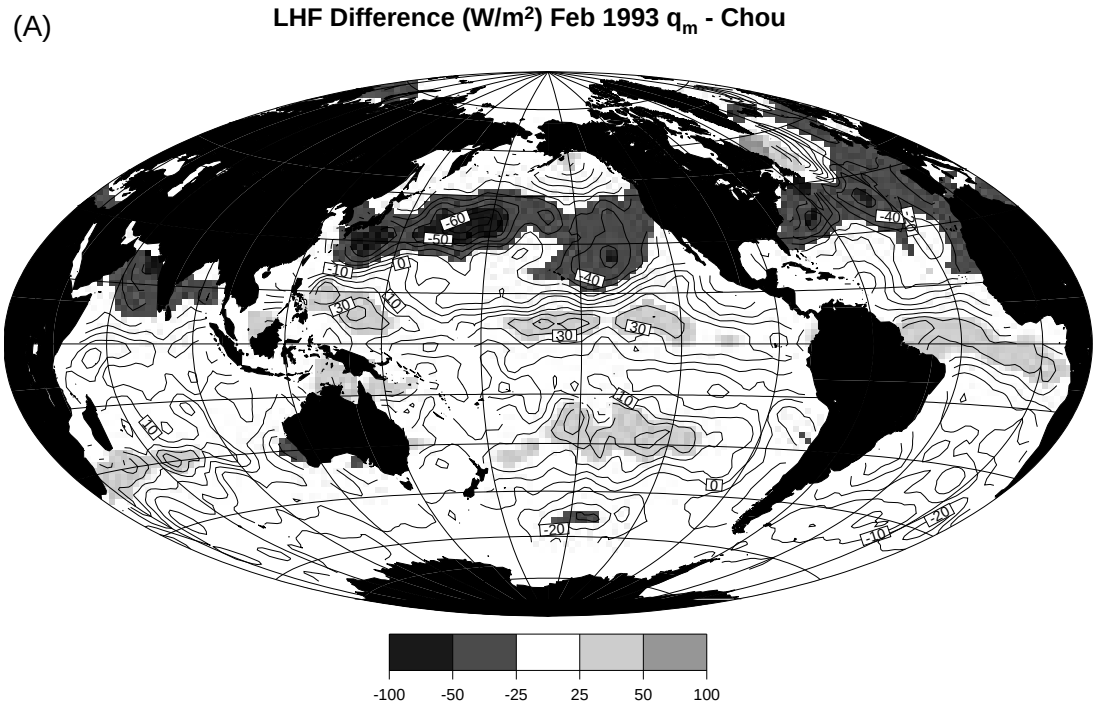

(B)

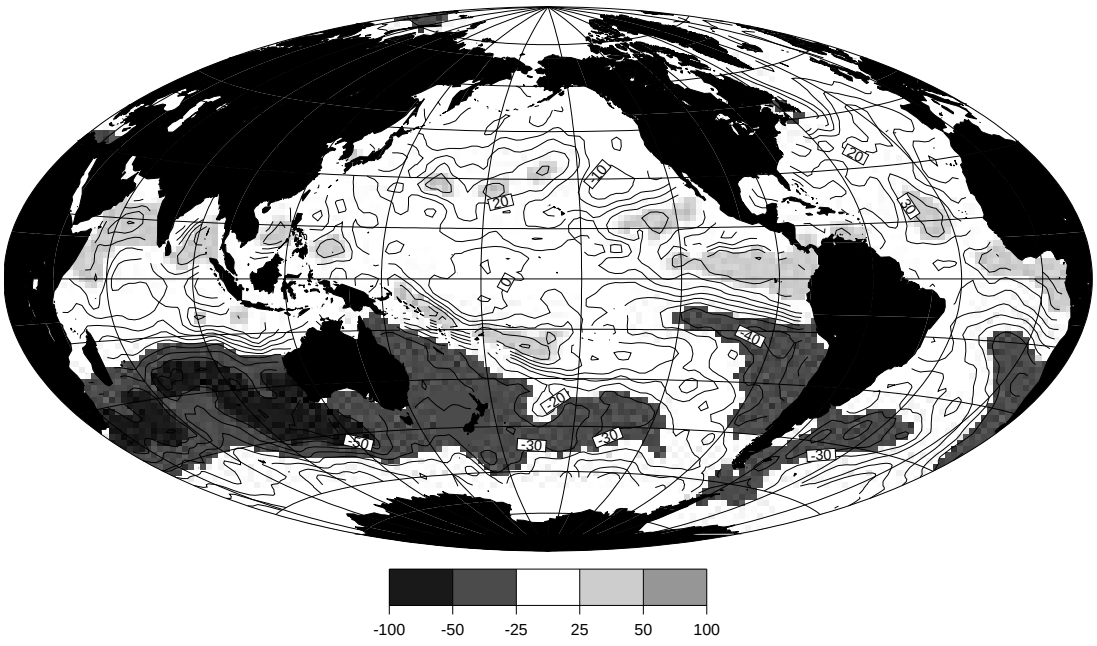

Figure 6.6 Difference between monthly averaged SSM/I latent heat fluxes from the ML-q_m method and Chou et al. (1997) for (A) February and (B) August 1993.

(A)

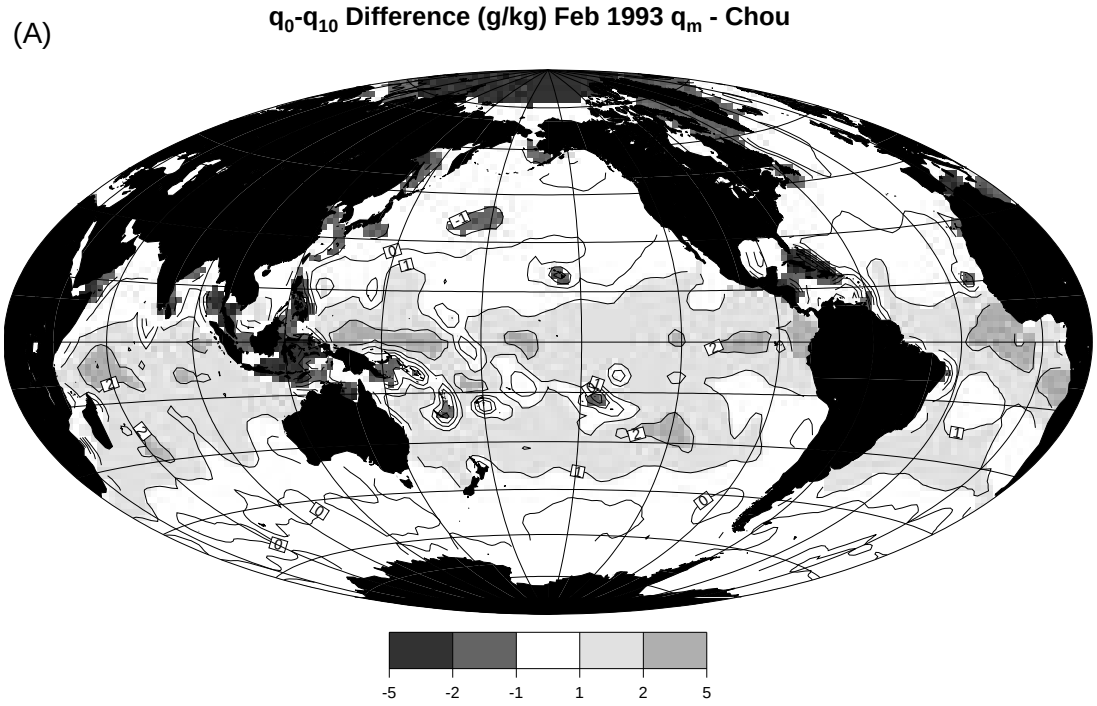

(B)

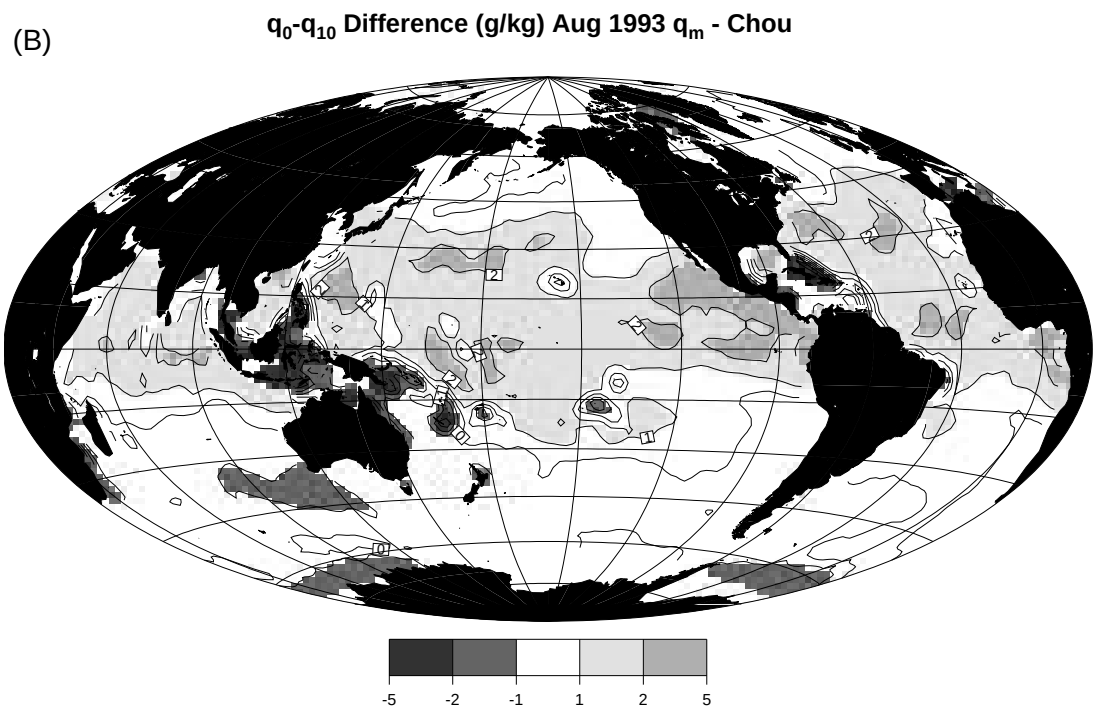

Figure 6.7 Difference between monthly-averaged sea-air humidity differences from the ML-q_m method and Chou et al. (1997) for (A) February and (B) August 1993.

in the model parameterizations must be responsible. Looking back to Figure 4.5 (page 71) we note that the largest difference between flux parameterization comes from the specification of k_E and k_H. The line labelled “FG” with k_H = 0.36 and k_E = 0.45 corresponds to the constants used in Chou et al (1995, 1997), while the line labelled “Kondo/Smith” (with $k_H = k_E$ = 0.4) corresponds to the current model. Without stating which one is ‘right’, we see that it explains 10 W/m^2 of difference at 15 m/s and 10°C, and 30 W/m^2 of difference at 15 m/s and 29°C. The regions of largest disagreement have SST’s of about 20°C, indicating that if they are in the higher-wind regime we can explain 20 W/m^2 for difference. For February, the monthly average of SSM/I U_{10} (Figure 6.8) for the portion of the Pacific maximum LHF difference West of the date line is >12 m/s, while the large region East of the date line has U_{10} > 10 m/s. The maxima in the midlatitude Atlantic also has U_{10} > 10 m/s. For August, the large and elongated region East of Australia has wind speeds >10 m/s at the Northwest end to >13 m/s at the Southeast end. The region off the coast of Chilé in the Pacific has U_{10} > 6 m/s. Thus about half the difference can be accounted for by model parameter differences. Note also the regions near the date line and the equator in both months where the wind speeds fall to low values -- the LHF difference also falls to low values there. The rest of the difference can be explained by the strong sensitivity of the LKB model to changes in q_0 - q_{10}.

Although it is difficult to pick out the ‘best’ set of parameters for the model, given the limited set of marine turbulence data available, the values from Francey and Garratt are not nearly as widely used as $k_H = k_E$ = 0.4 (*e. g.* the TOGA COARE bulk algorithm of Fairall et al. 1996). Chou et al. (1995) picked their values based on Chou et al. (1993) which used flight-level data in a cold-air outbreak near the East coast of North America to tune the LKB model. I have shown (Table 4.1) that this set of constants over-predicts the LHF by ~7 W/m^2 compared to turbulence data taken during COARE and ASTEX. Additionally, Figure 5.4(A), page 79, indicates that there is a ~10% systematic error in applying the LKB model at heights of ~50 m. The deviation of the higher $|q_*|$ points, and the consistent albeit small offset of q_* derived from heights where instrumented planes fly could lead to an incorrect value for k_E. The 10% factor that I was forced to use to make my ML-derived q_* match the ship-sensor q_* is close to the 12% difference in 0.4 vs. 0.45. If measurements taken at ~50 m were used to tune the model, using 10 m data will introduce a bias, based on Figure 5.4(A).

Chou et al. (1997) compared 2.5° x 2° SSM/I EOF retrievals of LHF with measurements made aboard the R/V Moana Wave during TOGA COARE, and found a standard error of 29 W/m^2 with a bias of 6.2 W/m^2. Even with the penalty of a smaller grid box over which to average (1° x 1°) the ML-q_m method obtains a standard error of 26.7 W/m^2 with a bias of 9.76 W/m^2 using a similar mix of turbulence and bulk reference fluxes. Chou et al. (1997) also compared SSM/I EOF retrievals of q_{10} collo-

(A)

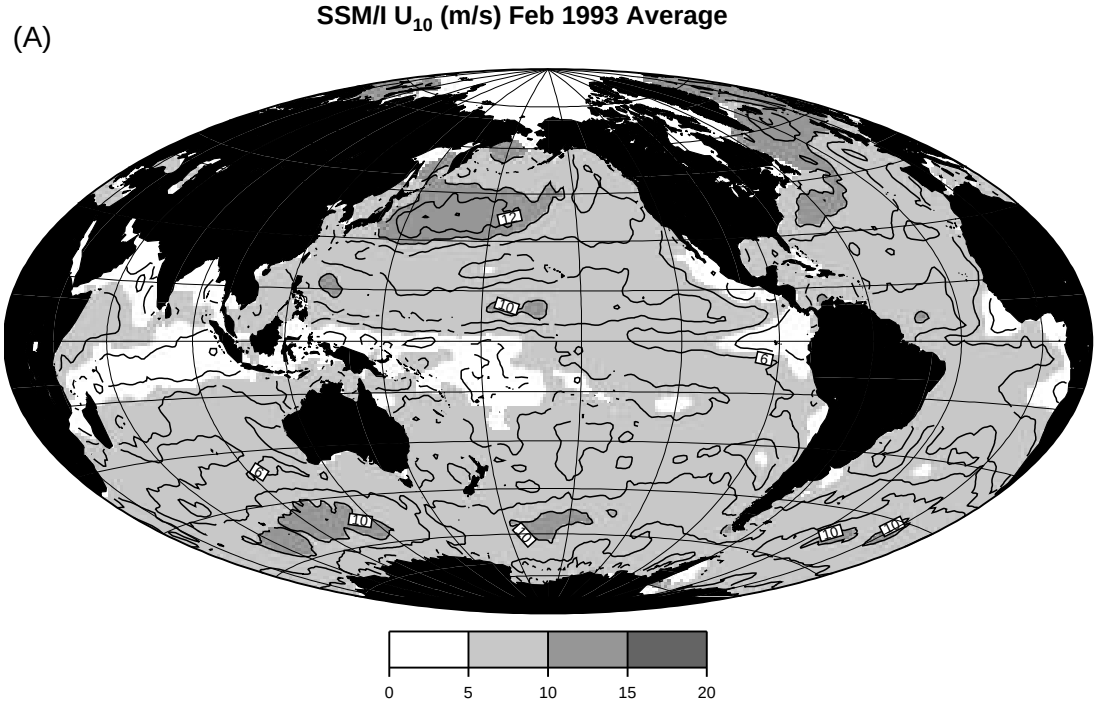

(B)

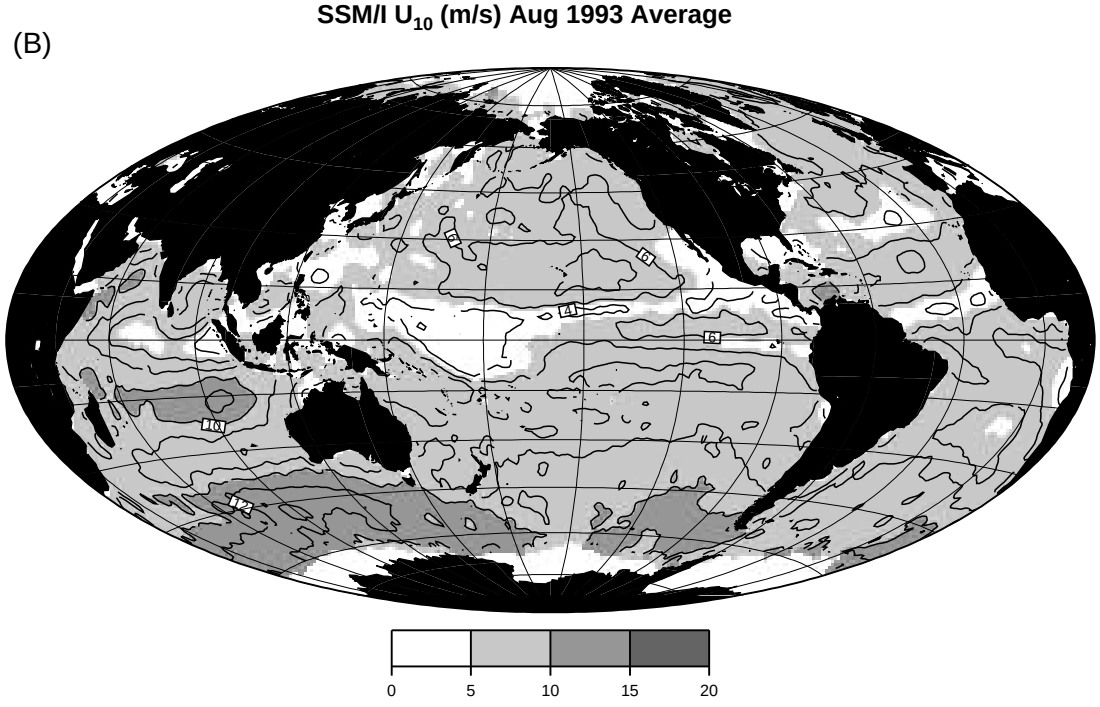

Figure 6.8 Monthly averaged SSM/I 10 meter wind speed for (A) February and (B) August 1993.

cated with RAOB soundings for all of 1993, using the lowest sounding level as a proxy for q_{10}. With 2054 points, they found an r.m.s. scatter of 1.83 g/kg, with a bias of 0.18 g/kg. Treating q_m as if it were q_{10}, the ML-q_m method's equivalent test result is 0.94 g/kg with a bias of 0.07 g/kg.

Schulz et al. (1997) presented a monthly climatology for September 1987, using their W_B(SSM/I T_B's) and linear W_B:q_{10} relationship. That time period is beyond the scope of this work, but a few comments are in order. Schulz' method suffers from the same problem of negative LHF at high latitudes in the North Pacific as Chou et al. (1995). It also appears to predict negative flux in the equatorial Pacific cold tongue. The estimated standard error of the retrieval, after deducting that portion of the variance attributed to collocation errors, is 30 W/m^2. This is larger than the 26 W/m^2 estimated standard error of the ML-q_m method. The estimated standard error of Schulz' monthly means for 2° x 2° grid boxes is 15 W/m^2, again after deducting 5 W/m^2 due to collocation and instrument errors.

6.3.2) Multi-year climatologies

As opposed to Chou et al. (1997), most climatologies are an average over many years' monthly climatologies, and are based on ship observations rather than satellite methods. In order to compare the current method with those long-term climatologies, the monthly-mean LHF fields from all six years were averaged month-by-month. The resulting maps for February and August are shown in Figure 6.9. The resulting fields are similar to the fields for February and August of 1993, but smoother and more zonally symmetric. The "bull's-eye" pattern in February 1993 just East of the date line and North of the equator, due to the El Niño of 1993, is not seen in the 6-year mean. Many of the same climatological features are still seen in the SSM/I data. The minimum over the equatorial cold tongue in the Pacific is still prevalent, and a hint of the season shift in the base of the tongue evident in the Atlantic cold tongue is seen. The much smaller minimum off the West coast of Indonesia (due to lower wind speeds) is visible, but larger in Northern Hemisphere winter.

Figure 6.10 shows the difference between the 6-year mean LHF and the Esbensen and Kushnir (1981) climatology. It was calculated from 25 years of ship data, mostly in the North Pacific and North Atlantic. In order to have enough measurements in each grid box to have statistical significance, a 5° x 4° grid was used. Figure 6.11 shows the same kind of difference field between the ML-q_m method and the Oberhuber (1988) climatology. This climatology is based on the comprehensive ocean-atmosphere data set (COADS, Woodruff et al. 1987). Figure 6.12 shows the difference between the ML-q_m method LHF and the climatology of da Silva et al. (1994). It is a seasonal climatology based on ship data between 1945-1989. The most striking thing about these climatologies is the similarity of their difference fields from the ML-q_m climatology. Over large parts of the tropics the model is >50 W/m^2 higher

(A)

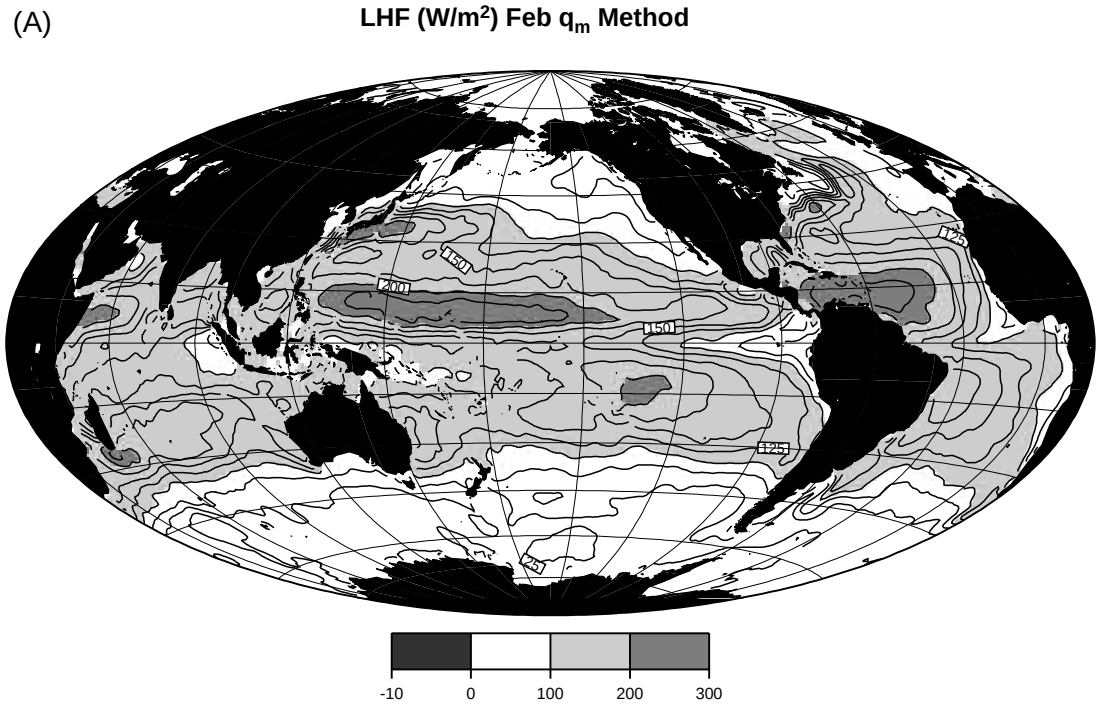

(B)

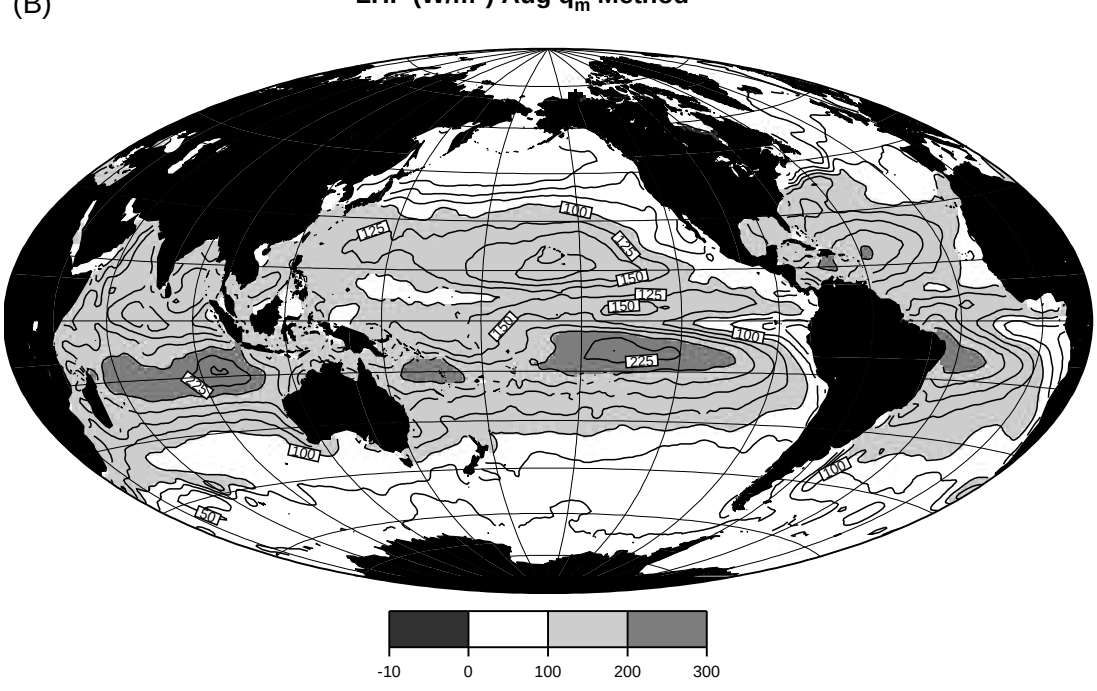

Figure 6.9 1992-1997 SSM/I LHF climatologies for (A) February and (B) August, using the ML-q_m method.

(A)

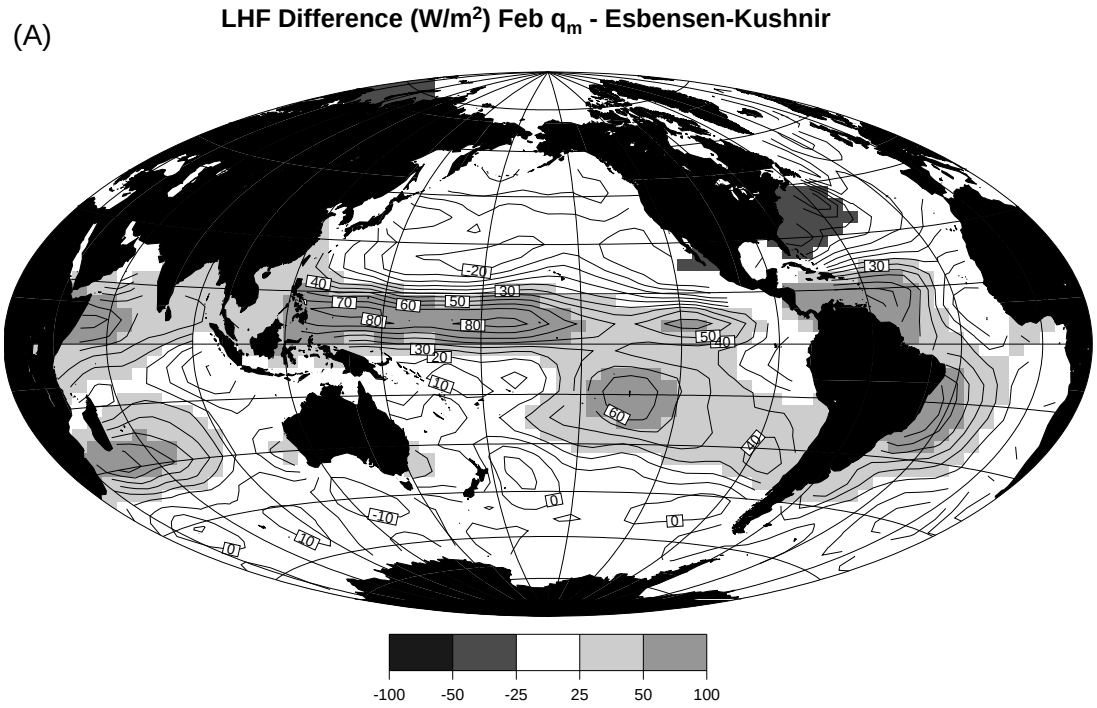

(B)

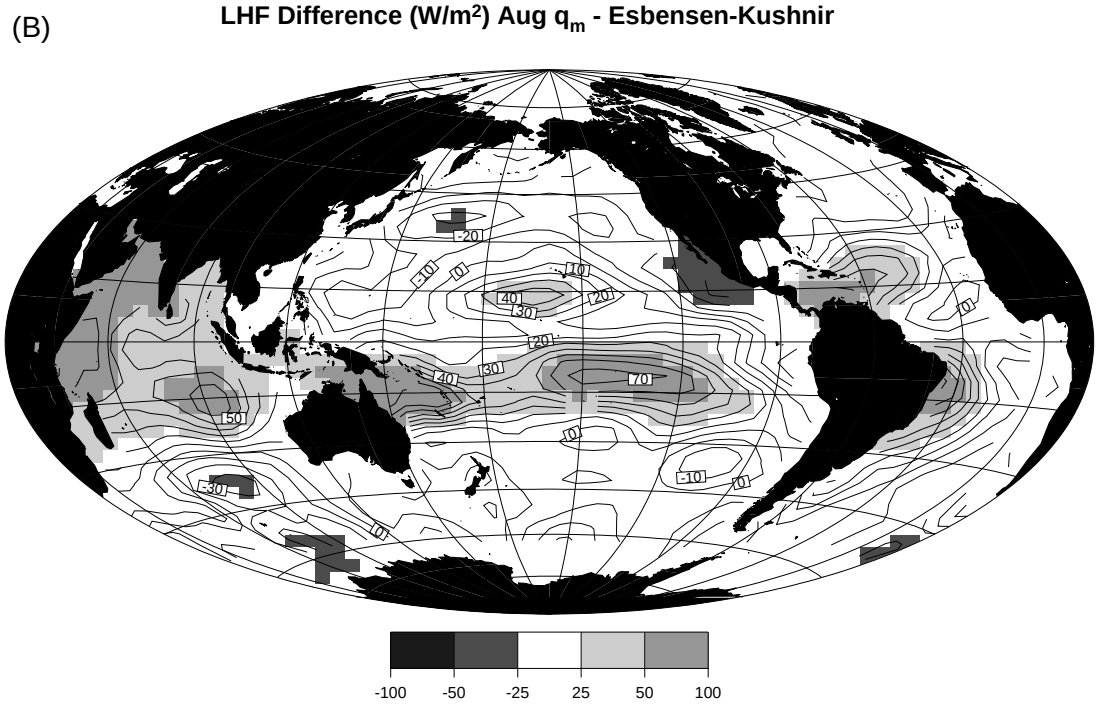

Figure 6.10LHF Difference fields between a 1992-1997 average using the SSM/I ML-q_m method and the Esbensen and Kushnir (1980) monthly multi-year average for (A) February and (B) August.

(A)

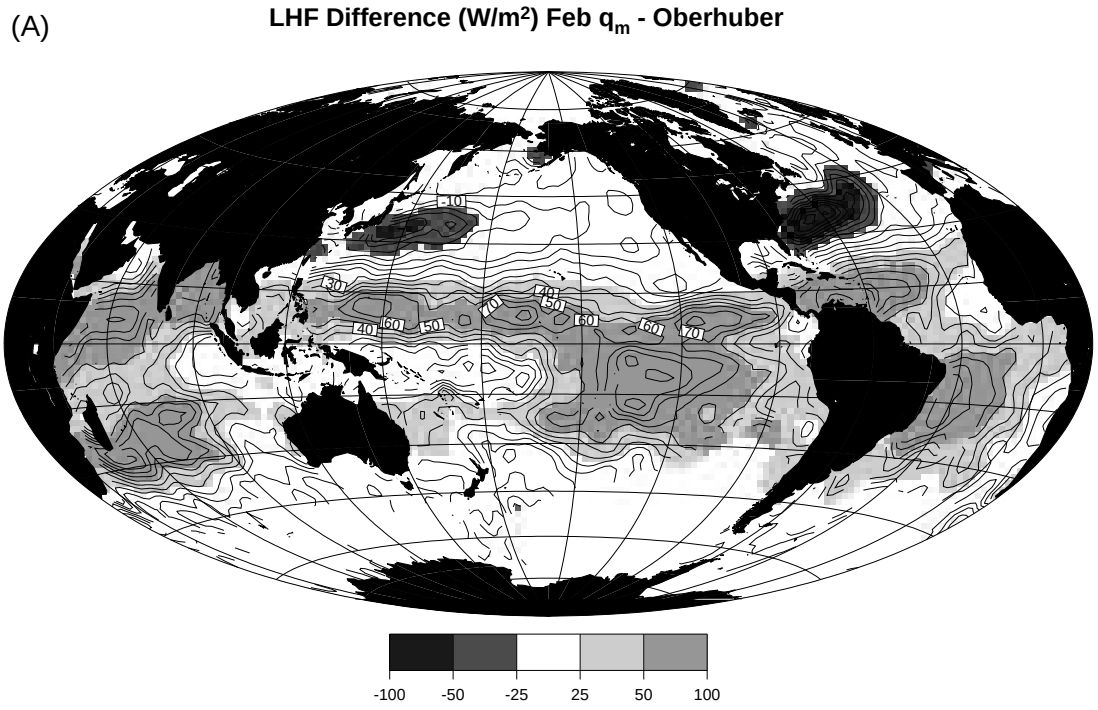

(B)

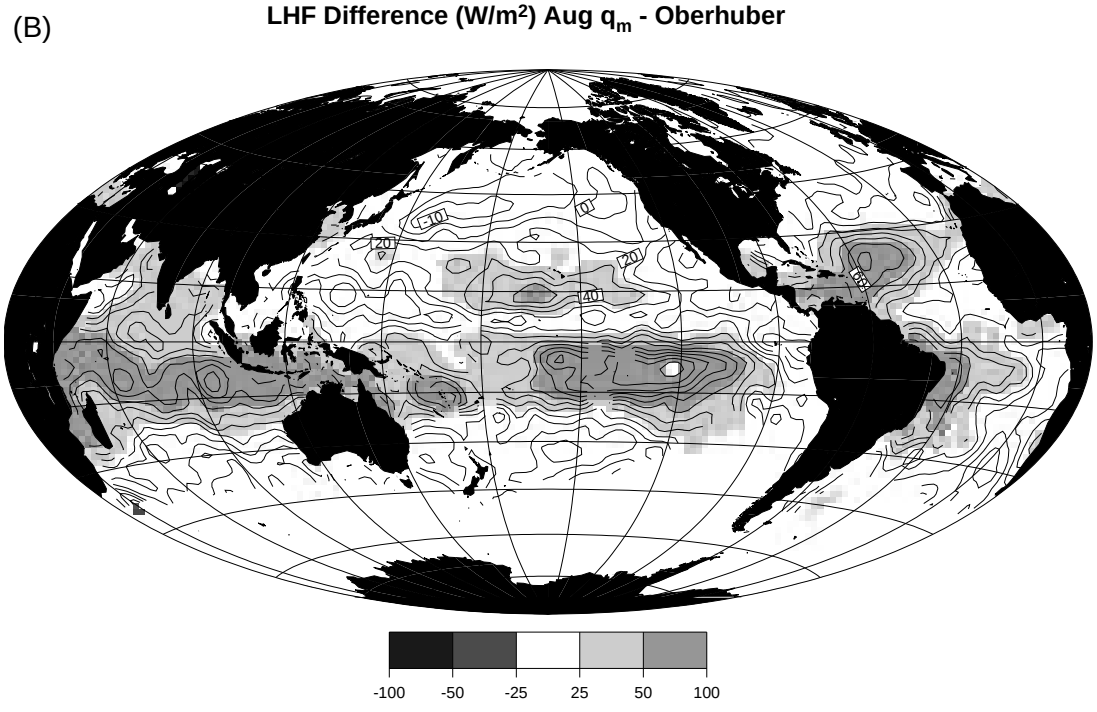

Figure 6.11LHF Difference fields between a 1992-1997 average using the SSM/I ML-q_m method and the Oberhuber (1988) COADS monthly multi-year average for (A) February and (B) August.

(A)

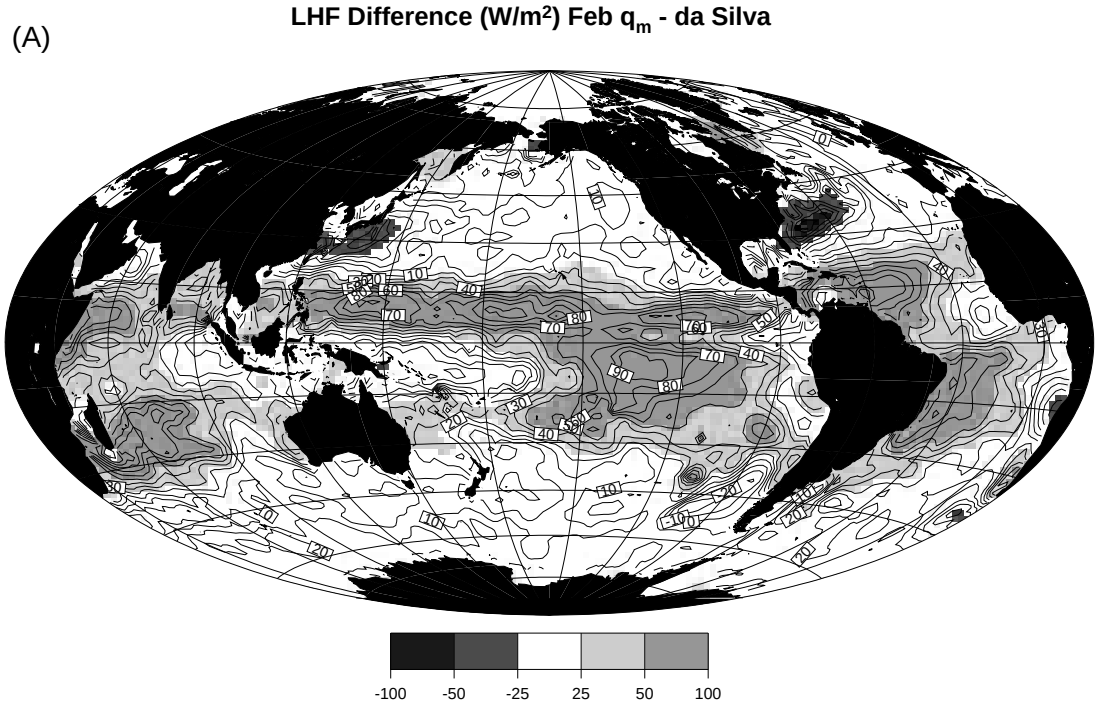

(B)

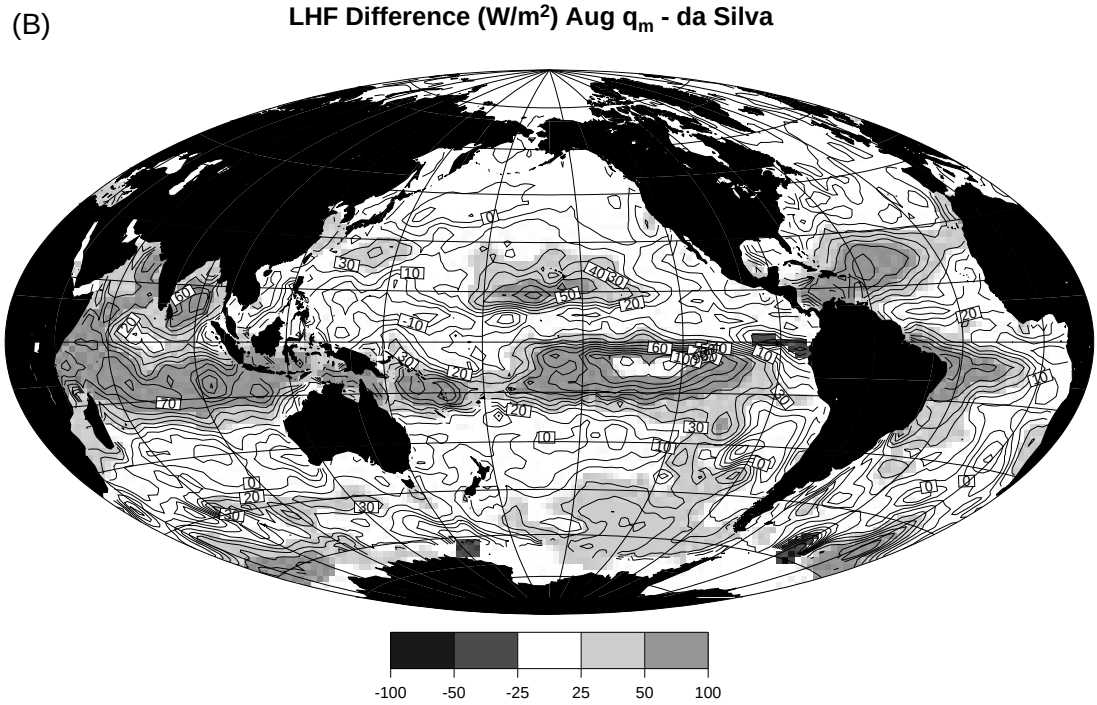

Figure 6.12LHF Difference fields between a 1992-1997 average using the SSM/I ML-q_m method and the da Silva et al. (1994) monthly multi-year average for (A) February and (B) August.

than these climatologies, while at higher latitudes especially in summer the agreement is better. There is a somewhat symmetric shape to the tropical error contours, with two zonal bands on either side of the equator. The band on the winter side is stronger than on the summer side, and they merge in February in the Easter Pacific. The Oberhuber climatology does not have enough data in the high Southern latitudes to compare to the SSM/I climatology, and I suspect that is the case for the Esbensen Kushnir product as well. The da Silva climatology shows the SSM/I climatology to be more than 25 W/m^2 high in the high Southern latitudes during austral summer.

There are some differences between these three marine ship-based climatologies. There is a pronounced minimum in the difference fields off the coast off Japan during February for the Oberhuber and da Silva climatologies, but no corresponding minimum in the Esbensen and Kushnir data. Additionally, the size of this feature is different, with Oberhuber being much larger and reaching further North. There is a hint of agreement among the three for the corresponding region off the East coast of North America, but again Oberhuber is largest and protrudes further North, and Esbensen's minimum is not nearly as strong as the other two. These regions are located in the storm track, and are commonly subject to advection of dry, cold continental air over the local warm Western boundary current, leading to large fluxes. The values of the ML-q_m method in these regions is closest to that of da Silva, in that Esbensen and Kushnir show very little in the way of a local maximum oriented with the storm track. Oberhuber features the largest and strongest such region.

These climatologies were calculated by first averaging the meteorological variables and then using the bulk aerodynamic method to calculate fluxes, rather than averaging the daily fluxes calculated from meteorological variables. This procedure can result in errors. Esbensen and Reynolds (1981) showed that "monthly averaged wind speeds, temperatures, and humidities can be used to estimate the monthly averaged sensible and latent heat fluxes from the bulk aerodynamic equations to within a relative error of approximately 10%." This conclusion is often cited in the literature (*e.g.* Chou et al. 1995, Liu 1988, Bates 1991). To assess the accuracy of this error, I performed the following experiment. I created files with one month of ECMWF 10 m wind, 2 m air and dew point temperatures, and sea surface temperature analyses on the ECMWF global ~1 degree grid. PBL-LIB was then used to calculate the LHF for each grid in the month, using the ECMWF roughness length parameterization. All variables were then scalar averaged (including the wind) for the month, and the resulting average wind speed, SST, air and dew point temperatures were used to calculate the LHF as well. Figure 6.13 shows the difference field between the two methods, for February and August 1993. The globally averaged difference for February 1993 is about 4 W/m^2. In the winter trade wind regions the error increases to more than 10 W/m^2 for significant areas. Chou et al. (1997) found similar results using her EOF method to calculate LHF, but

(A)

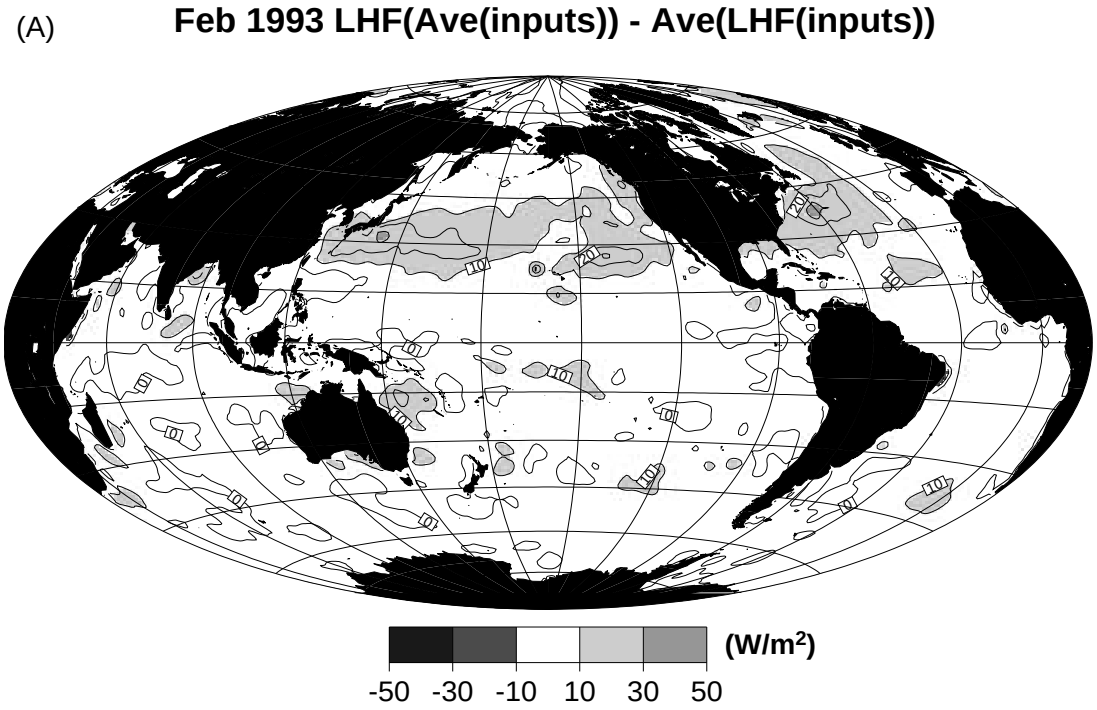

(B)

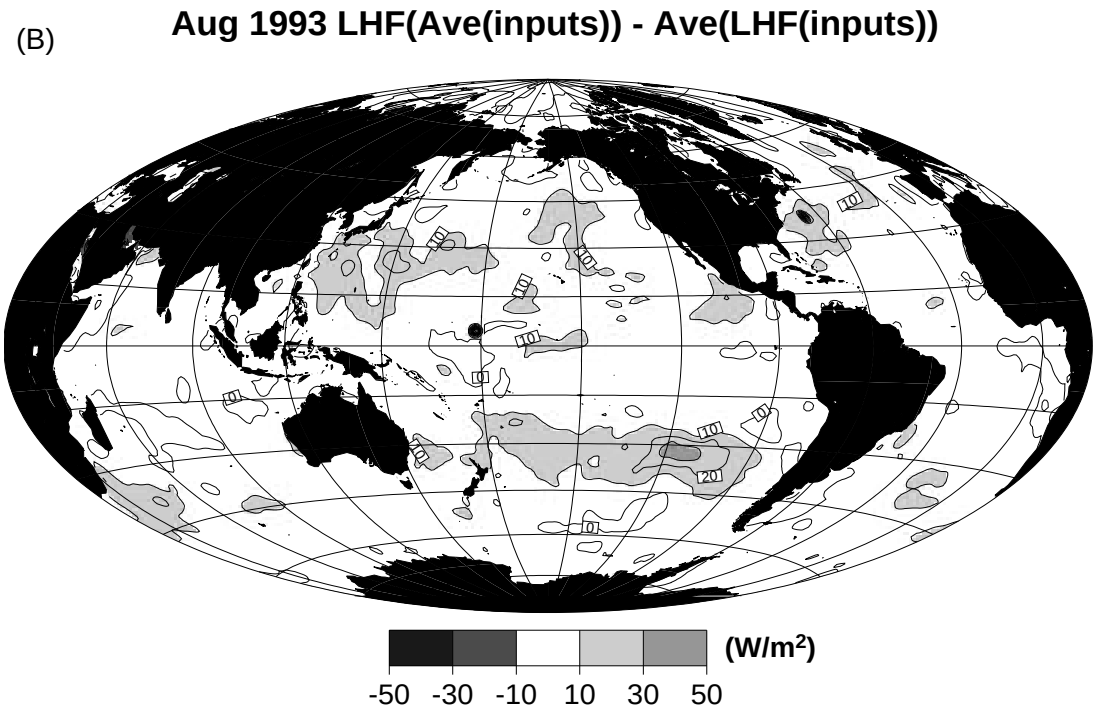

Figure 6.13The difference between LHF using ECMWF U_{10}, SST, T_{10}, and q_{10} calculated from monthly means of inputs and calculated from daily inputs and then averaged, for (A) February 1993 and (B) August 1993.

the error due to averaging is convolved with the errors of the EOF method. She found regions in the summertime extratropical oceans where the EOF method underestimated the LHF by 40-50%.

This difference is due to the non-linear nature of the surface layer equations and the variable nature of the winds and SST in the subtropical regions. Norris (1997) showed how the region of maximum SST gradient migrated seasonally. Since the latitude of maximum baroclinicity is closely tied to the latitude of maximum SST gradient, the monthly averaged winds and SST in this region introduces a local maximum in the error.

The result that SSM/I latent heat fluxes are larger than the ship-based climatological values is consistent with previous climatological studies (Bunker et al. 1982, Oberhuber 1988, da Silva et al. 1994). Bunker and da Silva both found from heat balance studies that there is a net surplus of heat going into the ocean, presumably due to errors in the calculation of the surface energy budget, including LHF. Ships in the subtropics tend to underestimate winds and overestimate dew point temperatures (Chou et al. 1997). Additionally, the wind speed used by Esbensen and Kushnir is about 1 m/s lower than that of da Silva and that of Oberhuber, both of which are in better agreement with the SSM/I wind speed (Chou et al, 1997).

6.4) Model Applicability

The question arises “where can we expect this SSM/I technique to work well? Under what conditions does it give substantial biases?” The answers lie in the filtering and availability of the input data. The turbulence data I had access to was from only two regimes. The Malcolm Baldrige took turbulence data between 28° and 35° N in the Eastern Atlantic ocean, where we expect predominantly cold advection conditions. The Hakuho Mara and the Moana Wave took turbulence data close to the equator in the Western Pacific warm pool, where convective conditions predominate. No turbulence data was available during a mid-latitude cold-air outbreak, or in the Western edge of an oceanic basin where we would expect to find warm advection. If we believe that the LKB model, which behaves well when compared to the available turbulence data, is applicable in wide-ranging conditions, then we can assess the SSM/I LHF model against the ship-sensor measurement estimates of LHF. But we can’t *prove* the SSM/I model behaves well outside of the sub-tropics. Since I used the available turbulence data to guide me in choosing the free parameters for the LKB model, it may have introduced a bias at mid-latitudes. For example, Chou et al. (1995) found a different combination of free parameters best fit observations made from aircraft flying at 50 m during a cold air outbreak off the East coast of North America, 35° to 40° N. As shown in Chapter 4, the choice of the empirical function $z_0(u_*)$ and the values for the ‘Von Karman’ constants k_E and k_H play a crucial role in determining the overall bias of the LKB model.

I also discarded soundings that were within 150 km of land, and those close to the ice edge (approximated by discarding soundings with SST < 1.5° C) in an attempt to avoid conditions of strong advection of continental air. The SSM/I retrievals of W and U_{10} are not valid when either land or ice is in the radiometer's field of view. I could have used soundings as close as 56 km (the pixel size of the 19 GHz channel) from land/ice, but chose to give the PBL some 'extra time' to develop a mixed layer. My regressions of W_B and q_m take advantage of the ubiquitousness of the mixed layer, and its self-similar structure. The regressions identify the most common mixed-layer humidity for a given SST and total integrated water vapor. I would hesitate to apply this method much closer to land/ice than 150 km, which limits the method's use for studying the largest fluxes during cold-air outbreaks and the fluxes over the Western Boundary Currents such as the Gulf Stream. These can be important contributors to the climatology of LHF. It is likely that the climatological LHF presented herein is underestimated in regions where these conditions occur often. In conditions where q_m is consistently dryer than its global mean relative to W and SST, this method under-predicts the flux.

In mid-latitude cyclones, the wind speed increases relative to its zonal average, tending to increase the surface fluxes. But at the same time, q_m is increasing relative to q_0, tending to decrease the fluxes. Near the convective bands, the SSM/I retrievals are not valid due to rain, prohibiting the use of this method. Here, the wind speed is often very high but the air has been hydrated by evaporation of rain. This method cannot tell us how much LHF from storms we're missing in our monthly climatologies.

6.4.3) Regional Errors

Because the DMSP satellites are in a sun-synchronous orbits, each point on the earth is sampled at most twice per day. The ascending node of the F10, F13 and F14 satellites is about 0600 local time, or near sunrise. The F11 is in a slightly different orbit. Since we sample near sunrise and near sunset, this method does not include the effect of the daily variation of LHF due to changes in the incoming solar flux. Zeng and Dickinson (1998) have calculated that the amplitude of the diurnal variation of LHF in the tropics is about 15 W/m^2 by comparing LHF from hourly data with LHF from daily and monthly data. The diurnal variation of SST was the largest contributor to the diurnal variation of LHF. They also found the error increased dramatically above SST = 30° C, to a maximum of about 50 W/m^2. Between 26° and 30° C, the error was small, but it changed sign at about 29° C and is nearly constant at about -10 W/m^2 between 20° and 24° C. Thus the SSM/I LHF method likely under-predicts the LHF in the Western Pacific warm pool, and slightly overpredicts it in the rest of the tropics.

6.5) Conclusions

In this thesis, I have collected a large quantity of oceanic soundings, launched from high-quality research vessels. Each of the vessels time series of meteorological observations was also obtained, allowing a high-quality independent estimates of surface latent heat flux (LHF). I have used Monin-Obukhov similarity theory (the LKB model, Liu et al., 1979) to estimate bulk fluxes. I have shown how to calculate surface fluxes using mixed-layer averages of specific humidity (q_m) and potential temperature (θ_m). The validity of this approach has been addressed, and it is found to be valid for a much wider variety of conditions than previous researchers had thought. The errors associated with this approach have been examined, and found to be similar to the errors in using the bulk method with the more traditional 10-meter data.

Using a statistical approach, I have developed two new retrievals using the total integrated water vapor (W) and the sea surface temperature (SST). This represents a departure from most retrievals involving the SSM/I which use only the channels available on the sensor. Instead, I have used a two-satellite approach where the SSM/I is intended to furnish measurements of W, and the AVHRR is intended to furnish measurements of SST. The problem of the AVHRR not being able to retrieve SST in cloudy conditions has been circumvented by using Reynolds and Smith (1994) optimally interpolated (OI) SST, which is largely controlled by AVHRR measurements but also uses those relatively few buoy and ship observations as well. The retrieved parameters are q_m and W_B, the "bottom layer" (500 m) integrated water vapor. The errors associated with these statistical retrievals have been quantified.

The new method incorporating SSM/I-derived wind speed and mixed-layer humidity, ECMWF air-sea temperature difference, and NCEP optimal interpolation SST has been used to calculate global grids of monthly-averaged latent heat flux for the period January 1992 to December 1997. All available SSM/I data was used, from the DMSP F10, F11, F13 and F14 satellites. Daily ECMWF sea level pressure was used, mainly to calculate potential temperatures and mixing ratios, but also in an analytical equation relating q_m to W_B. This equation, along with the technique of driving the LKB model with mixed-layer values, is a replacement for the statistical relationship of Schulz et al. (1993). Twice-daily ECMWF air-sea temperature differences (T_{10} - SST) were used in the calculations. Weekly Reynolds OI SST data were used. All SSM/I data were reduced from a 0.25° by 0.25° grid to a 1° by 1° grid, and all other input data were interpolated first in space to the same grid, then in time to the time of each SSM/I observation. The calculations were performed three times, once using the q_m retrieval, once using the W_B retrieval, and once using the bulk SSM/I C_E method. The overall errors of the methods have been examined, and found to be smaller than the existing best (and nearly equivalent) methods of Chou et al.

(1997), Schulz et al. (1993) and Schlüssel et al. (1995). This will be the first SSM/I LHF climatology to be calculated for the full run of the SSM/I sensors and made available to the general scientific community.

The pattern and seasonal variation of both versions of PBL-LIB LHF and both versions of SSM/I LHF show good agreement with Chou et al. (1997), Esbensen and Kushnir (1981), Oberhuber (1988), and da Silva et al (1994). All capture the local maximum where the atmospheric storm track interacts with the western boundary currents off the coasts of Asia and North America during February and Africa during August. All show a local maximum over the subtropical trade wind regions during summer. PBL-LIB fails near the equator, but the SSM/I LHF captures the local minimum over the pacific cold tongue the atlantic cold tongue during August.

Discrepancies between the published climatologies and the current climatology have been addressed. The major differences between the ML-q_m method and Chou et al (1997) has been identified as partially a model parameter choice issue, and partially differences in the SSM/I retrievals of humidity.

6.6) Model implications

The resulting grids of monthly SSM/I LHF will be made available to the scientific community, perhaps via NOAA PMEL's climate server at "http://ferret.wrc.noaa.gov/fbin/climate_server".

One of the largest uncertainties comes from using the weekly OI SST product. The next level of complication would be to parameterize the SST diurnal cycle. This has been done by e.g. Clayson and Curry (1996) for the TOGA-COARE retrievals of SSM/I LHF, with some success. It requires some parameterization of the incoming solar radiation, which is highly affected by cloud cover. The SSM/I retrieval of cloud liquid water may prove useful for such an endeavor.

It may also prove advantageous to examine the effect of using different surface-layer parameterizations with the ML-method in place of the LKB model. The model of Clayson et al. (1996) seems especially promising to me, as it has been shown to produce good results both in the TOGA-COARE region and at mid-latitudes. Like LKB, it is based on the surface renewal theory of Brutsaert (1965), which at its heart postulates a time-scale for interaction between the viscous sub-layer and the Kolmogorov-scale eddies. LKB has only a time-scale for shear-driven turbulence while Clayson et al. (1996) includes both shear and convective flows. Additionally, the roughness at the surface caused by capillary waves is included directly in this time-scale, rather than as an empirical relation between u_* and z_0 (e.g. Smith

1989). This approach alleviates the need for the gustiness parameterization used here and in Fairall et al. (1996).

The retrieval technique developed in section 3.10, page 41, holds great promise for the Advanced Microwave Scanning Radiometer (AMSR) scheduled for launch in Autumn of 1999 aboard the ADEOS-II satellite, and aboard the EOS PM-1 satellite scheduled for launch in the year 2000. AMSR is a passive microwave radiometer with eight frequency bands at 6.925, 10.65, 18.7, 23.8, 36.5 and 89.0 GHz that is a sort of combination of the AVHRR and SSM/I sensors. The aperture diameter of AMSR's antenna is 2 m, giving it a field of view of about 5km (89GHz) to about 50 km (6.9 GHz), with a swath width of 1600 km. Since it has channels both below 10 GHz and close to the SSM/I channels, it can retrieve SST and W simultaneously. The conclusion from this thesis is that a direct parameterization of q_m in terms of brightness temperatures will be possible. This will increase the accuracy of LHF calculations using the ML-method, since the current calculations use weekly SST values and thus miss diurnal and other short-timescale variations.

It may be advantageous to keep the two retrievals (q_m and SST) separate, since it may not be possible to fully account for the influence clouds have on the lower frequency channels with the cloud information contained in the upper channels. AVHRR cannot retrieve instantaneous SST over the cloud-covered part of the world's oceans (a significant percentage) which forced me to use the weekly OI SST data. Still, the advantages of having retrievals of SST and q_m from the same platform are tremendous.

References

Albrecht, B. A., C. S. Bretherton, D. Johnson, W. H. Schubert, and A. S. Frisch, 1995: The atlantic stratocumulus transition experiment - ASTEX. *Bull. Amer. Meteor. Soc.*, **76,** 889-904.

Alishouse, J. C., S.A. Snyder, J. Vongsathorn, and R. R. Ferraro 1990: Determination of oceanic total precipitable water from the SSM/I. *IEEE Transactions on Geoscience and Remote Sensing*, **28**(5), 811-816..

Bates, T.S , B. J. Huebert, J.L. Gras, F. B Griffiths and P. A. Durkee, [in press]: The International Global Atmospheric Chemistry (IGAC) Project's First Aerosol Characterization Experiment (ACE-1) - Overview, submitted to *J. Geophys. Res*.

Blanc, T. 1989: Accuracy of bulk-method-determined flux, stability, and sea surface roughness. *J. Geophys. Res.*, **92**, 3867-3876.

Bolton, D., 1980: The computation of equivalent potential temperature. *Mon. Wea. Rev.*, **108**, 1046-1053.

Brown, R.A., 1970: A secondary flow model for the planetary boundary layer. *J. Atmos. Sci.*, **27**, 742-757.

Brown, R.A., 1972: On the inflection point instability of a stratified Ekman boundary layer. *J. Atmos. Sci*., **29**, 850-859.

Brown, R. A., 1974: Matching classical boundary layer solutions toward a geostrophic drag coefficient relation. *Bound. Lay. Meteor.*, **7**, 489-500.

Brown, R.A., 1980: Longitudinal instabilities and secondary flows in the planetary boundary layer: a review. *Rev. Geophys. Space Phys.* **18**, 683-697.

Brown, R.A., 1981: Modeling the geostrophic drag coefficient for AIDJEX. *J. Geophys. Res*., **86**, 1989-1994.

Brown, R. A., and W. T. Liu, 1982: An operational large-scale marine planetary boundary layer model. *J. Appl. Meteor.,* **21,** 261-269.

Brown, R. A., 1982a: On two-layer models and the similarity functions for the planetary boundary layer. *Bound. Lay. Meteor.*, **24**, 451-463.

Brown, R. A. and G. Levy, 1986: Ocean surface pressure fields from satellite-sensed winds. *Monthly Weather Review*, **114**, 2197-2206.

Brown, R. A., 1991: *Fluid Mechanics of the Atmosphere*. Academic Press, San Diego. 489 pp.

Brutsaert, W., 1965: A model for evaporation as a molecular diffusion into a turbulent atmosphere. *J. Geophys. Res.*, **70**, 5017-5024.

Businger, J. A., J. C. Wyngaard, Y. Izumi and E. F. Bradley, 1971: Flux-profile relationships in the atmospheric surface layer. *J. Atmos. Sci.*, **28**, 181-189.

Businger, J. A,. 1973a: Turbulent transfer in the atmospheric surface layer. *Workshop in Micrometeorology.*, Amer. Meteor. Soc., 67-100.

Businger, J. A,. 1973b: A note on free convection. *Bound.-Layer Meteor.*, **4**, 323-326.

Charnock, H., 1955: Wind stress on water surface. *Quart. J. Roy. Meteorol. Soc.*, **81**, 639-640.

Chou, S.-H., 1993: A comparison of airborne eddy correlation and bulk aerodynamic methods for ocean-air turbulent fluxes during cold-air outbreaks. *Bound.-Layer Meteor.*, **64,** 75-100.

Chou, S.-H., R. M. Atlas, C. L. Shie, and J. Ardizzone, 1995: Estimates of surface humidity and latent heat fluxes over oceans from SSM/I data. *Monthly Wea. Rev.*, **123**, 2405-2425.

Chou, S.-H., C.-L. Shie, R. M. Atlas, and J. Ardizzone, 1996: Evaporation estimates over global oceans from SSM/I data, paper presented at 8th Conference on Satellite Meteorology and Oceanography, Am. Meteorol. Soc., Altanta, GA.

Chou, S.-H., C.-L. Shie, R. M. Atlas, and J. Ardizzone, 1997: Air-sea fluxes retrieved from special sensor micorwave imager data. *J. Geophys. Res.*, **102**, 12705-12726.

Clayson, C. A. and J. A. Curry, 1996: Determination of surface turbulent fluxes for the tropical ocean - global atmosphere coupled ocean-atmosphere response experiment: comparison of satellite retrievals and in situ measurements. *J. Geophys. Res.*, **101**, 28,515-29,528.

Cole, H., 1993: “The TOGA COARE ISS Radiosonde Temperature and humidity sensor errors”. *Technical Report, Surface and Sounding Systems Facility (SSSF)*, National Center for Atmospheric Research (NCAR), Boulder, 26 p.

da Silva, A., A. C. Young, and S. Levitus, 1994: Atlas of Surface Marine Data 1994, Volume 1: Algorithms and Procedures. *NOAA Atlas NESDIS 6*, U.S. Department of Commerce, Washington, D.C., 416 pp.

Deardorff, J.W., 1972: Numerical investigation of neutral and unstable planetary boundary layers. *J. Atmos. Sci.* **29**, 91-115.

Deardorff, J. W. 1970: Convective velocity and temperature scales for the unstable planetary boundary layer and for Rayleigh convection. *J. Atmos. Sci.*, **27**, 1211-1213.

Dickinson, S. and R. A. Brown, 1996: A study of near-surface winds in marine cyclones using multiple satellite sensors. *J. Appl. Meteor.*, **35**, 769-81.

Dyer, A. J., 1974: A review of flux-profile relationships. *Bound.-Layer Meteor.*, **7**, 363-372.

Dyer, A. J. and E. F. Bradley, 1982: An alternative analysis of flux-gradient relationships at the 1976 ITCE. *Bound.-Layer Meteor.*, **22**, 3-19.

Ekman, V. W., 1905: On the influence of the earth’s rotation on ocean currents. *Arkiv. Math. Astron. Fysik*, **2**, 1-54.

Elliot, W. P., and D. J. Gaffen, 1991: On the utility of radiosonde humidity archives for climate studies. *Bull. Amer. Meteor. Soc.*, **72,** 1507-1520.

Esbensen, S. K. and Y. Kushnir, 1981: The Heat Budget of the Global Ocean: An Atlas Based on Estimates from Surface Marine Observations. *Rep. 29*, Clim. Res. Inst., Oreg. State Univ., Corvalis, 27 pp.

Ebensen, S. K. and R. W. Reynolds, 1981: Estimating monthly averaged air-sea transfers of heat and momentum using the bulk aerodynamic method. *J. Phys. Ocean.*, **11**, 457-465.

Esbensen, S. K., D. B. Chelton, D. Vickers, and J. Sun, 1993: An analysis of errors in Special Sensor Microwave Imager Evaporation Estimates over the global oceans. *J. Geophys. Res.*, **98 (C4)**, 7081-7101.

Fairall, C. W., E. F. Bradley, D. P. Rogers, J. B. Edson, and G. S. Young, 1996: Bulk parameterization of air-sea fluxes for Tropical Ocean-Global Atmosphere Coupled-Ocean Atmosphere Response Experiment. *J. Geophys. Res.*, **101**, 3747-3764.

Fairall, C. W., A. B. White, J. B. Edson, and J. E. Hare, 1997: Integrated shipboard measurements of the marine boundary layer. *J. Atmos. Ocean Tech*., **14**, 338-359

Flamant, C., J. Pelon, B. Brashers and R. A. Brown,1998: Evidence of a Mixed-Layer Dynamics Contribution to the Entrainment Process" (in preparation).

Foster, R. C. and R. A. Brown, 1994a: On large-scale PBL modelling: surface layer models. *The Global Atmosphere and Ocean System*, **2**, 185-198.

Foster, R. C. and R. A. Brown, 1994b: On large-scale PBL modelling: wind and latent heat flux comparisons. *The Global Atmosphere and Ocean System*, **2**, 199-219.

Francey, R. J. and Garratt, J. R., 1981: Interpretation of flux-profile observations at ITCE (1976). *J. Appl. Meteor.*, **20**, 603-618.

Gautier, C., R. Frouin and J.-Y. Simonot, 1988: An attempt to remotely sense from space the surface heat budget over the Indian ocean during the 1979 monsoon. *Geophys. Res. Lett*, **21**, 193-196.

Godfrey, J. S. and A. C. M. Beljaars, 1991: On the turbulent fluxes of buoyancy, heat and moisture at the air-sea interface at low wind speeds. *J. Geophys. Res.*, **96**, 22,043-22,048.

Grody, N. C., 1976: Remote sensing of atmospheric water vapor content from satellites using microwave radiometry. *IEEE Trans. on Antennas and Propagation*, **AP-24**, 155-161.

Hollinger, J. P., R. Lo, G. Poe, R. Savage, and J. Peirce, 1987: *Special Sensor Microwave/Imager user's guide* (Washington, DC: Naval Research Laboratory).

Högström, U 1988: Nondimensional wind and temperature profiles in the atmospheric surface layer: a re-evaluation. *Bound.-Layer Meteor.*, **42**, 55-78

Högström, U. 1996: Review of some basic characteristics of the atmospheric surface layer. *Bound.-Layer Meteor.*, **78**, 215-246.

Hsu, S. A., and B. W. Blanchard, 1989: The relationship between total precipitable water and surface-level humidity over the sea surface: a further evaluation. *J. Geophys. Res.*, **94 (C10)**, 14,539-14545.

Jourdan, D. and C. Gautier, 1995: Comparison between global latent heat flux computed from multisensor (SSM/I and AVHRR) and from in situ data. *J. Atmos. Ocean. Tech*., **12**, 46-72.

Konda, M., N. Imasato, and A. Shibata, 1996: A new method to determine near-sea surface air termperature by using satellite data. *J. Geophys. Res.*, **101**, 14,349-14360.

Kondo, J., 1975: Air-sea bulk transfer coefficients in diabatic conditions. *Bound.-Layer Meteor.*, **9,** 91-112.

König-Langlo, G. and B. Marx 1997: The Meteorological Information System at the Alfred Wegener Instiute. *Climate and Environmental Database Systems*, Edited by M. Lautenschlager and M. Reinke. Kluwer Academic Publisher. 197 pp.

Kraus, E. B., 1972: Oceanic response and feedback to atmospheric forcing. *Dynamics of the tropical atmosphere: notes from a colloquium, Summer 1972*. National Center for Atmospheric Research, Boulder, p. 421-431.

Large, W. G., J. Morzel, and G. B. Crawford, 1995: Accounting for surface wave distortion of the marine wind profile in low-level ocean storms wind measurements. *J. Phys. Oceanogr.*, **25**, 2959-2971.

Leovy, C. B., 1969: Bulk transfer coefficient for heat transfer. *J. Geophys. Res.*, **13**, 3313-3321.

Levy, G. and R. A. Brown, 1986: Southern Hemisphere synoptic weather from a satellite scatterometer. *Monthly Weather Review*, **119**, 2803-2813.

Liu, W. T. and J. A. Businger, 1975: Temperature profile in the molecular sublayer near the interface of a fluid in turbulent motion. *Geophys. Res. Lett.*, **2**, 403-404.

Liu, W. T., K.B. Katsaros, and J. A. Businger, 1979: Bulk parameterization of air-sea exchange of heat and water vapor including molecular constraints at the interface. *J. Atmos. Sci.*, **36**, 1722-1735.

Liu, W. T., and P. P. Niiler, 1984: Determination of monthly mean humidity in the atmospheric surface layer over oceans from satellite data. *J. Phys. Oceanogr.*, **14**, 1451-1457.

Liu, W. T., 1986: Statistical relation between monthly mean precipitable water and surface-level humidity over global oceans. *Monthly Weather Review,* **14**, 1591-1602.

Miller, D. K., 1990: Estimation of surface latent heat flux patterns in a rapidly intensifying cyclone derived from the Special Sensor Microwave/Imager. M.S. Thesis, Dept. of Atmospheric Sciences, University of Washington, 223 pp.

Miller, D. K. and K. B. Katsaros, 1992: Satellite-derived surface latent heat fluxes in a rapidly intensifying marine cyclone. *Mon. Wea. Rev.*, **120**, 1093-1107.

Norris, J. R., 1997: Interannual variability in cloudiness, sea surface temperature, and atmospheric circulation over the midlatitude North Pacific during summer. Ph.D. Thesis, Dept. of Atmospheric Sciences, University of Washington, 199 pp.

Oberhuber, J. M. , 1988: An atlas based on `COADS' data set. *Tech. Rep. 15*, Max-Planck-Instutut für Meteorologie.

Petty, G. W., 1990: On the response of the Special Sensor Microwave/Imager the marine environment - implications for atmospheric parameter retrievals. Ph. D. Thesis, Dept. of Atmospheric Sciences, University of Washington, 291 pp.

Randall, D. A., R. D. Cess, J. P. Blanchet, G. J. Boer, D. A. Dazlich, A. D. Del Genio, M. Deque, V. Dymnikov, V. Galin, S. J. Ghan, A. A. Lacis, H. Le Treut, Z. X. Li, X. Z. Liang, B. J. McAvaney, V. P. Meleshko, J. F. B. Mitchell, J. J. Morcrette, G. L. Potter, L. Rikus, E. Roeckner, J. F. Royer, U. Schlese, D. A. Sheinin, J. Slingo, A. P. Sokolov, K. E. Taylor, W. M. Washington, R. T. Wetherald, I. Yagai, and M. H. Zhang, 1992: Intercomparison and interpretation of surface energy fluxes in atmospheric general circulation models. *J. Geophys. Res.*, **97 (D4)**, 3711-3724.

Reynolds, R. W. and T. S. Smith, 1994: Improved global sea surface temperature analyses using optimum interpolation. *J. Climate*, **7**, 929-948.

Schulz, J., P. Schlüssel, and H. Grassl, 1993: Water Vapour in the atmospheric boundary layer over oceans from SSM/I measurements. *Int. J. Remote Sensing*, **14**, 2773-2789.

Schlüssel, P., W. J. Emery, H. Grassl, and T. Mammen, 1990: On the bulk-skin temperature difference and its impact on satellite remote sensing of sea surface temperature. *J. Geophys. Res.*, **95 (C8)**, 13,341-13,356.

Schlüssel, P., L. Schanz, and G. Englisch, 1995: Retrieval of latent heat and longwave irradiance at the sea surface from SSM/I and AVHRR measuremtents. *Adv. Space Res.*, **16**, (10)107-(10)116.

Smith, S. D., 1989: Water vapor flux at the sea surface. *Bound.-Layer Meteor.*, **47**, 277-293.

Stage, S. A. and J. A. Businger, 1981: A model for entrainment into a cloud-topped marine boundary layer. Part I: model description and application to a cold-air outbreak episode. *J. Atmos. Sci.*, **38**, 2213-2229.

Stull, R. B., 1994: A convective transport theory for surface fluxes. *J. Atmos. Sci.*, **51**, 3-22

Wallace, J. M., and P. V. Hobbs 1991: *Atmospheric Science*. Academic Press, San Diego. 467 pp.

Webster, P. J., and R. Lukas, 1992: TOGA COARE: the Coupled Ocean-Atmosphere Response Experiment. *Bull. Amer. Met. Soc.*, **73**, 1377-1416.

Wentz, F. J., 1989: User's manual: SSM/I geophysical tapes. *Tech. Rep. 060989*, 16 pp., Remote Sens. Syst., Santa Rosa, Calif.

Wentz, F. J., 1995: A well calibrated ocean algorithm for SSM/I. *Tech. Rep. 101395*, 18 pp., Remote Sens. Syst., Santa Rosa, Calif.

Wentz, F. J. and C. K. Smith, 1997: Vapor Algirithms for SSM/I and AMSR. *Tech. Rep. 063097-V,* 16 pp., Remote Sens. Syst., Santa Rosa, Calif.

Woodruff, S. D., R. J. Slutz, R. L. Jenne, and P. M. Steurer, 1987: A comprehensive ocean-atmosphere data set. *Bull. Amer. Meteor. Soc.*, **68,** 1239-1250.

Yuter, S. E., 1998: Convection and stratus in the tropical eastern Pacific: The 1997 Pan American Climate Studies Tropical Eastern Pacific Process Study. In preparation.

Zeng, L. and G. Levy, 1995: Space and time aliasing structure in monthly mean polar-orbiting satellite data. *J. Geophys. Res.*, **100(D3)**, 5133-5142.

Vita

Bart Alan Brashers

Education:

Ph.D., Atmospheric Sciences, University of Washington (Seattle), 1998. Thesis: “Oceanic Latent Heat Flux from Satellite Data”.

B.S., Engineering-Physics, University of California (Berkeley), 1987.

Employment:

1987-1988: Montör, Volvo Kompanenter AB, Köping, Sweden.

1989-1991: Manager of Computer Services, Tracer Technologies, Inc., San Marcos, CA.

1991-1997: Research Assistant, Department of Atmospheric Sciences, University of Washington.

Publications:

Conference Proceedings:

“A Model for Oceanic Evaporation from Special Sensor Microwave/Imager Data”, B. Brashers, Pacific Ocean Remote Sensing Conference (PORSEC), July 9-13, 1996, Victoria, BC.

“Oceanic Latent Heat Flux from Simulated SSM/I Data”, B. Brashers, 12th Symposium on Boundary Layers and Turbulence, AMS, July 28-August 1, 1997, Vancouver, B.C.

Journal Articles:

Flamant, C., Pelon, J., Brashers, B., and Brown, R. A., “Evidence of a Mixed-Layer Dynamics Contribution to the Entrainment Process” (in preparation).

Awards:

Third place for first-time presenters at the 12th Symposium on Boundary Layers and Turbulence, Vancouver B.C., 30 July 1997.

Scholarship, NATO Advanced Study Institute: “Convection in Geophysical Flows”, March 17-27, 1997, Pforzheim, Germany.

Post-doctoral Research Associateship, National Research Council, at the National Oceanic and Atmospheric Administration, Research Triangle Park, NC., to begin August 1998.